Supporting Information for Examining the Effects of Monomer and Catalyst Structure on the Mechanism of Ruthenium-Catalyzed Ring-Opening Metathesis Polymerization

William J. Wolf, Tzu-Pin Lin, and Robert H. Grubbs

Table of Contents

General Considerations

Unless otherwise stated, all chemicals were purchased from commercial suppliers and used as received. All glassware was oven dried for at least 12 h prior to use and synthetic manipulations were performed under a nitrogen atmosphere inside a Vac/Atm glovebox or under Ar using standard Schlenk techniques. BPh_3 was recrystallized from Et_2O in the glovebox. Norbornene monomers were prepared according to literature procedures (dimethyl norbornene,[1,2] all other monomers[3]). Macromonomers were prepared according to literature procedures: polystyrene[4] poly(lactic acid) and poly(dimethylsiloxane).[3,5] Ru benzylidene phosphine complexes and NHC ligands were received as a gift from Materia Inc. and used without further purification. The SIMes[6] and SIPr[7] Ru benzylidene bispyridine complexes were prepared according to literature procedures. Solvents were dried by passage through activated alumina columns, degassed by sparging with Ar and stored over activated 3 Å molecular sieves under inert atmosphere. Deuterated solvents were purchased from Cambridge Isotope Laboratories, degassed by three freeze-pump-thaw cycles, and stored over activated 3 Å molecular sieves under inert atmosphere.

NMR spectra were recorded on Varian 300, 400, 500, and 600 MHz spectrometers or a Bruker Avance 400 MHz spectrometer. 1D and 2D spectra were processed using MestReNova v12.0. DOSY NMR spectra were processed using VNMRj software with convection corrections. Dynamic NMR lineshape analysis was performed using the DNMR package in TopSpin v4.0.6. Variable temperature NMR spectra were recorded using a Varian 500 or Varian 600 MHz spectrometer or a Bruker Avance 400 equipped with a calibrated thermocouple to regulate temperature. The probe temperature was corroborated by using a CH_3OH standard.

GPC analysis was performed using an Agilent 1260 Infinity equipped with Agilent PLgel Mixed-BLS columns. Single crystal X-ray diffraction was performed by the staff at the Caltech X-ray Crystallography Facility using a Bruker AXS D8 VENTURE diffractometer: all data was collected at 100K. Mass Spectrometry was performed by the staff at the Multi-User Mass Spectrometry Laboratory of the Department of Chemistry at Caltech.

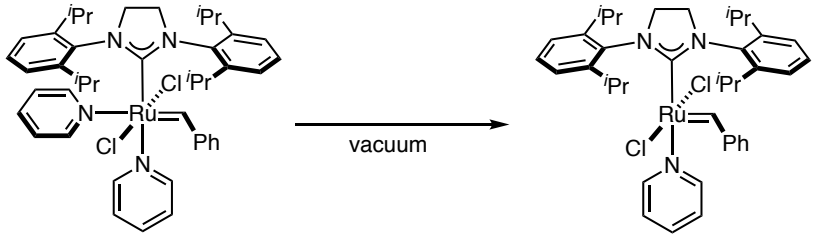

A solution of **6** (100 mg, 0.12 mmol) in benzene (3 mL) was frozen and then evaporated to dryness. This procedure was repeated a total of three times to yield the monopyridyl complex **6a** in quantitative yield. X-ray quality crystals were grown by slow evaporation of a THF solution of **6a**.

^{1}H NMR (500 MHz, CD_2Cl_2) δ 19.02 (s, 1H), 7.96 (d, J = 5.5 Hz, 2H), 7.53 (t, J = 7.6 Hz, 1H), 7.50 – 7.44 (m, 4H), 7.43 (t, J = 7.4 Hz, 1H), 7.29 (d, J = 7.8 Hz, 2H), 7.23 (s, 7H), 6.99 (dt, J = 16.0, 7.2 Hz, 4H), 4.19 (d, J = 91.9 Hz, 4H), 3.88 (s, 2H), 3.40 (s, 2H), 1.63 – 0.81 (m, 24H) ppm.

^{13}C NMR (101 MHz, CD_2Cl_2) δ 314.11, 313.86, 219.86, 152.99, 151.13, 149.69, 147.78, 136.74, 129.82, 129.51, 129.20, 127.89, 124.27, 123.60, 54.69, 28.96, 28.09, 27.18, 26.15, 23.22 ppm.

Note: the resonances for the monopyridine complex **6a** do not deviate from those reported by Piers for the bispyridine complex **6** due to the full dissociation of one of the pyridine ligands in solution.

HRMS [FAB+]: $[M]^+$ calcd for $C_{39}H_{49}Cl_2N_3Ru$ 731.2369; found 731.2348

%V Bur was calculated using the single crystal structure of the monopyridine complexes **5a**[8] and **6a** using the SambVca 2.0 application.[9] The z-axis was defined along the Ru–pyridine bond as shown in Figure SXX and the spherical radius was set to 3.5 or 5 Å.

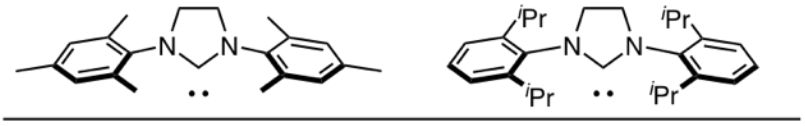

ν_{CO}(av)	2024.6 cm^{-1}	2024.9 cm^{-1}
TEP	2049.6 cm^{-1}	2051.1 cm^{-1}
%V Bur (3.5 Å)	34.2	34.2
%V Bur (5 Å)	35.8	39.7

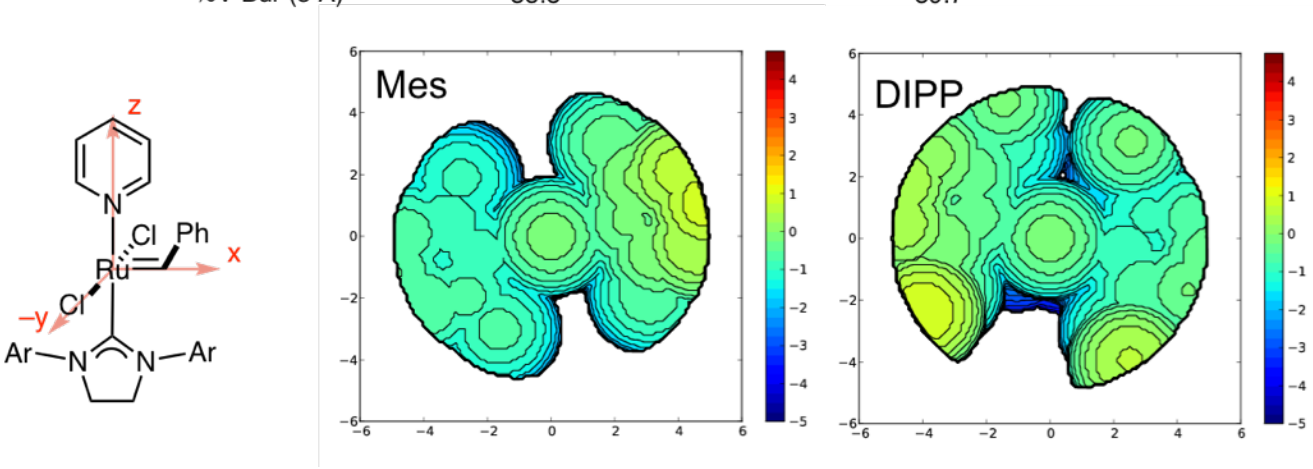

Figure S1. The defined coordinate system for the Ru benzylidene complexes for the SambVca application. The space filling model for **5a** at a radius of 5 Å. The space filling model for **6a** at a radius of 5 Å.

Synthesis of Norbornene Monomers

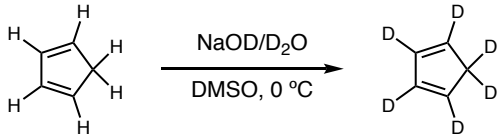

C_5D_6 was prepared according to literature procedure[10] using 25 mL of freshly cracked cyclopentadiene. Deuterium incorporation was measured using ^1H NMR against an internal standard of benzene and determined to be 94%.

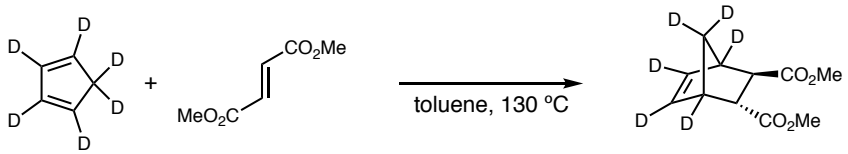

(±)

A 100 mL round bottom flask equipped with a magnetic stirbar was charged with dimethyl fumarate (1.03 g, 7.14 mmol, 1 equiv.) and toluene (20 mL). To the resulting solution was added cyclopentadiene-d_6 (660 µL, 7.14 mmol, 1 equiv) via syringe. The flask was fitted with a reflux condenser and heated with stirring to 130 ºC for 2.5 h. After cooling to ambient temperature, the reaction mixture was concentrated and purified by flash chromatography (SiO_2, 10% Et_2O in pentane, R_f = 0.15) to give a clear, colorless oil that solidified upon standing (1.4 g, 90%). Deuterium incorporation was measured by ^{1}H NMR and determined to be 93% based on integration against the methyl ester resonances.

^{1}H NMR (400 MHz, $CDCl_3$) δ 3.65 (s, 3H), 3.58 (s, 3H), 3.30 (d, J = 4.6 Hz, 1H), 2.61 (d, J = 4.5 Hz, 1H) ppm.

^{2}H NMR (61 MHz, $CDCl_3$) δ 6.31 (s, 1D), 6.12 (s, 1D), 2.95 (s , 2.76, 1.46 ppm.

^{13}C NMR (101 MHz, CD_2Cl_2) δ 200.39, 181.43, 168.55, 138.87, 135.74 (br), 131.16, 130.05 (br), 128.97, 126.77, 53.39, 17.70 ppm.

HRMS [FAB+]: $[M–H]^+$ calcd for $C_{11}H_9D_6O_2$ 217.1347; found 217.1322

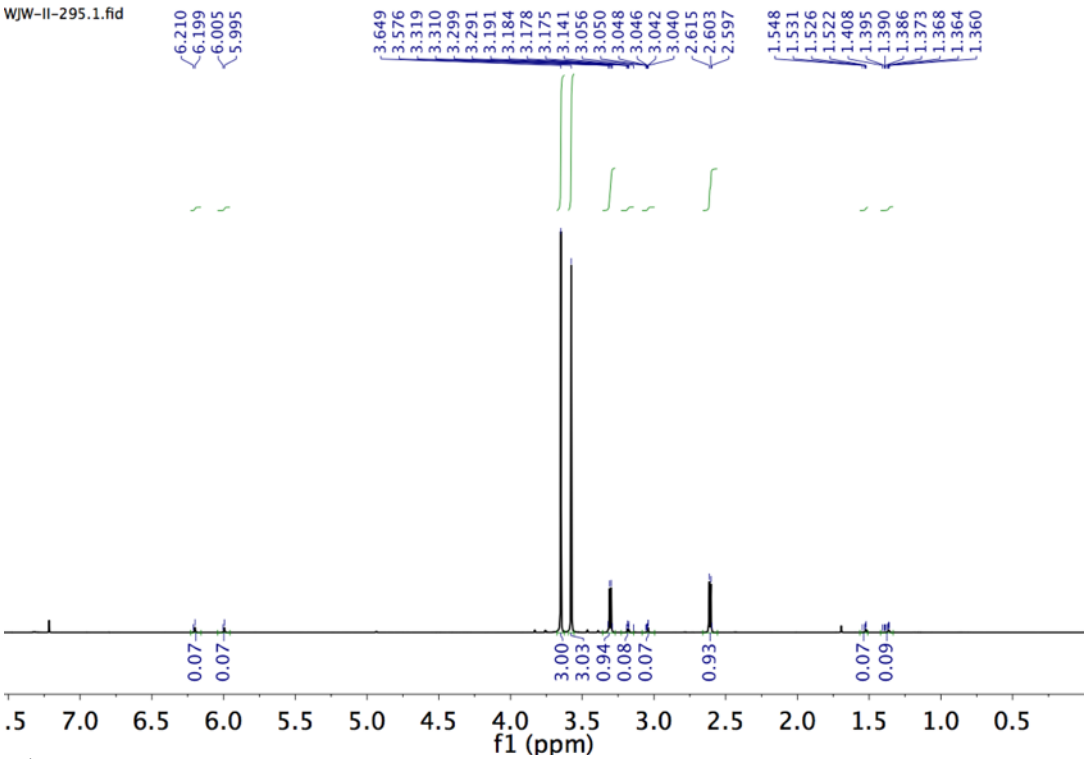

Figure S2. ^{1}H NMR spectrum of *dx*-DME-d_6 showing 93% D incorporation.

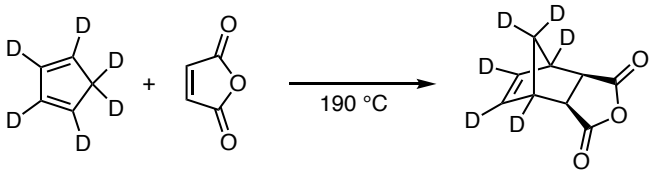

Cyclopentadiene-d_6 (19.0 g, 263 mmol, 1 equiv) was added to a 250 mL round bottom flask equipped with a magnetic stirbar and cooled to 0 °C. Maleic anhydride (25.8 g, 263 mmol, 1 equiv) was added slowly portionwise (caution: potential exotherm). The flask was fitted with a water cooled condenser and the reaction mixture was heated to 190 °C under Ar for 6 h to isomerize *endo* carbic anhydride to the *exo* isomer. The reaction mixture was cooled to 120 °C and toluene (40 mL) was added. The reaction mixture was cooled to ambient temperature to induce crystallization. The crystals were isolated by filtration and purified by flash chromatography (SiO_2, 20% EtOAc in hexanes, $R_f = 0.35$) to give a white solid. The isomeric purity was determined by comparing the chemical shift of the protons at the 2,3 position of the norbornene (2.9 ppm) to those of the protio analogue (2.9 ppm) as shown in Figure S3.

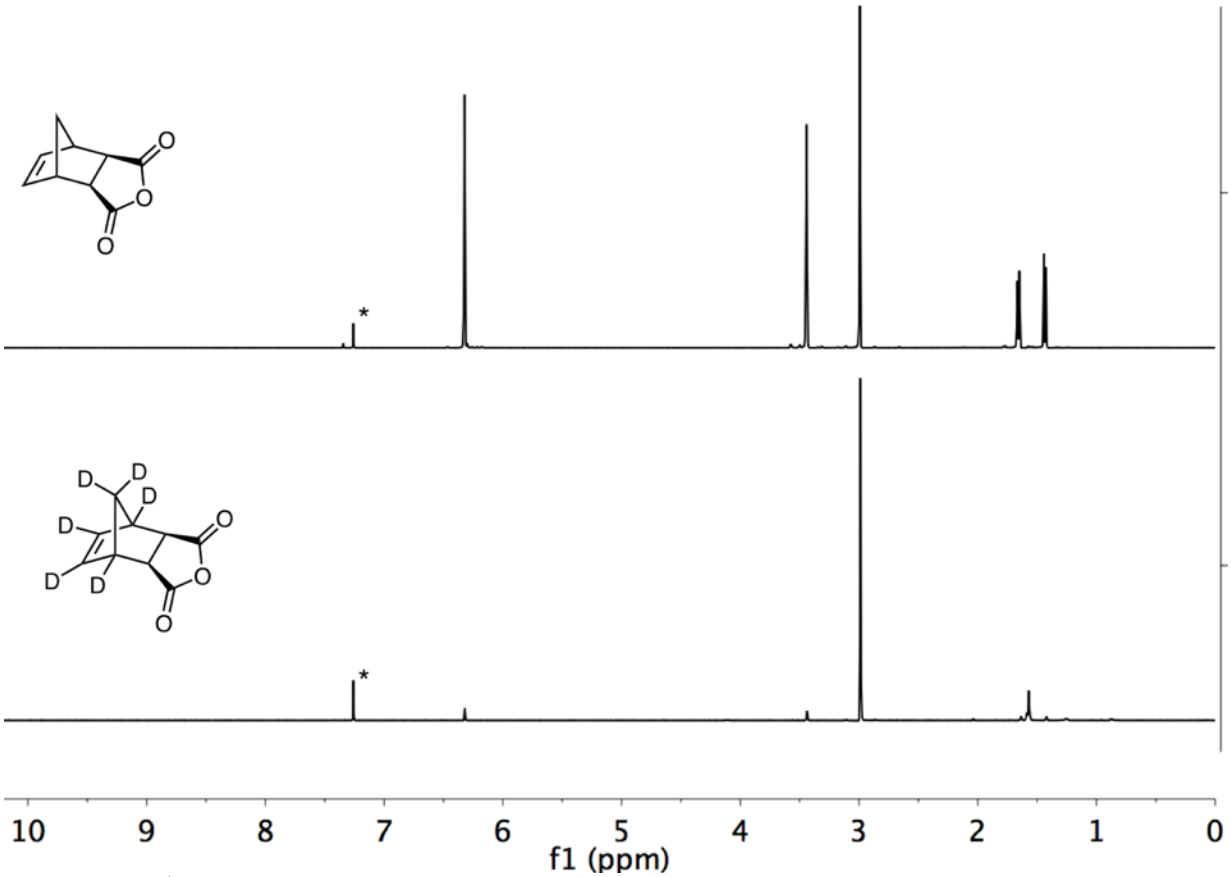

Figure S3. ^{1}H NMR spectra of carbic anhydride (top) and carbic anhydride-d_6 (bottom) showing deuterium incorporation. Residual $CHCl_3$ indicated by *.

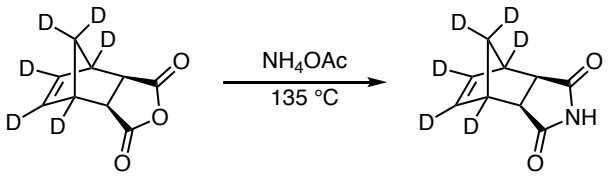

exo-Carbic anhydride-d_6 (2.3 g, 13.5 mmol, 1 equiv) and NH_4OAc (5.2 g, 67.5 mmol, 5 equiv) were combined in a 50 mL round bottom flask and heated to 135 °C for 15 h. The reaction mixture was cooled to ambient temperature and EtOAc (50 mL) and water (30 mL) were added. The organic layer was separated and washed with water (20 mL), sat. aq. $NaHCO_3$ (2 x 20 mL), and brine (20 mL), dried over $MgSO_4$, filtered, and concentrated to a white solid (2.28 g, quantitative yield).

^{1}H NMR (600 MHz, $CDCl_3$) δ 8.30 (br s, 1H), 2.72 (s, 2H) ppm.

^{2}H NMR (61 MHz, $CDCl_3$) δ 6.34 (s, 2D), 3.30 (s, 2D), 1.56, 1.48 (overlapping s, 2D) ppm.

^{13}C NMR (101 MHz, $CDCl_3$) δ 178.30, 137.39 (t, $J_{C\text{-}D}$ =), 49.24, 45.06, 44.77, 44.54 ppm.

HRMS [EI+]: $[M+H]^+$ calcd for $C_9H_4D_6NO_2$ 170.1088; found 170.1084.

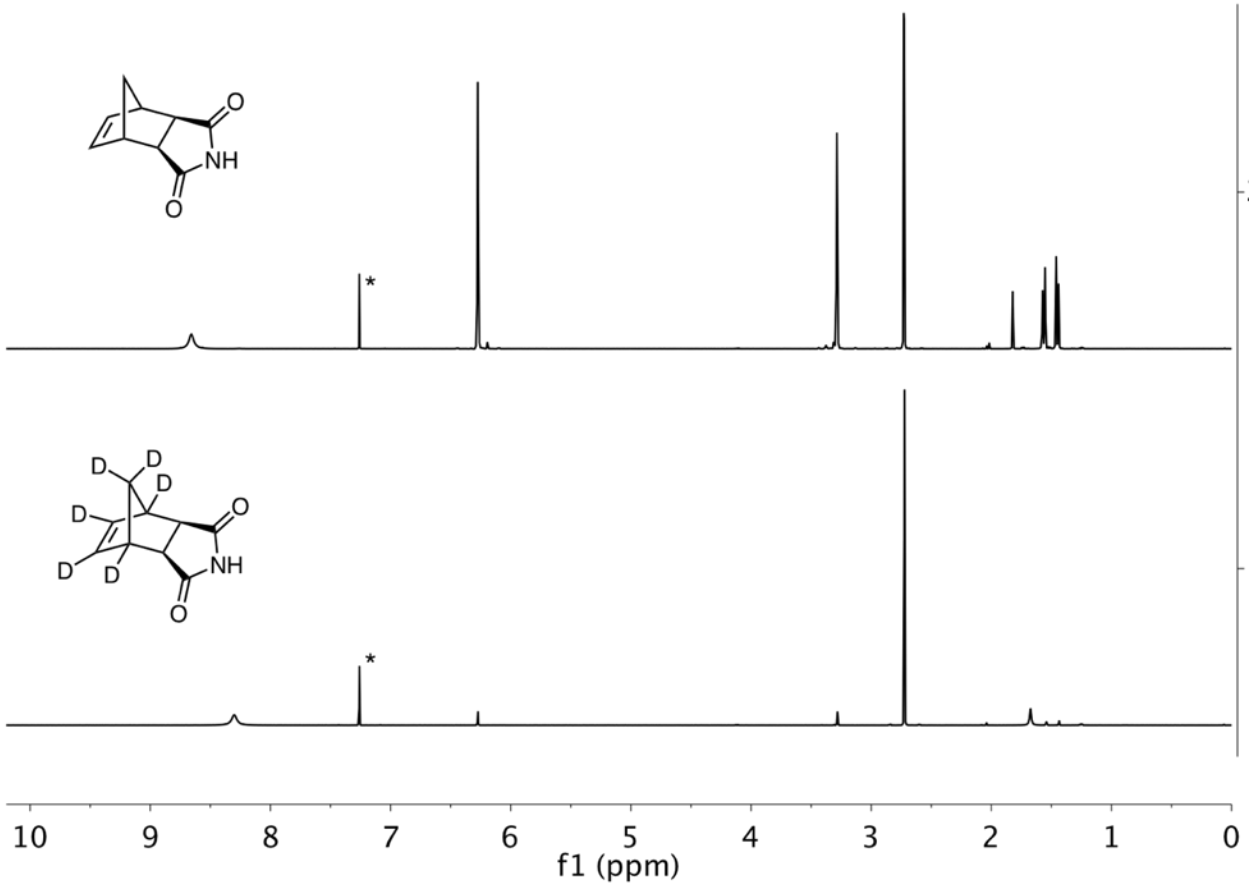

Figure S4. ^{1}H NMR of *xx*-NHI (top) and *xx*-NHI (bottom). Residual $CHCl_3$ indicated by *.

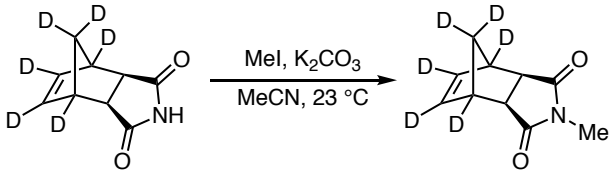

To a 100 mL round bottom flask equipped with a magnetic stirbar was added ***xx*-NHI** (2.28 g, 13.5 mmol, 1 equiv), K_2CO_3 (3.7 g, 27 mmol, 2 equiv) and MeCN (45 mL). MeI (1.7 mL, 27 mmol, 2 equiv) was added via syringe, a reflux condenser was attached, and the reaction mixture was rapidly stirred for 20 h. MeCN was removed *in vacuo* and the residue was extracted with EtOAc (50 mL) and water (25 mL). The organic layer was separated and washed with water (25 mL) and brine (15 mL), dried over $MgSO_4$, filtered and concentrated. Flash chromatography (SiO_2, 20% EtOAc in hexanes, $R_f = 0.2$) gave the desired compound as a white solid (1.6 g, 65%).

^{1}H NMR (600 MHz, $CDCl_3$) δ 2.95 (s, 3H), 2.67 (s, 2H) ppm.

^{2}H NMR (61 MHz, $CDCl_3$) δ 6.31 (s, 2D), 3.26 (s, 2D), 1.48 (s, 1D), 1.16 (s, 1D) ppm.

^{13}C NMR (101 MHz, $CDCl_3$) δ 178.25, 137.28 (t, J_{CD} = 27 Hz), 47.92, 44.93–44.41 (m), 42.68–41.75 (m), 24.66 ppm.

HRMS [EI+]: $[M+Na]^+$ calcd for $C_{10}H_5D_6NO_2Na$ 206.1064; found 206.1053.

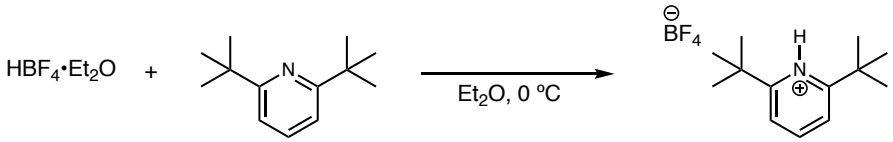

To a 20 mL scintillation vial equipped with a magnetic stirbar was added 2,6-di-*tert*-butylpyridine (1.15 mL, 5.22 mmol, 1.00 equiv.) and Et_2O (10 mL). The solution was cooled to 0 ºC and HBF_4•Et_2O (710 µL, 5.22 mmol, 1.00 equiv) was added dropwise with rapid stirring. A white precipitate formed, and the reaction mixture was rapidly stirred for 10 min. The precipitate was isolated by filtration, washed with Et_2O (3 x 10 mL) and dried *in vacuo* to give a white solid (1.30 g, 89%).

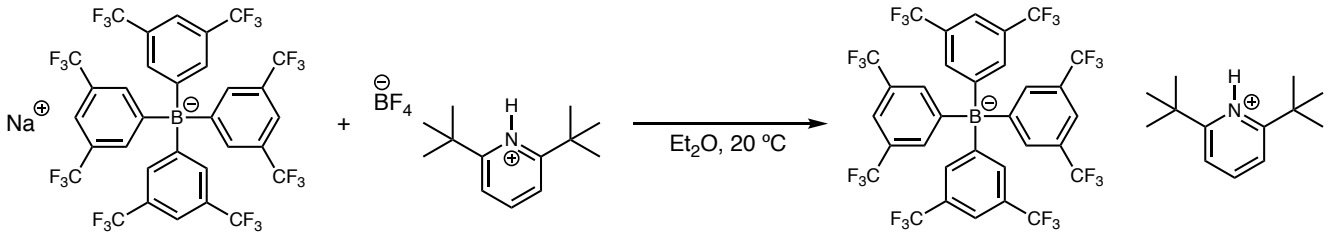

In the glovebox, a 4 mL vial was equipped with a magnetic stirbar and charged with 2,6-di-*tert*-butylpyridinium tetrafluoroborate (50 mg, 0.18 mmol, 1.0 equiv.) and Et_2O (2 mL). To this mixture was added a solution of $NaBArF_{24}$ (158 mg, 0.18 mmol, 1 equiv.) in Et_2O (1 mL) via pipette. The resulting reaction mixture was sealed with a screw cap and rapidly stirred for 5 h. The reaction mixture was then filtered through a 0.45 µM PTFE syringe filter and concentrated *in vacuo* to give a white solid (160 mg, 84%).

^{1}H NMR (400 MHz, CD_2Cl_2) δ 10.92 (t, J = 56.2 Hz, 1H), 8.44 (t, J = 8.1 Hz, 1H), 7.83 (d, J = 8.2 Hz, 2H), 7.73 (s, 8H), 7.57 (s, 4H), 1.54 (s, 18H) ppm.

^{19}F NMR (376 MHz, CD_2Cl_2) δ –62.85 ppm.

^{13}C NMR (126 MHz, CD_2Cl_2) δ 163.47, 161.72 (q, $J_{C–B}$ = 50 Hz) , 148.28, 134.77, 129.01, 128.99, 128.96, 128.94, 128.76, 128.73, 128.71, 128.69, 124.57 (q, $J_{C–F}$ = 272 Hz) 122.77, 117.48, 36.91, 28.60 ppm.

General procedures for kinetic measurements

All ROMP reactions were performed in oven-dried glassware using dry and degassed solvents inside an Ar filled glovebox or using standard NMR techniques at 25±0.5 °C. We observed rate constants that were consistent when measured by *in situ* NMR spectroscopy or by aliquots taken from a batch reaction.

Quenching vials were prepared by charging GC vials (Agilent 5183-2068) with 1 mL of a solution of ethyl vinyl ether in $CDCl_3$ or THF (10% v:v). For reactive monomers, the addition of Silicycle SilaMet® S dimercaptotriazine Ru scavenger (5–10 mg per vial) was necessary to sequester Ru species. These quenching vials were tightly sealed with screw top septum vials. Batch reaction were performed in 4 mL vials equipped with a magnetic stir bars. A 4 mL vial was charged with the appropriate monomer, dissolved in CH_2Cl_2 to give a 0.05 M solution and sealed with a screw top septum. In a separate vial sealed with a screw top septum, the Ru catalyst was dissolved in CH_2Cl_2. An appropriate amount of the catalyst solution was then quickly added to the rapidly stirred monomer solution using a gas-tight microsyringe. Aliquots of the reaction mixture were taken at regular intervals and rapidly injected into the quenching vials. Once the reaction was complete, the quenching vials were removed from the glovebox and submitted directly for ^{1}H NMR analysis ($CDCl_3$ solutions) or for GPC analysis (THF solutions). The THF solutions can be dried in vacuo and submitted for subsequent ^{1}H NMR analysis. The consumption of the norbornene monomer was measured by integrating the resonance at δ 6.3 ppm against the ^{13}C satellite peaks from the DCM solvent used for the ROMP.

Rate behavior was also monitored by NMR using a Varian 600 MHz spectrometer equipped with a with 5 mm penta inverse probe. In the glovebox, solutions of norbornene monomer (0.05 M, CD_2Cl_2) were prepared using calibrated glassware. Oven dried 5 mm NMR tubes was charged with 0.5 mL of this stock solution, sealed with a rubber septum and secured using vinyl tape. The tubes were removed from the glovebox and inserted into the spectrometer that was equilibrated to the desired temperature. The spectrometer was locked onto the deuterated solvent and shimmed to the sample, and then the sample was removed and the appropriate catalyst solution (20 μL) was injected via microsyringe. The tube was quickly inverted to mix and then transferred to the spectrometer where an automated acquisition was used to collect ^{1}H spectra (1 scan) at regular intervals.

Low Temperature NMR studies

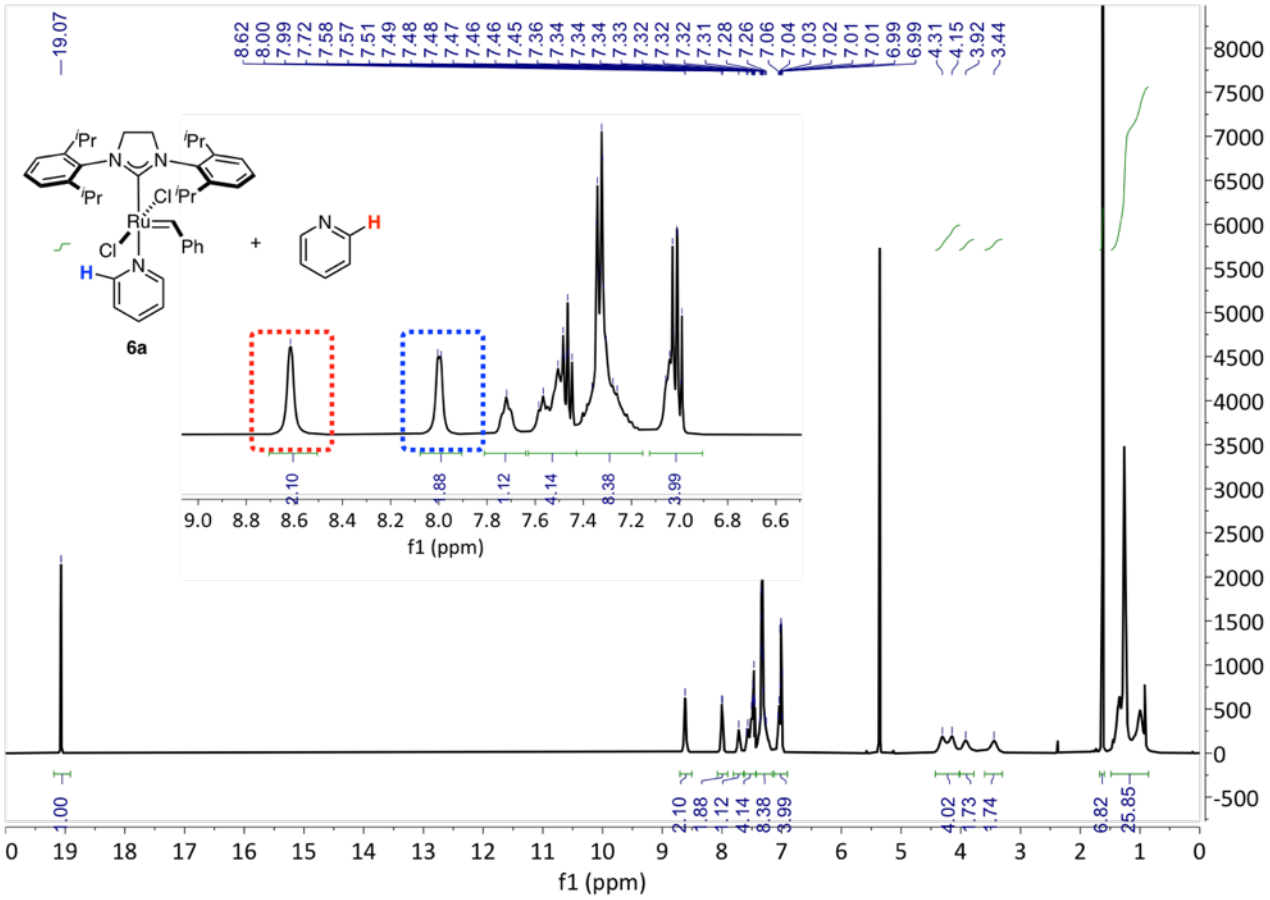

Figure S5. ^{1}H NMR spectrum of **6** in solution showing the free and bound pyridine ligands. The exchange of these signals was monitored by EXSY. The benzylidene resonance at 19.07 ppm was used to monitor the formation of the 6-coordinate complex.

Measuring K_1 for 6

In the glovebox, a 5 mm screw top NMR tube was charged with 6 mg (7 umol) of **6**. The tube was sealed with a Teflon lined screw top septum, removed from the box, and cooled to –78 ºC in a dry ice/acetone bath. To the NMR tube was added $CDCl_2F$ (0.52 mL, 0.014 M solution) via syringe (after the NMR experiment, the volume of the solvent was double checked by marking the level with a grease pencil and filling the empty tube to the mark with a calibrated syringe). The NMR tube was then transferred to the precooled NMR (–80 ºC) spectrometer and a series of ^{1}H NMR spectra were recorded at a number of temperatures. The benzylidene resonance for both **6** and **6a** were integrated and a Van't Hoff plot was constructed to determine K_1.

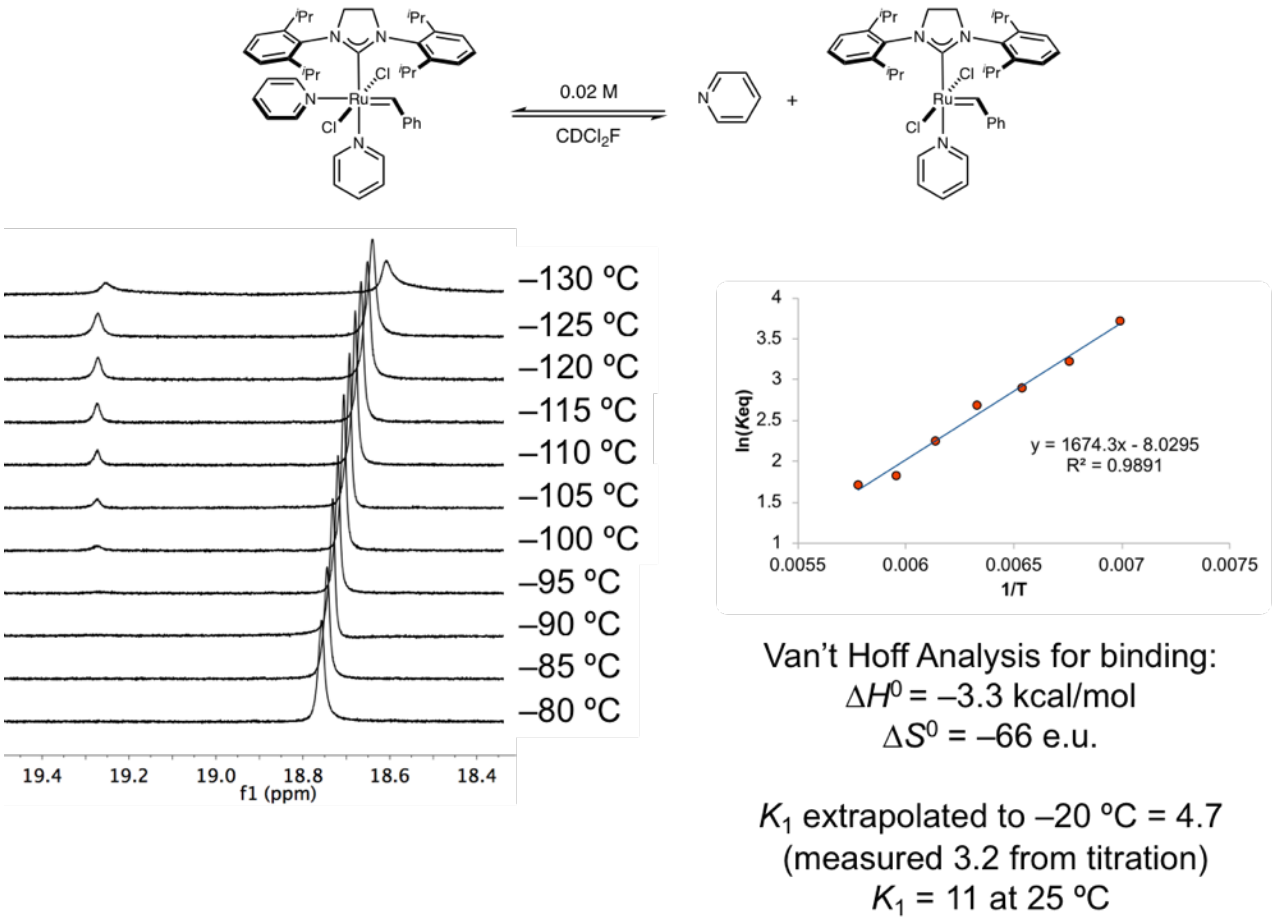

Figure S6. ^{1}H NMR array of **6** in $CDCl_2F$ solution showing the formation of the bis pyridine species at low temperature and the Van't Hoff plot and thermodynamic parameters for the dissociation of pyridine from **6**.

NMR titration of 6

Solution 1 was prepared by dissolving 14.5 mg of **6a** in CD_2Cl_2 (3.00 mL). 700 uL of this solution was transferred to a screw top NMR tube and sealed with a screw top septum. A second solution was prepared by adding 2.00 mL of solution 1 to 290 mg of pyridine to create solution 2. The NMR tube was inserted into the precooled (–20 °C) NMR tube and aliquots of solution 2 were added according to the volumes outlined in Table S1. The benzylidene shift was plotted against [pyridine] and fit according to

Table S1. NMR titration of **6a** with pyridine in CD_2Cl_2.

Compound(mg)	14.5	Anion(mg)	290	Final (eq)	277.55	
MW	731.81	MW	79.1			
volume(uL)	3000	volume(uL)	2000			
M	0.006604629	M	1.83E+00			
in tube(uL)	700					
number	add(ul)	add sum (ul)	sum	receptor(M)	Anion(M)	Anion/Receptor (eq)
No.0	0	0	700	6.60E-03	0.00E+00	0.00
No.1	5	5	705	6.60E-03	1.30E-02	1.97
No.2	5	10	710	6.60E-03	2.58E-02	3.91
No.3	5	15	715	6.60E-03	3.85E-02	5.82
No.4	5	20	720	6.60E-03	5.09E-02	7.71
No.5	10	30	730	6.60E-03	7.53E-02	11.41
No.6	15	45	745	6.60E-03	1.11E-01	16.76
No.7	20	65	765	6.60E-03	1.56E-01	23.58
No.8	30	95	795	6.60E-03	2.19E-01	33.17
No.9	50	145	845	6.60E-03	3.15E-01	47.63
No.10	80	225	925	6.60E-03	4.46E-01	67.51
No.11	150	375	1075	6.60E-03	6.39E-01	96.82
No.12	250	625	1325	6.60E-03	8.65E-01	130.92
No.13	400	1025	1725	6.60E-03	1.09E+00	164.92
No.14	700	1725	2425	6.60E-03	1.30E+00	197.43

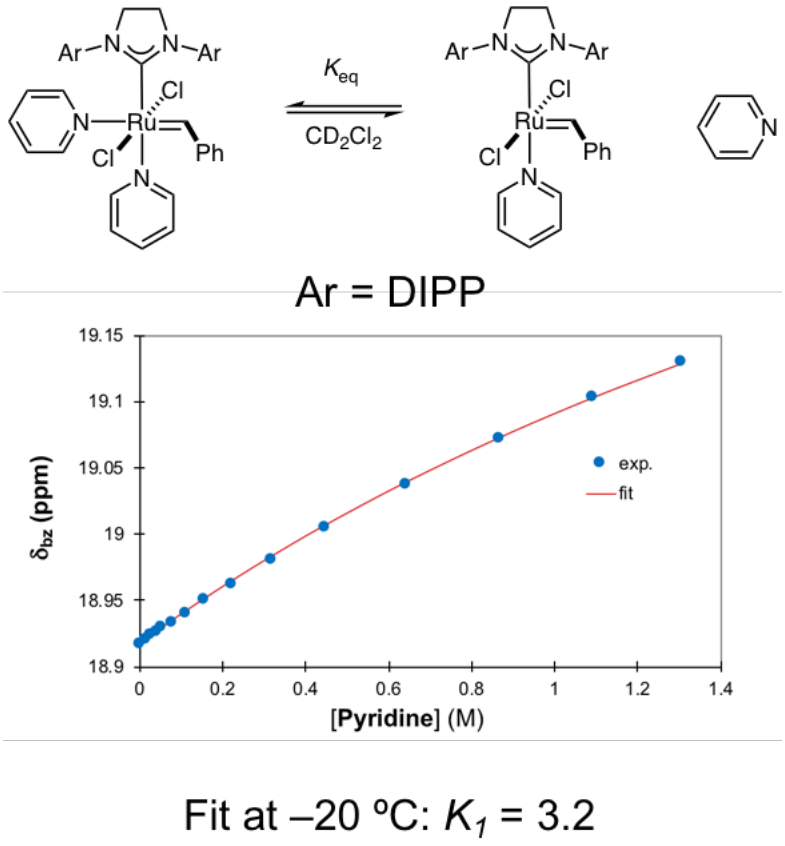

Figure S7. ^{1}H NMR titration for **6a** at –20 °C showing the best fit for K = 3.2.

Exchange Spectroscopy

A 0.02 M solution of each Ru complex was prepared in CD_2Cl_2 and added to a 5 mm NMR tube under a nitrogen atmosphere. The NMR samples were placed the thermally equilibrated NMR probe and ^1H–^1H NOESY spectra were recorded. For each temperature, two spectra were collected: one with 0 ms mixing time and one with 500 ms mixing time. Rates of exchange were calculated using the EXSYCALC program.

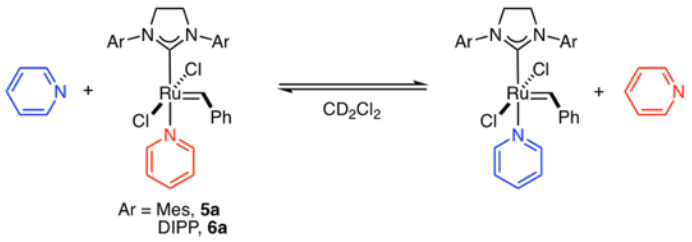

associative

rate = k_1[**5a**][py]

$\frac{k'}{[py]} = k_1$

dissociative

rate = k_1[**5a**]

$k' = k_1$

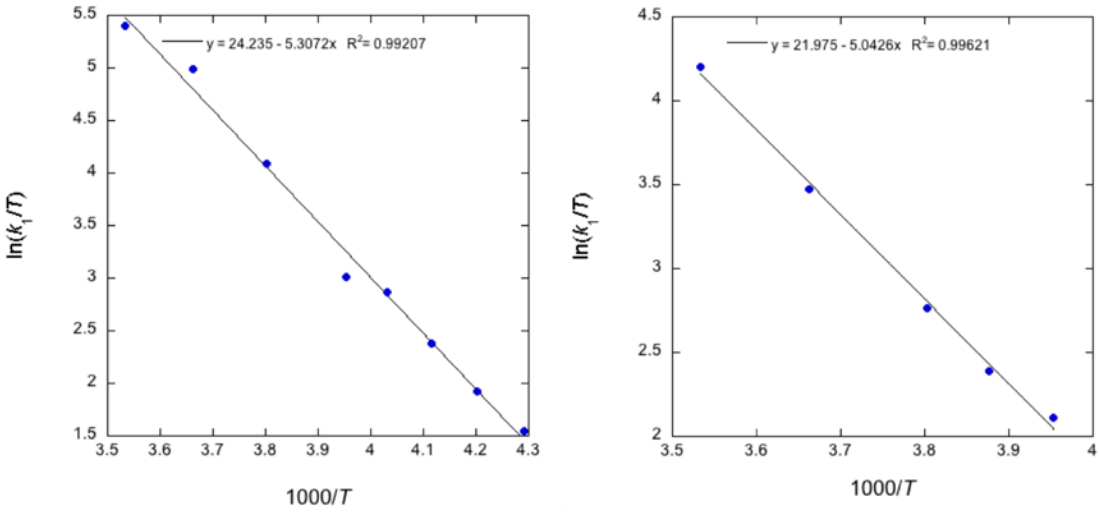

Figure S8. Degenerate pyridine exchange for **5** and **6** and the plots of Eyring plots for the second order exchange for **5** (left) and **6** (right).

A dissociative mechanism is assumed to be a first-order process for degenerate exchange ($k' = k_1$), while an associative mechanism is assumed to be a second-order process ($k'/[py] = k_1$). The EXSY experiments could not be conducted above 10 °C because the cross-peaks for exchange were non-zero at 0ms mixing time.

Table S2. Pyridine exchange rates measured for **5** and **6** by EXSY NMR, calculated using EXSYCALC.

5

°C	K	1000/T (K^{-1})	k' (s^{-1})	k_1 ($M^{-1}s^{-1}$)	ln(k'/T)	ln(k_1/T)
-40	233	4.29	0.103	4.68	-7.72	1.54
-35	238	4.20	0.151	6.84	-7.37	1.92
-30	243	4.12	0.238	10.8	-6.93	2.38
-25	248	4.03	0.388	17.6	-6.46	2.87
-20	253	3.95	0.450	20.4	-6.33	3.02
-10	263	3.80	1.31	59.7	-5.30	4.09
0	273	3.66	3.22	146	-4.44	4.99
10	283	3.53	4.88	222	-4.06	5.40
0[a]	283	3.66	3.90			

[a]Frequency of exchange measured with 2 equivalents of pyridine relative to **5a** ([py]:[Ru] = 3:1)

6

°C	K	1000/T (K^{-1})	k' (s^{-1})	k_1 ($M^{-1}s^{-1}$)	ln(k'/T)	ln(k_1/T)
-20	253	3.95	0.182	8.27	-7.24	2.11
-15	258	3.88	0.240	10.9	-6.98	2.39
-10	263	3.80	0.348	15.8	-6.63	2.76
0	273	3.66	0.710	32.3	-5.95	3.47
10	283	3.53	1.47	66.7	-5.26	4.20
0[a]	283	3.66	0.722			

[a]Frequency of exchange measured with 2 equivalents of pyridine relative to **6a** ([py]:[Ru] = 3:1)

Plots of 1000/T against ln(k'/T) are linear, but lead to large, negative entropies of activation, which are inconsistent with a dissociative exchange mechanism. Plots of 1000/T against ln(k_1/T) are also linear and provide smaller entropies of activation which are more consistent with an associative interchange type of mechanism.

	5	**6**
$\Delta H^{\ddagger}$	10.5±0.4 kcal/mol	10.0±0.4 kcal/mol
$\Delta S^{\ddagger}$	4±6 J/mol K	–15±6 J/mol K

The addition of one additional equivalent of pyridine to **5** or **6** does not lead to an increase in the frequency of exchange, though the rate of exchange does increase.

$(0.710\ s^{-1})(0.022\ M\ Py) = 0.015\ M/s$
$(0.722\ s^{-1})(0.033\ M\ Py) = 0.023\ M/s$

Measuring K2

A 5 mm NMR tube was charged with a solution of **5a** or **6a** in CD_2Cl_2 and fitted with a rubber septum and secured with vinyl tape. A 4 mL vial was charged with BPh_3 and CD_2Cl_2 and secured with a screw top septum. The NMR tube was cooled to –78 °C in a dry ice/acetone bath and the solution of BPh_3 was added via microsyringe (final [Ru] = 0.02 M). The tube was quickly inserted into the NMR probe and ^1H NMR spectra were recorded.

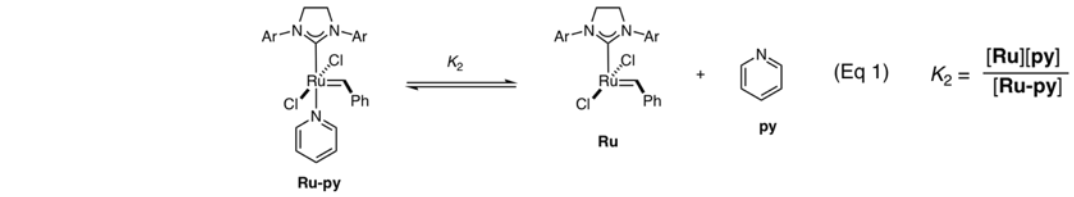

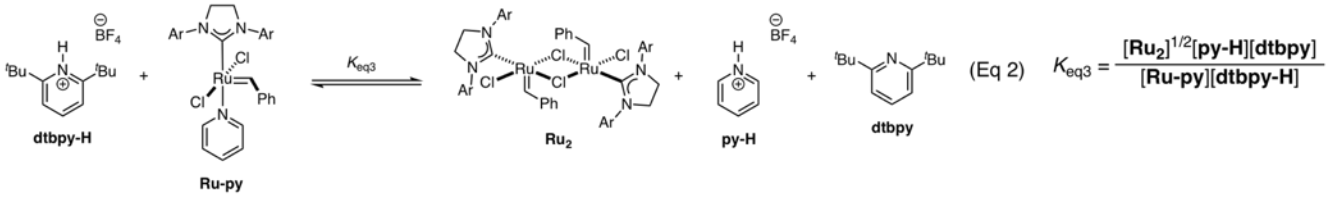

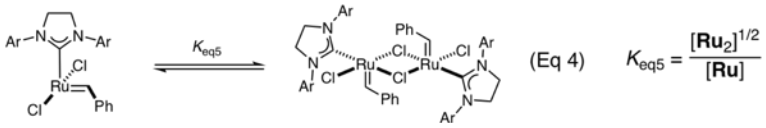

$$K_2 = \frac{[Ru][py]}{[Ru\text{-}py]} = \frac{[Ru_2]^{1/2}[py\text{-}H][dtbpy]}{[Ru\text{-}py][dtbpy\text{-}H]} \cdot \frac{[dtbpy\text{-}H][py]}{[py\text{-}H][dtbpy]} \cdot \frac{[Ru]}{[Ru_2]^{1/2}}$$

$$= K_{eq3} \cdot 1/K_{eq4} \cdot 1/K_{eq5}$$

$K_{eq4} = 10^{-(pKa-pKb)} = 10^{-(0.81-3.45)} = 10^{2.36} = 436$

pK_a of (2,6-di-*tert*-butylpyridinium)tetrafluoroborate in DMSO from *Can. J. Chem.* **1988**, *66*, 1159.[11]

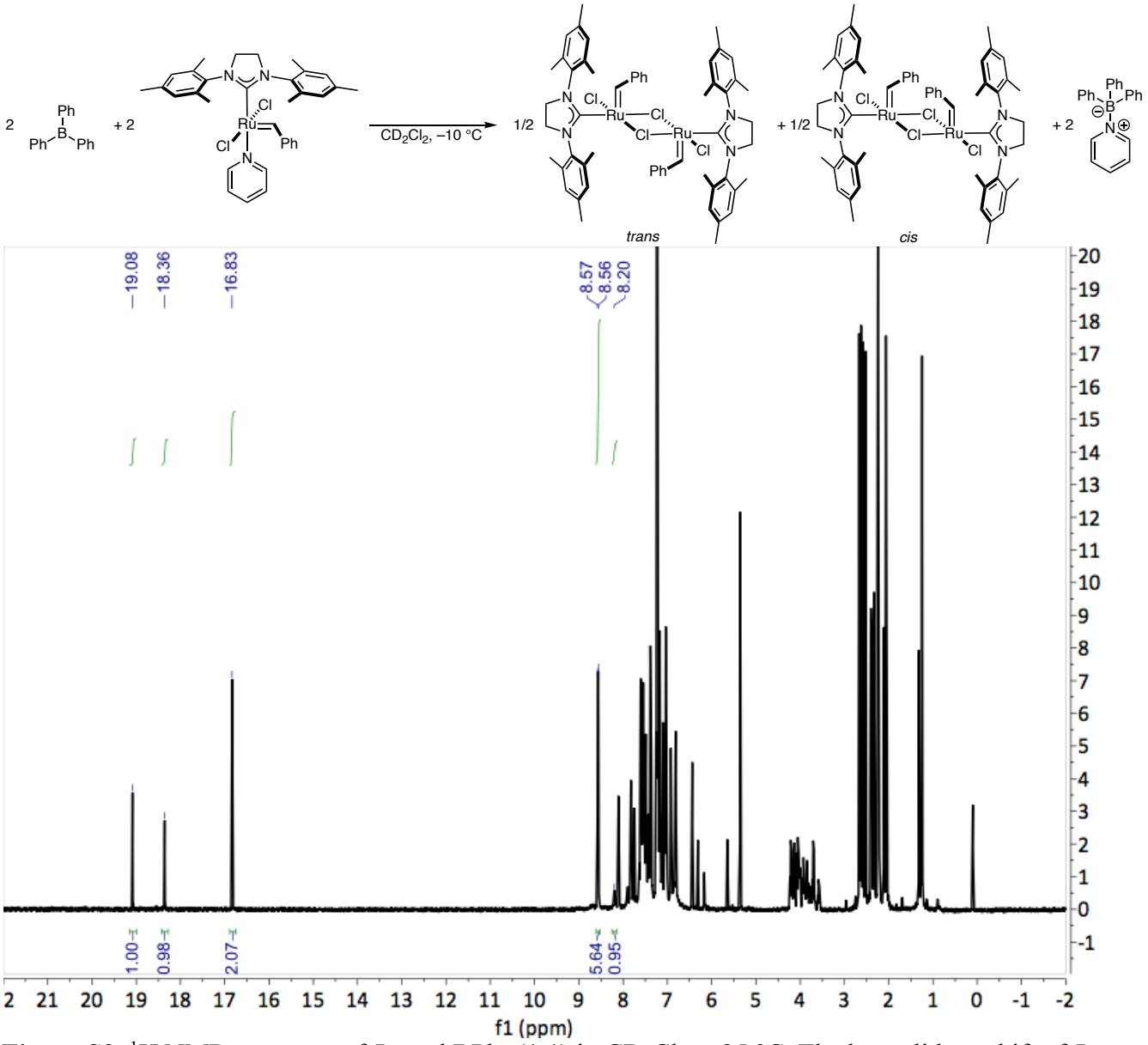

Figure S9. ^{1}H NMR spectrum of **5a** and BPh_3 (1:1) in CD_2Cl_2 at 25 °C. The benzylidene shift of **5a** appears at 19.08 ppm and the dimeric species appear at 18.36 and 16.83 ppm.

BPh_3 trap:

$$K_{eq3} = \frac{(0.015)^{\frac{1}{2}}(0.015)}{(0.005)(0.005)} = 74$$

$$\frac{K_{eq3}}{K_4 K_5} = \frac{74}{(10^7)(100)} = 7 \times 10^{-8}$$

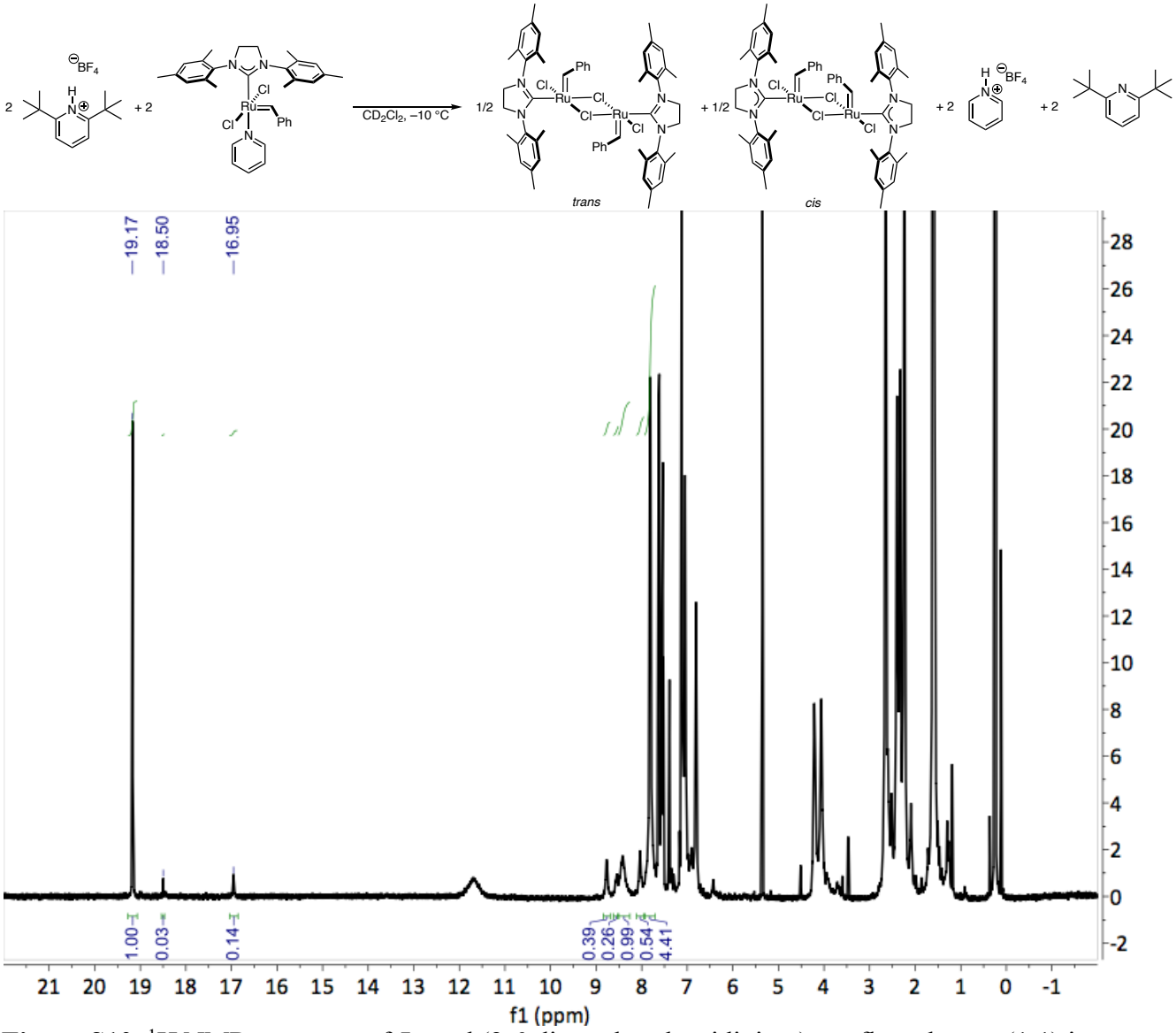

Figure S10. ^{1}H NMR spectrum of **5a** and (2,6-di-*tert*-butylpyridinium)tetrafluoroborate (1:1) in CD_2Cl_2 at 25 °C. The benzylidene shift of **5a** appears at 19.08 ppm and the dimeric species appear at 18.36 and 16.83 ppm

Pyridinium trap:

$$K_{eq3} = \frac{(0.0029)^{\frac{1}{2}}(0.0029)(0.0029)}{(0.0171)(0.0171)} = 0.0016$$

$$\frac{K_{eq3}}{K_4 K_5} = \frac{0.0016}{(438)(100)} = 3 \times 10^{-8}$$

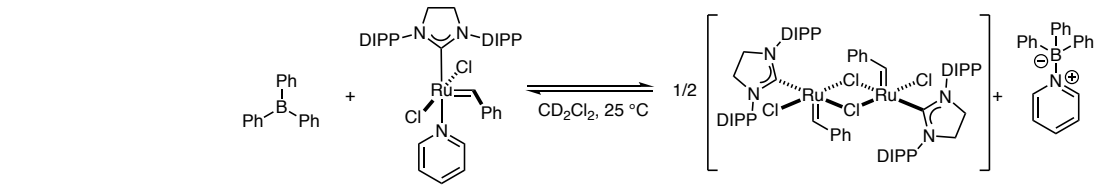

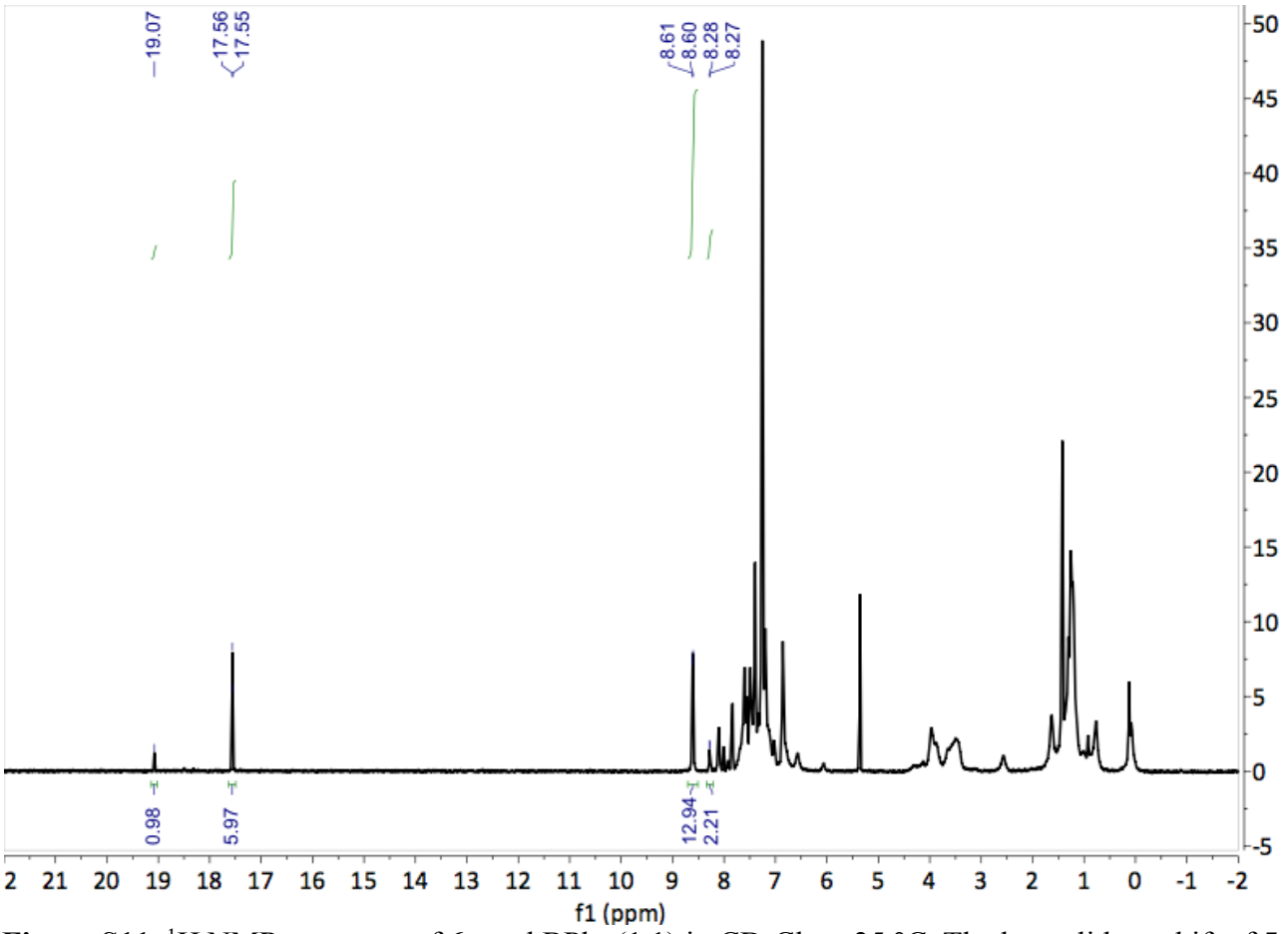

Figure S11. ^{1}H NMR spectrum of **6a** and BPh_3 (1:1) in CD_2Cl_2 at 25 °C. The benzylidene shift of **5a** appears at 19.07 ppm and the dimeric species appears at 17.55 ppm.

BPh_3 trap:

$$K_{eq3} = \frac{(0.017)^{\frac{1}{2}}(0.017)}{(0.0029)(0.0029)} = 275$$

$$\frac{K_{eq3}}{K_4 K_5} = \frac{275}{(10^7)(100)} = 2.7 \times 10^{-7}$$

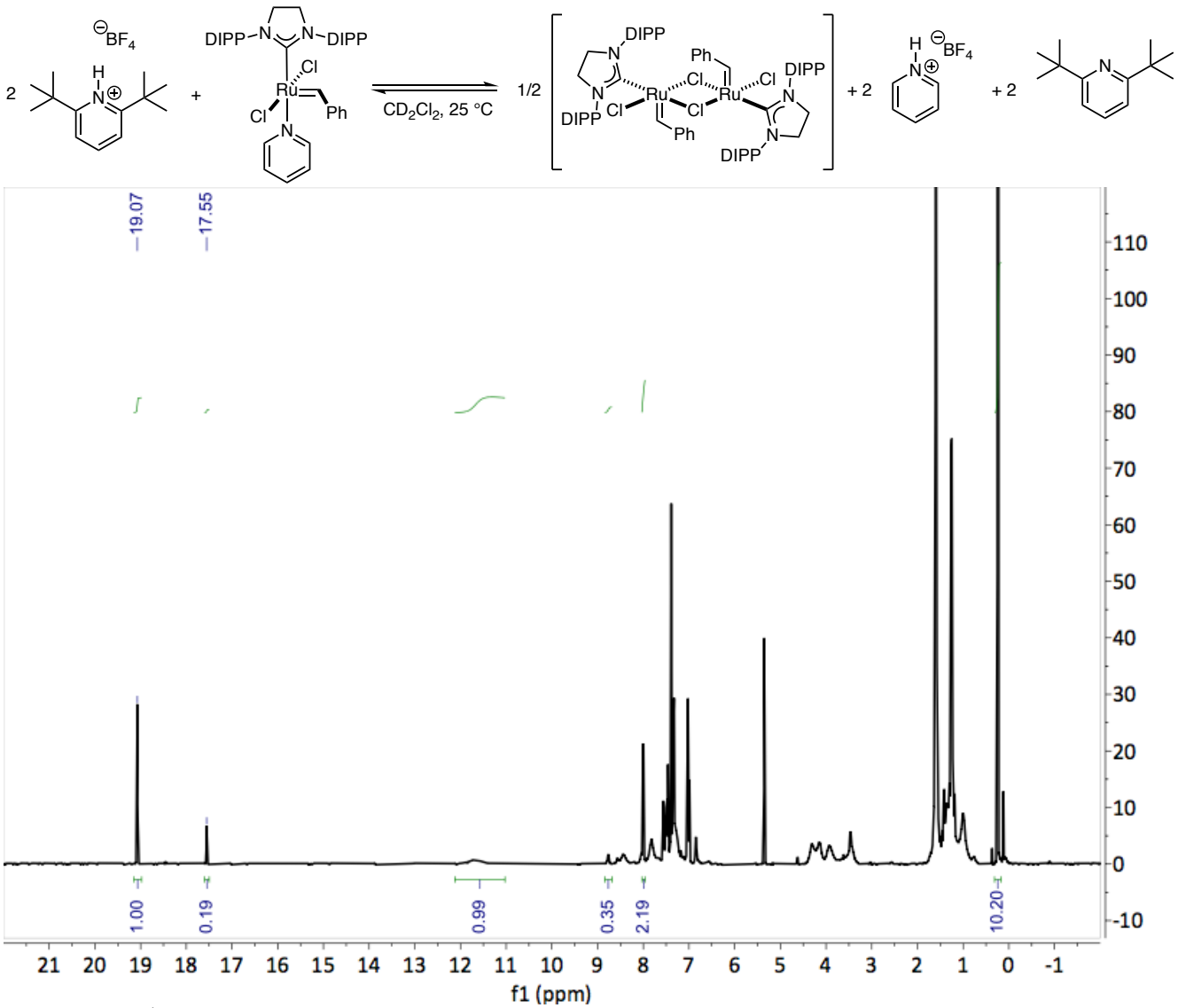

Figure S12. ^{1}H NMR spectrum of **6a** and (2,6-di-*tert*-butylpyridinium)tetrafluoroborate (1:1) in CD_2Cl_2 at 25 °C. The benzylidene shift of **6a** appears at 19.08 ppm and the dimeric species appear at 18.36 and 16.83 ppm

Pyridinium trap:

$$K_{eq3} = \frac{(0.003)^{\frac{1}{2}}(0.003)(0.003)}{(0.017)(0.017)} = 0.00232$$

$$\frac{K_{eq3}}{K_4 K_5} = \frac{0.0232}{(438)(100)} = 5 \times 10^{-8}$$

The structure of the dimeric Ru complexes was assigned based on DOSY NMR, ESI mass spectrometry, and EXSY. EXSY at 20 °C showed exchange between the two dimers containing the SIMes ligand.

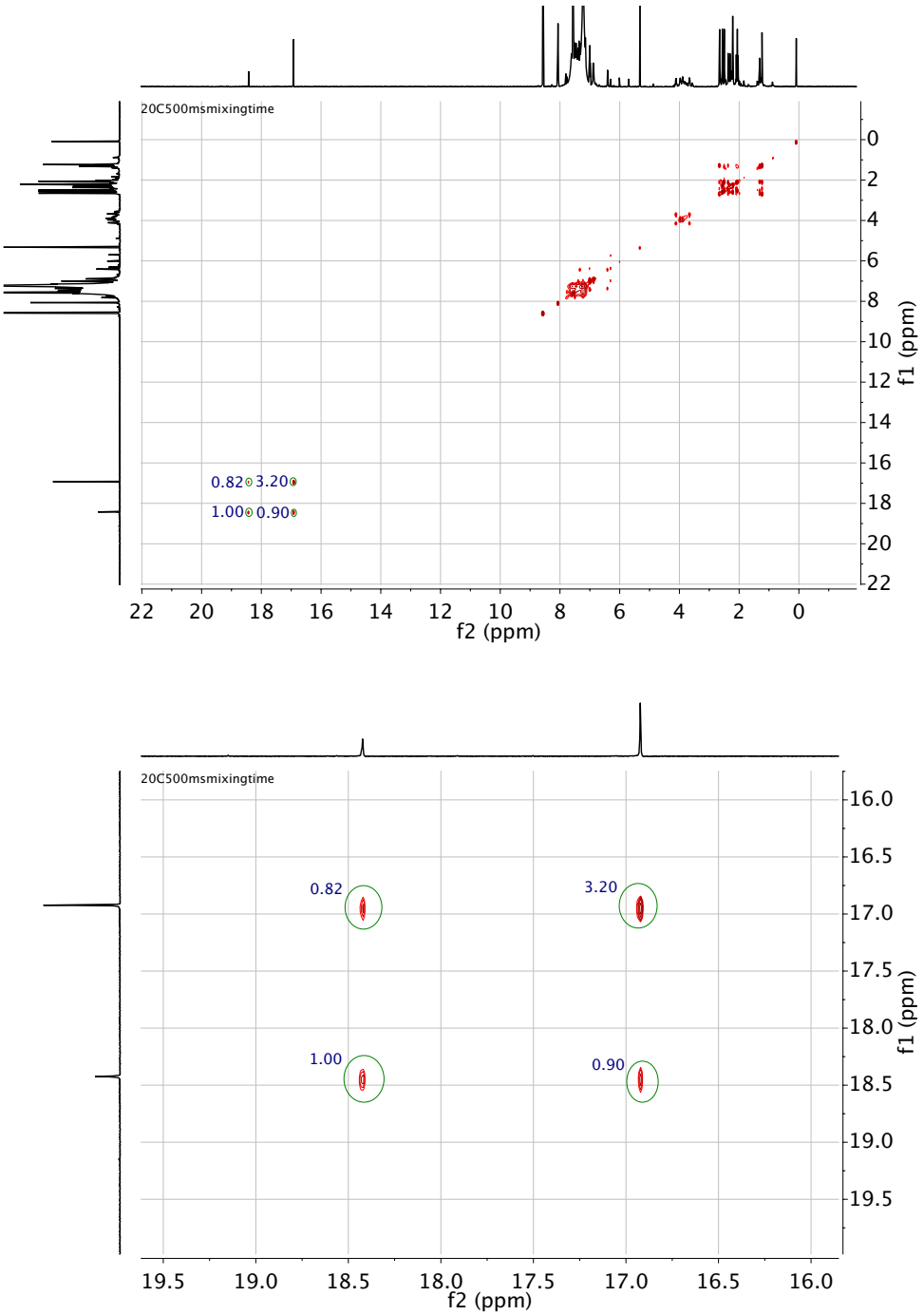

Figure S13. ^{1}H-^{1}H EXSY spectrum showing exchange between the two dimeric species generated from **5a** and BPh_3.

Diffusion constant measured for **5a** at –10 °C: 5.57 x 10^{-10} m^2/s
Diffusion constants measured for new species: 18.3 ppm: 4.35 x 10^{-10} m^2/s. 16.8 ppm: 4.52 x 10^{-10} m^2/s.

Diffusion constant measured for **6a** at –10 C:
Diffusion constants measured for new species: 17.5 ppm: 4.35 x 10^{-10} m^2/s. 16.8 ppm.

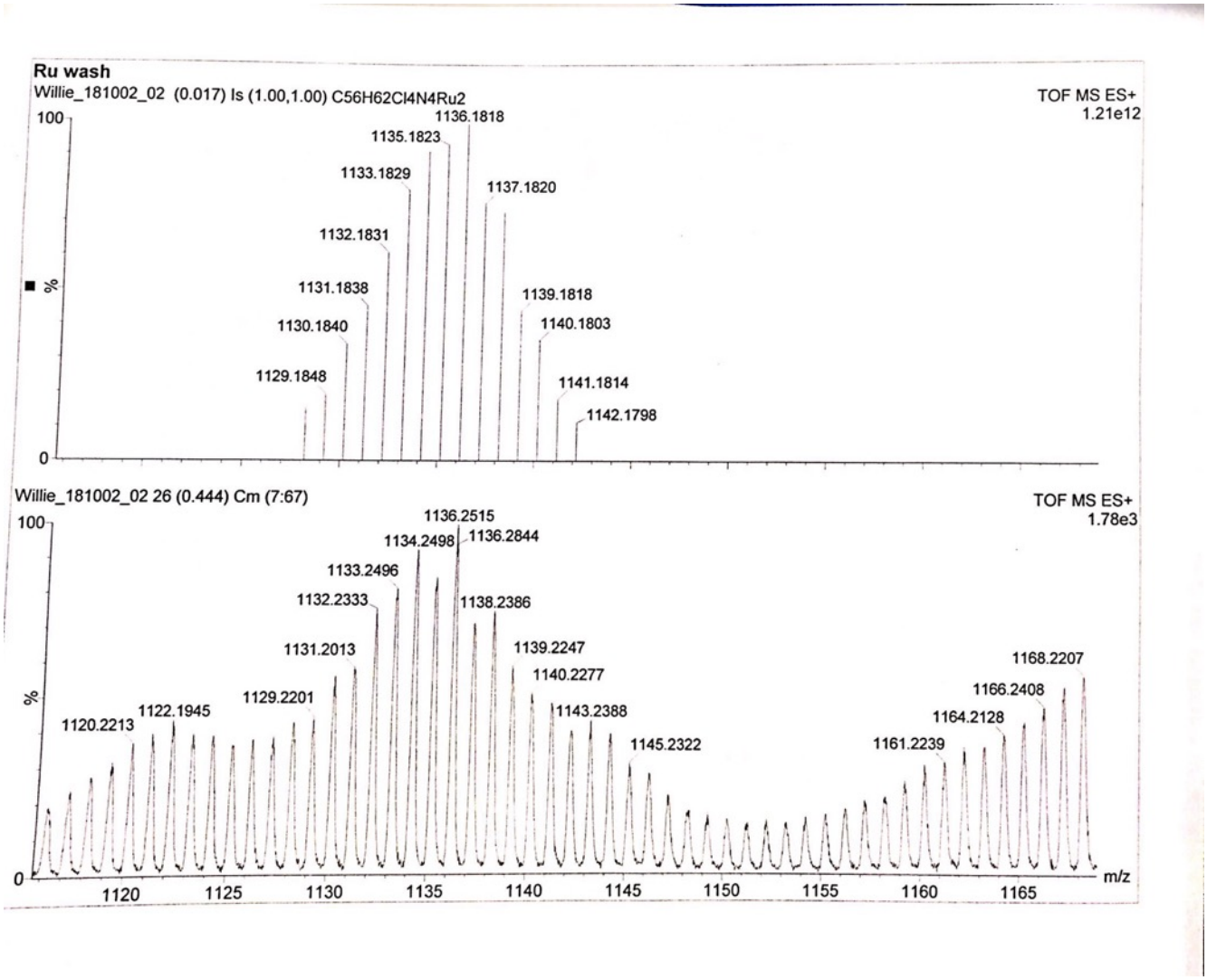

Figure S14. HRMS of the dimeric Ru species generated from **5a** and BPh_3. *m/z* calc'd for $C_{56}H_{62}Cl_4N_4Ru_2$ 1136.1818; found 1136.2515.

Kinetic Isotope Effects

The observed rate constants for each catalyst and each monomer are shown in Table S3. The rate constants and corresponding errors were calculated by linear regression of natural log plots of concentration vs time using the LINEST function in Microsoft Excel 2016.

The weighted average and variance of at least four separate experiments were calculated according to Eq 5 and 6[12] and are summarized in Table S3.

Table S3

	5	**6**
Isotopologue	k_{obs} (x 10^{-3} s^{-1})	k_{obs} (x 10^{-3} s^{-1})
DME-H_6	6.9(3)	1.62(5)
	7.3(5)	1.65(5)
	8.2(2)	1.71(8)
	9.4(9)	1.37(5)
	10.3(5)	1.52(6)
	8.0(3)	
	8.02±0.13	**1.56 ± 0.03**
DME-D_6	9.3(4)	1.8(2)
	9.9(8)	1.9(2)
	9.7(4)	2.21(5)
	8.4(6)	1.49(9)
	9.0(3)	2.26(8)
	8.9(6)	1.82(6)
	11.1(6)	1.72(6)
	10.3(3)	
	9.49±0.15	**1.93±0.03**
k_H/k_D	**0.85(2)**	**0.81(2)**

	5	**6**
Isotopologue	k_{obs} (x 10^{-3} s^{-1})	k_{obs} (x 10^{-3} s^{-1})
NMI-H_6	28.9(2)	19.6(6)
	28.6(2)	19.5(9)
	41.4(3)	21.6(4)
	26.5(4)	23.7(2)
		21.5(1)
		23.4(2)
Weighted Average	**28.5±0.01**	**22.1±0.01**
NMI-D_6	26.0(6)	26.8(6)
	25.1(6)	25.5(3)
	26.4(3)	24.0(2)
	28.9(4)	22.2(2)
		22.7(2)
Weighted Average	**26.9±0.02**	**23.4±0.01**
k_H/k_D	**1.06(2)**	**0.94(3)**

Weighted average:

$$\bar{x} = \frac{\sum x_i/\sigma_i^2}{\sum 1/\sigma_i^2} \qquad \text{Eq 5}$$

Variance:

$$\sigma_{\bar{x}}^2 = \frac{1}{\sum 1/\sigma_i^2} \qquad \text{Eq 6}$$

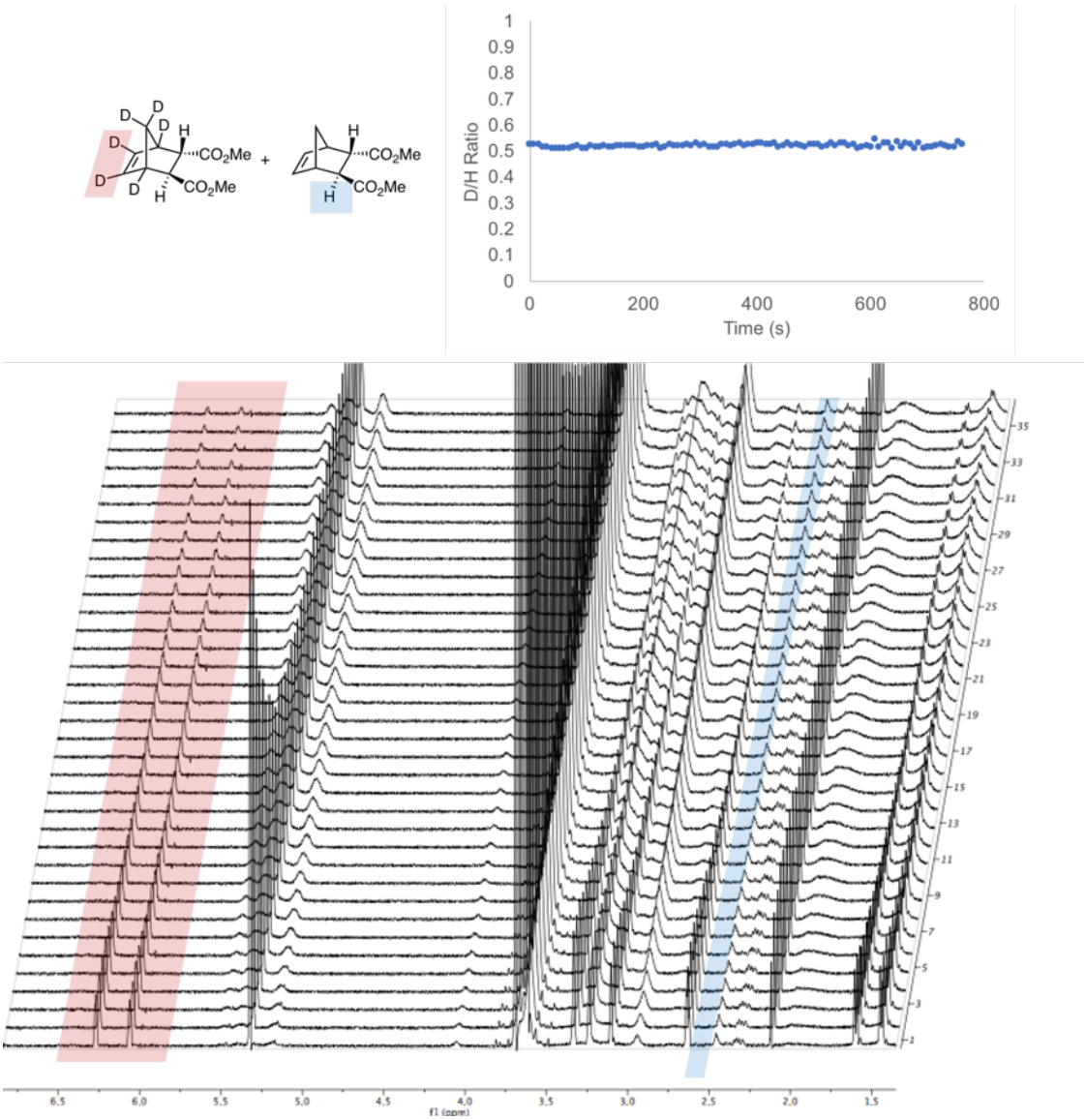

Figure S15. The ROMP of a 1:1 mixture of ***dx*-DME-H$_6$** and ***dx*-DME-D$_6$** shows that the H:D ratio is maintained throughout the course of the reaction. The proton α to the ester group is simultaneously monitored as a fully protiated internal standard.

NMR studies of the catalytic resting state

To a magnetically stirred solution of the norbonene monomer in CD_2Cl_2 (0.1 M) was added a solution of **5** (CD_2Cl_2, 0.04 M, 0.25 mL) in the glovebox at ambient temperature (final [Ru] = 0.02 M). The reaction mixture rapidly turned a dark brown color and was transferred to an NMR tube, sealed with a polyethylene cap, taken from the glovebox and to the NMR spectrometer, where ^{1}H spectra were recorded at 25 ºC. The benzylidene resonance of the starting Ru complex was fully consumed and the appearance of new alkylidene resonances was consistent with the observations of Bielawski for phosphine supported Ru catalysts.[13] The presence of a resonance at approximately 8.0 ppm indicated the absence of competitive binding by the polymer chain to the Ru center (a non-chelating monomer). Chelating monomers were characterized by the presence of a single (often broad) resonance around 8.4 ppm.

The full ^{1}H spectra for each monomer are shown below, with an inset showing the aromatic region with the appropriate pyridine resonances.

dx-DME

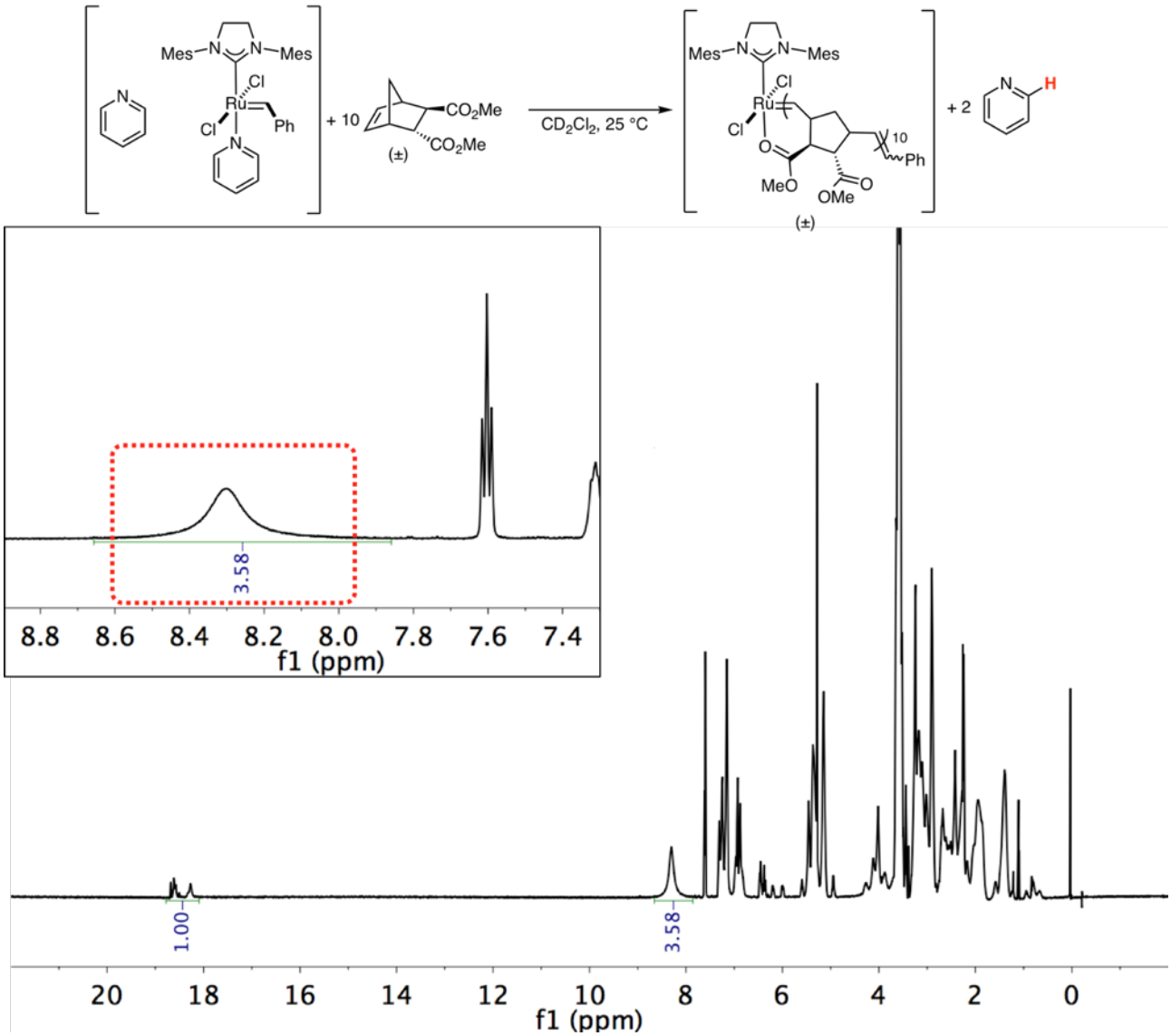

Figure S16. ^{1}H NMR spectrum of the poly(*dx*-DME) bound Ru alkylidene species. Inset: the dissociated pyridine is highlighted in red.

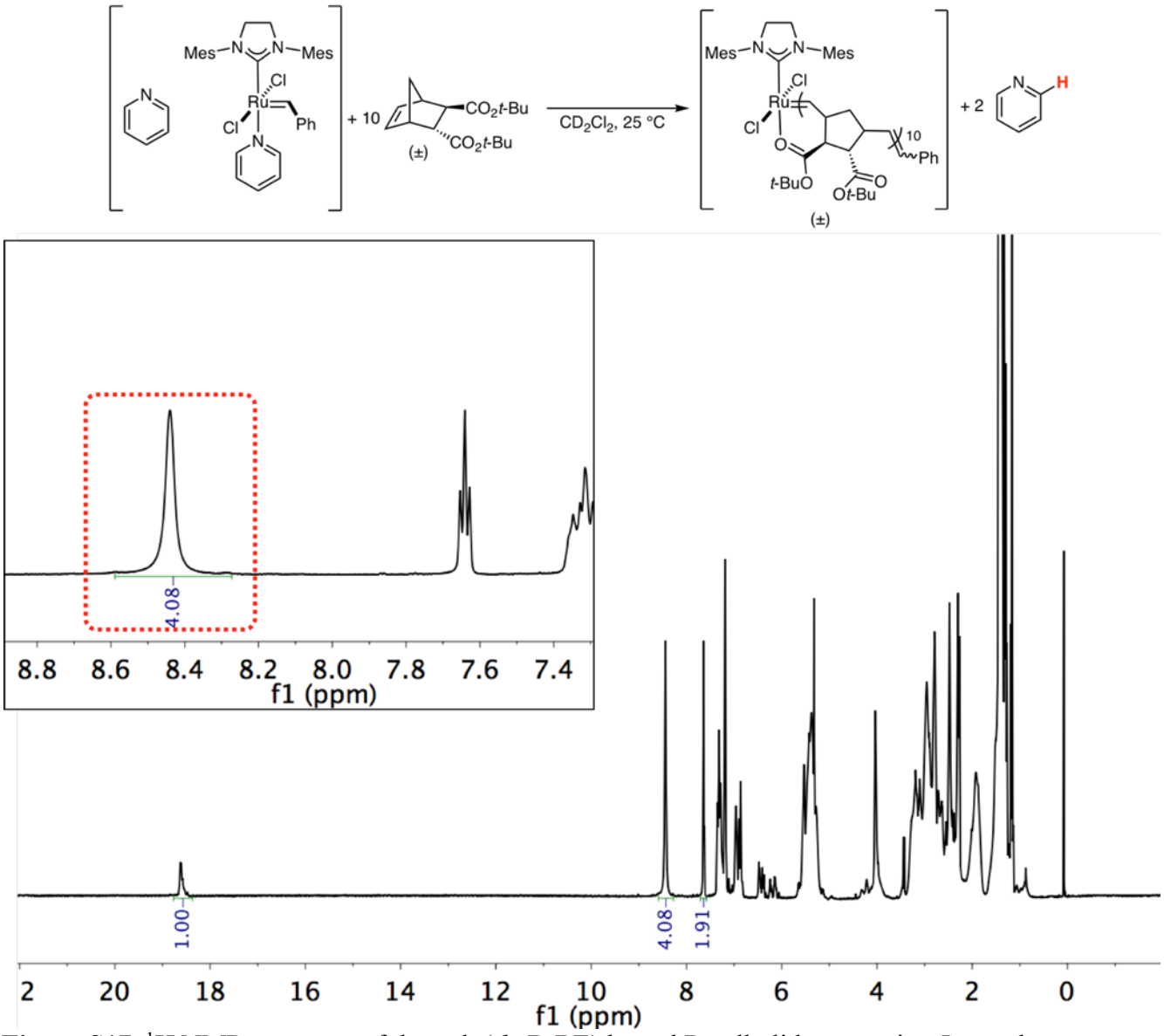

Figure S17. ^{1}H NMR spectrum of the poly(*dx*-DtBE) bound Ru alkylidene species. Inset: the dissociated pyridine is highlighted in red.

xx-NMI

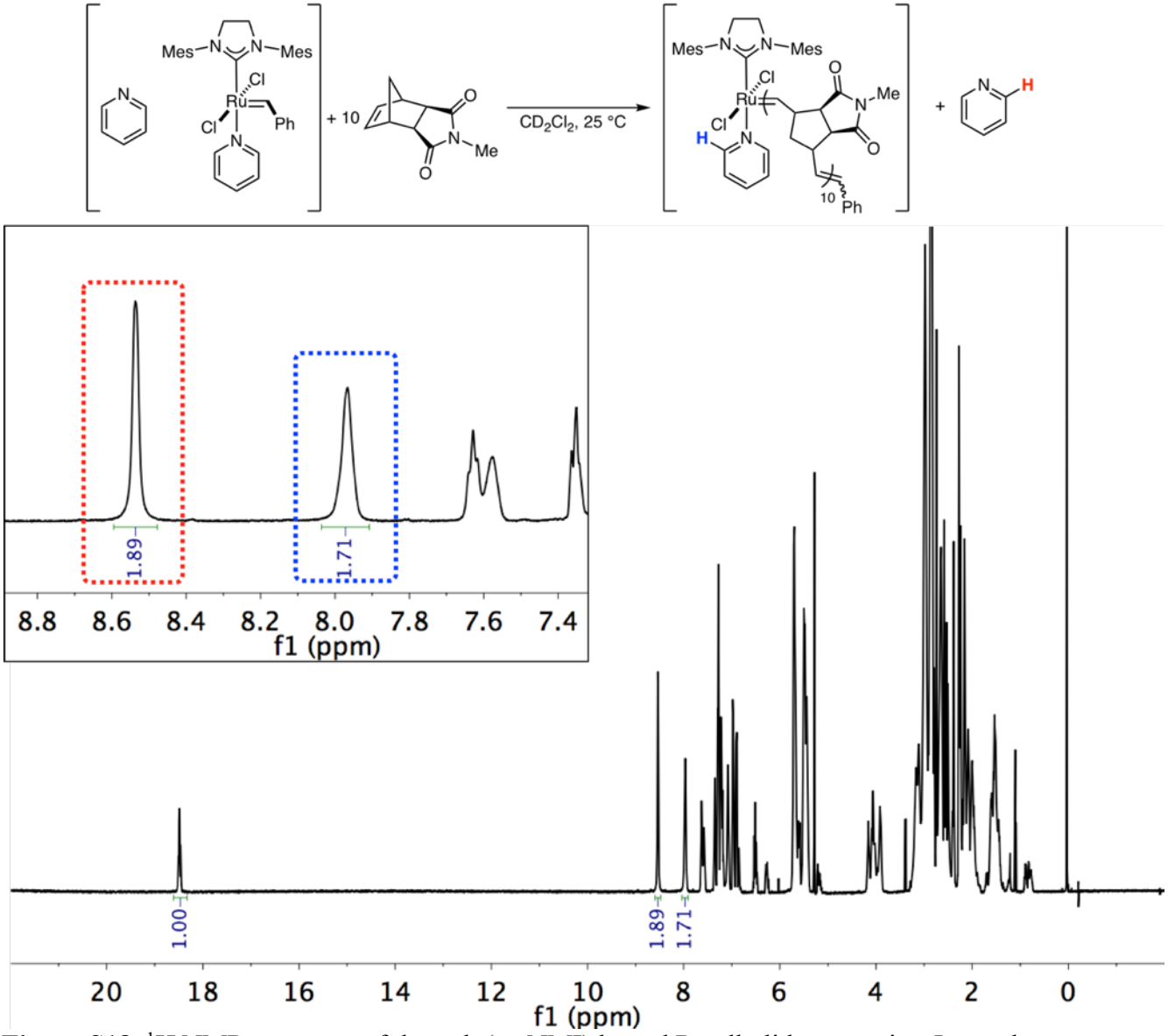

Figure S18. ^{1}H NMR spectrum of the poly(*xx*-NMI) bound Ru alkylidene species. Inset: the dissociated pyridine is highlighted in red and the bound pyridine is highlighted in blue.

dd-NMI

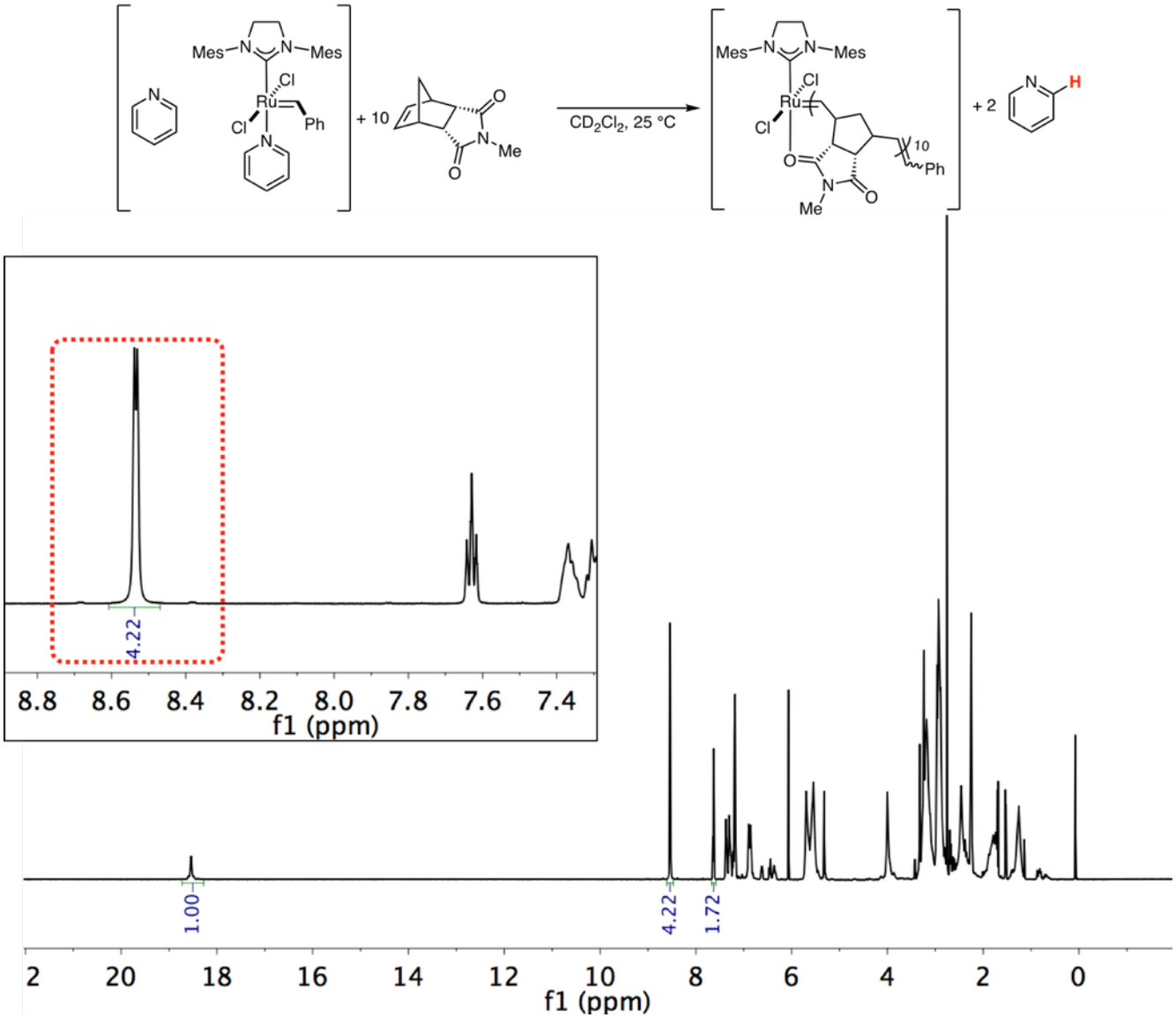

Figure S19. ^{1}H NMR spectrum of the poly(*dd*-NMI) bound Ru alkylidene species. Inset: the dissociated pyridine is highlighted in red.

x-ME

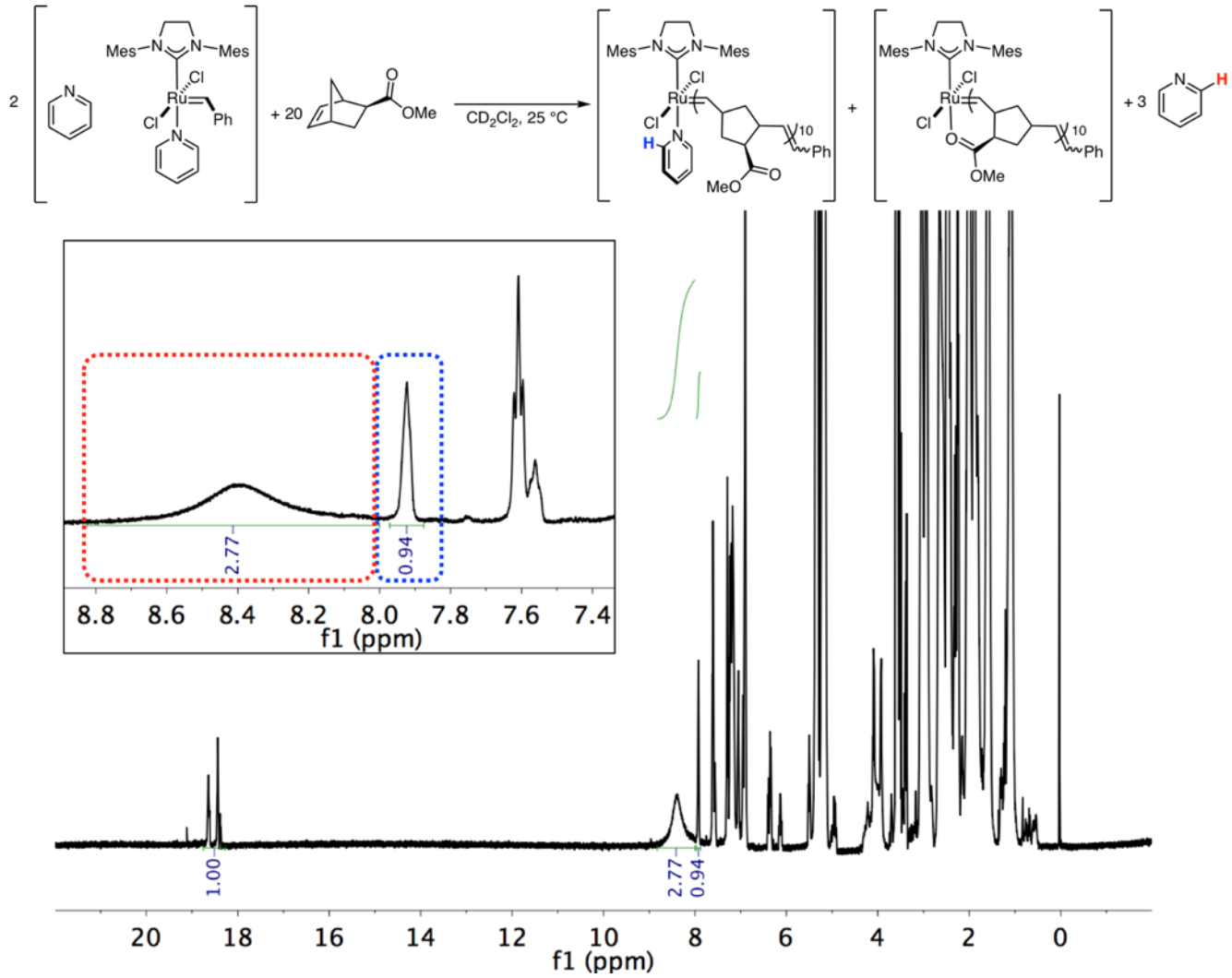

Figure S20. ^{1}H NMR spectrum of the poly(*x*-ME) bound Ru alkylidene species. Inset: the dissociated pyridine is highlighted in red and the bound pyridine is highlighted in blue. The ratio of free:bound pyridine is 3:1, indicating a 1:1 mixture of the two isomers shown above.

PDMS

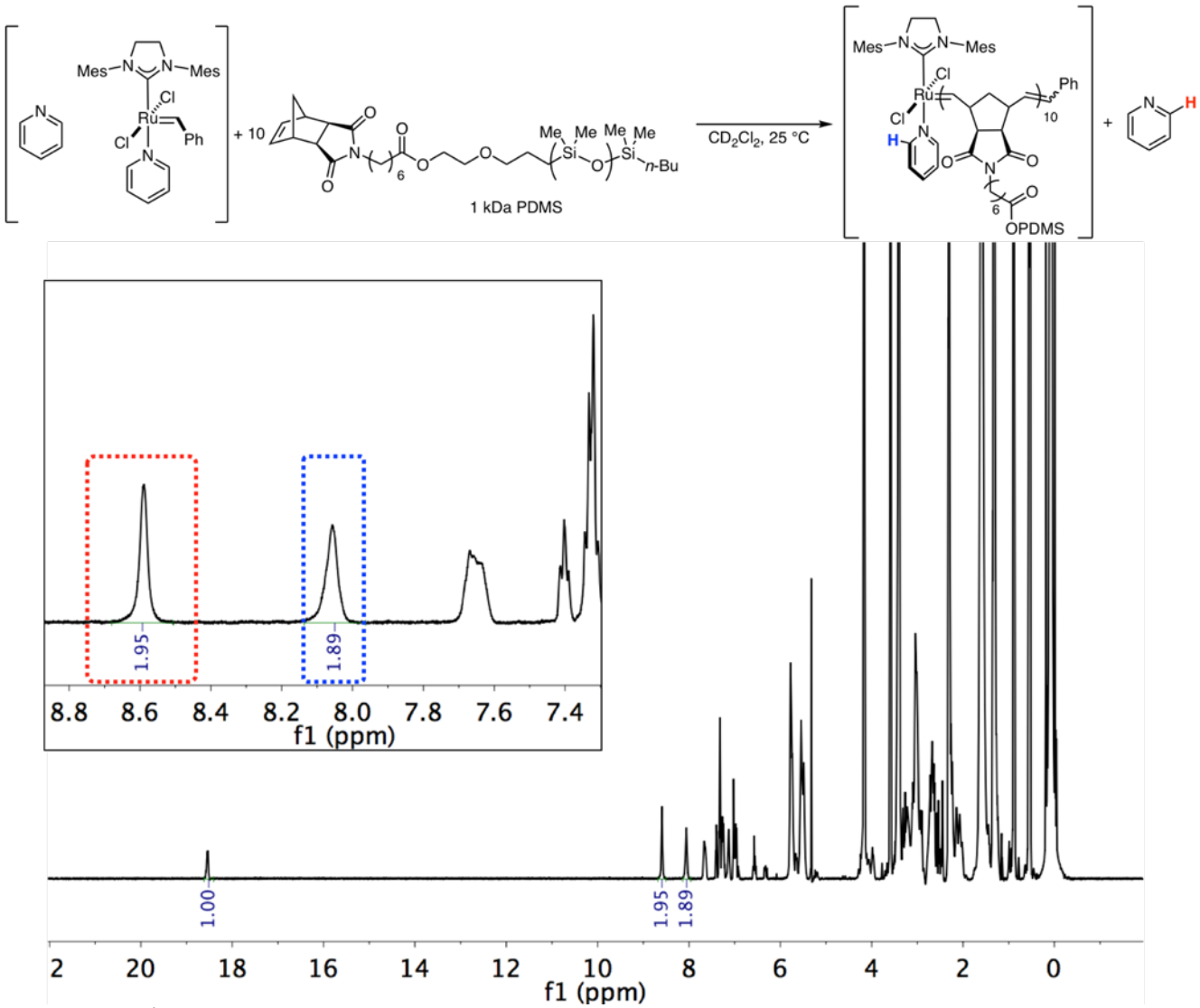

Figure S21. ^{1}H NMR spectrum of the poly(PDMS) bound Ru alkylidene species. Inset: the dissociated pyridine is highlighted in red and the bound pyridine is highlighted in blue.

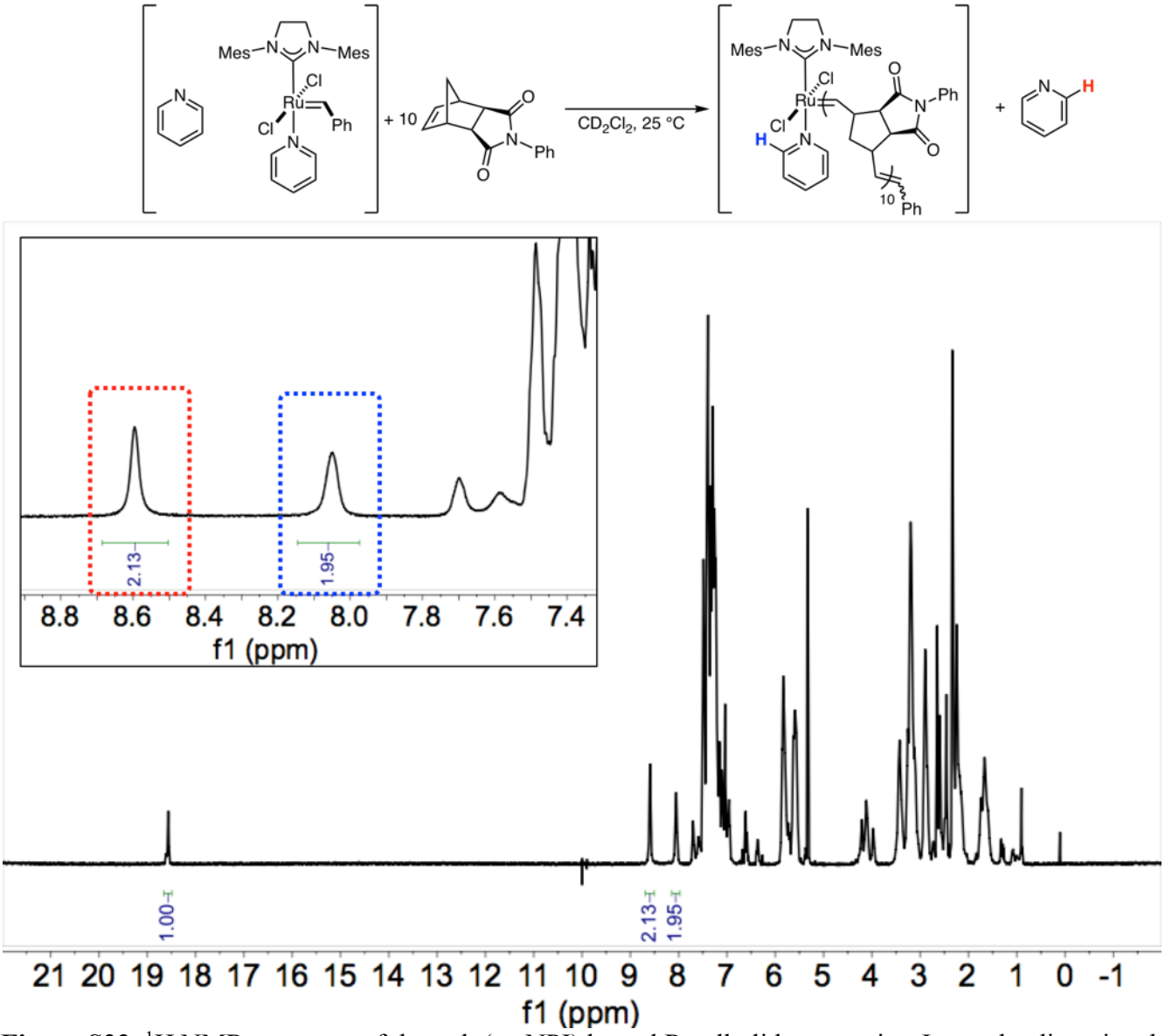

Figure S22. ^{1}H NMR spectrum of the poly(*xx*-NPI) bound Ru alkylidene species. Inset: the dissociated pyridine is highlighted in red and the bound pyridine is highlighted in blue.

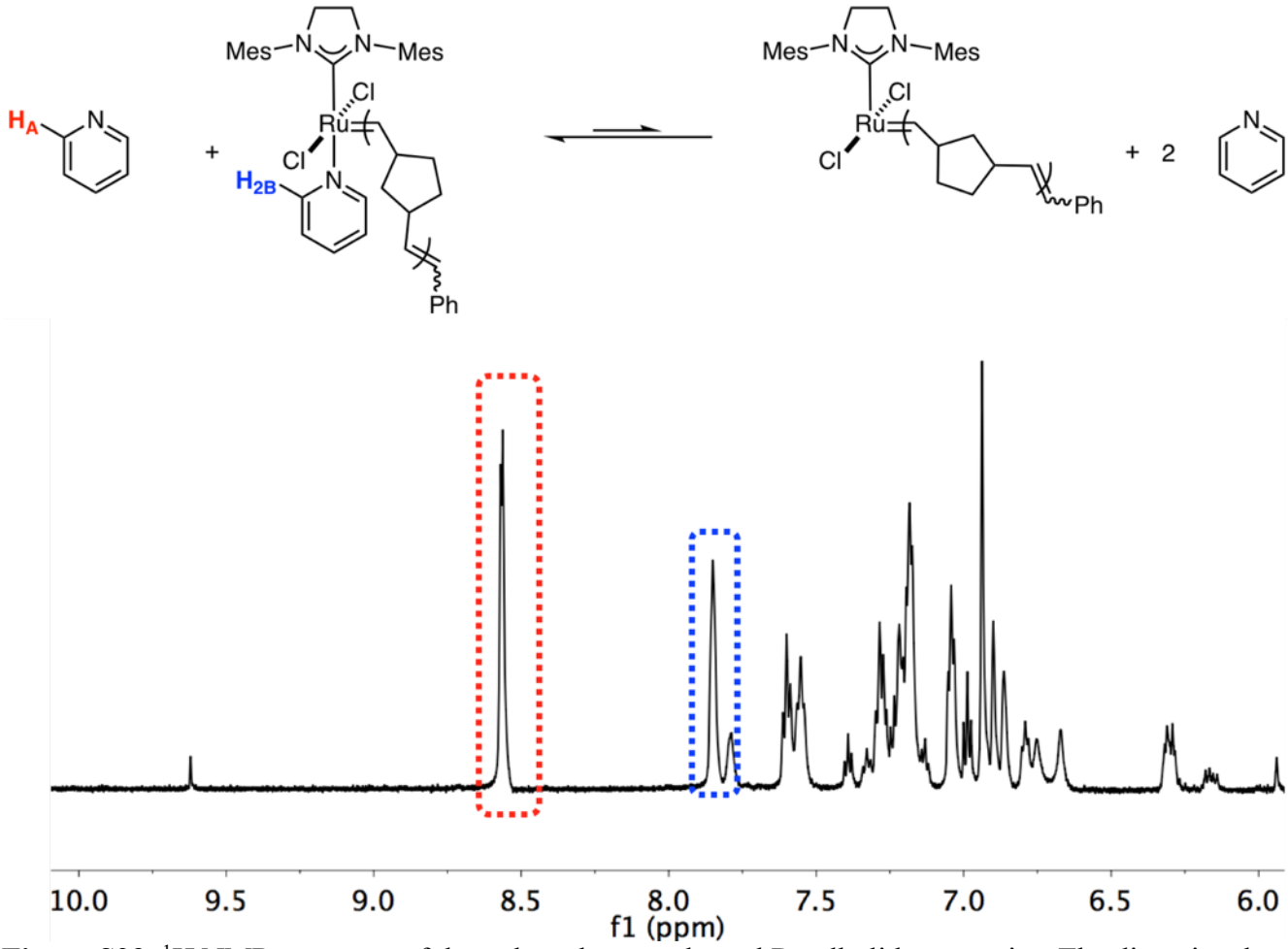

Figure S23. ^{1}H NMR spectrum of the polynorbornene bound Ru alkylidene species. The dissociated pyridine is highlighted in red and the bound pyridine is highlighted in blue.

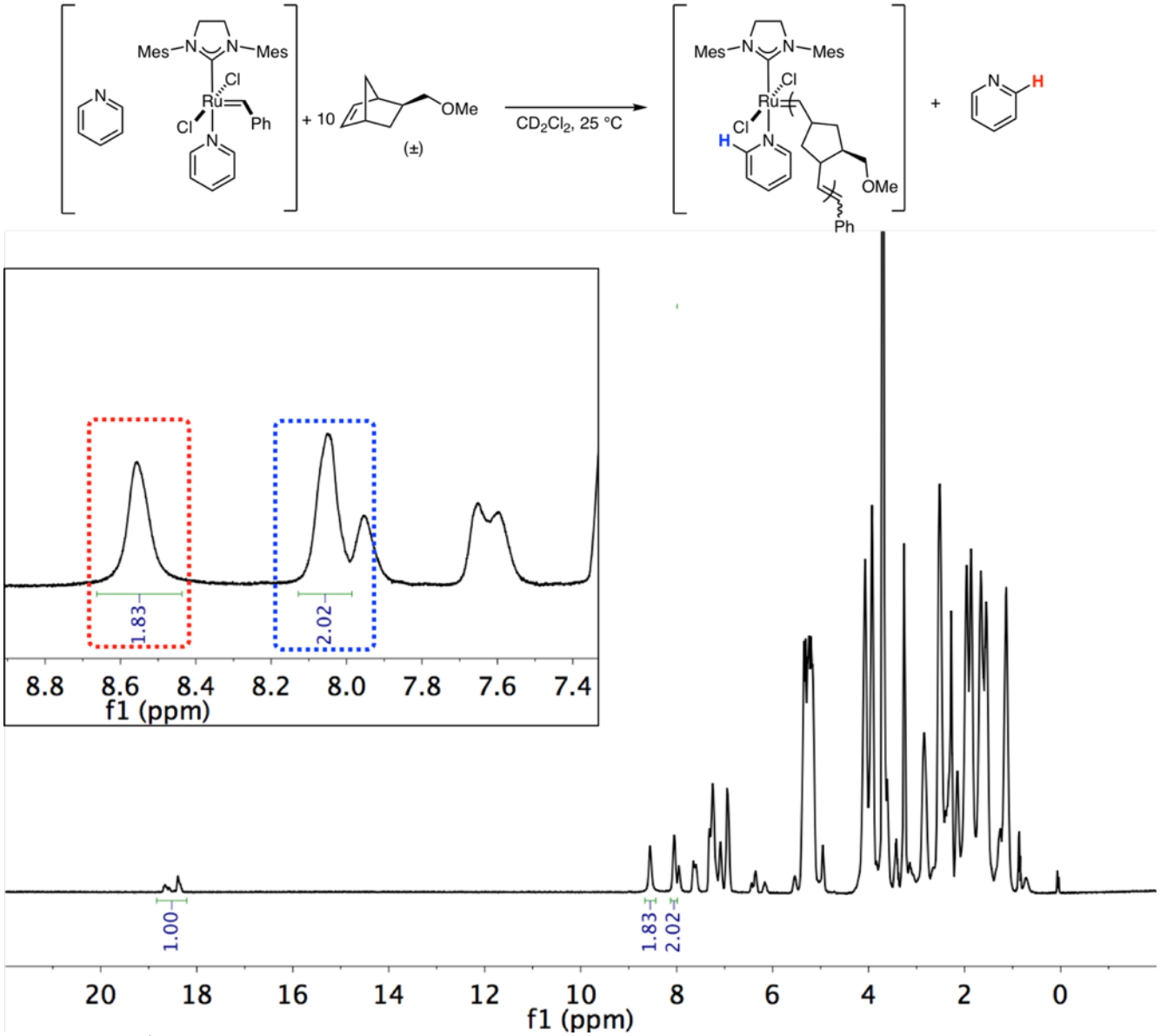

Figure S24. ^{1}H NMR spectrum of the polynorbornene bound Ru alkylidene species. The dissociated pyridine is highlighted in red and the bound pyridine is highlighted in blue.

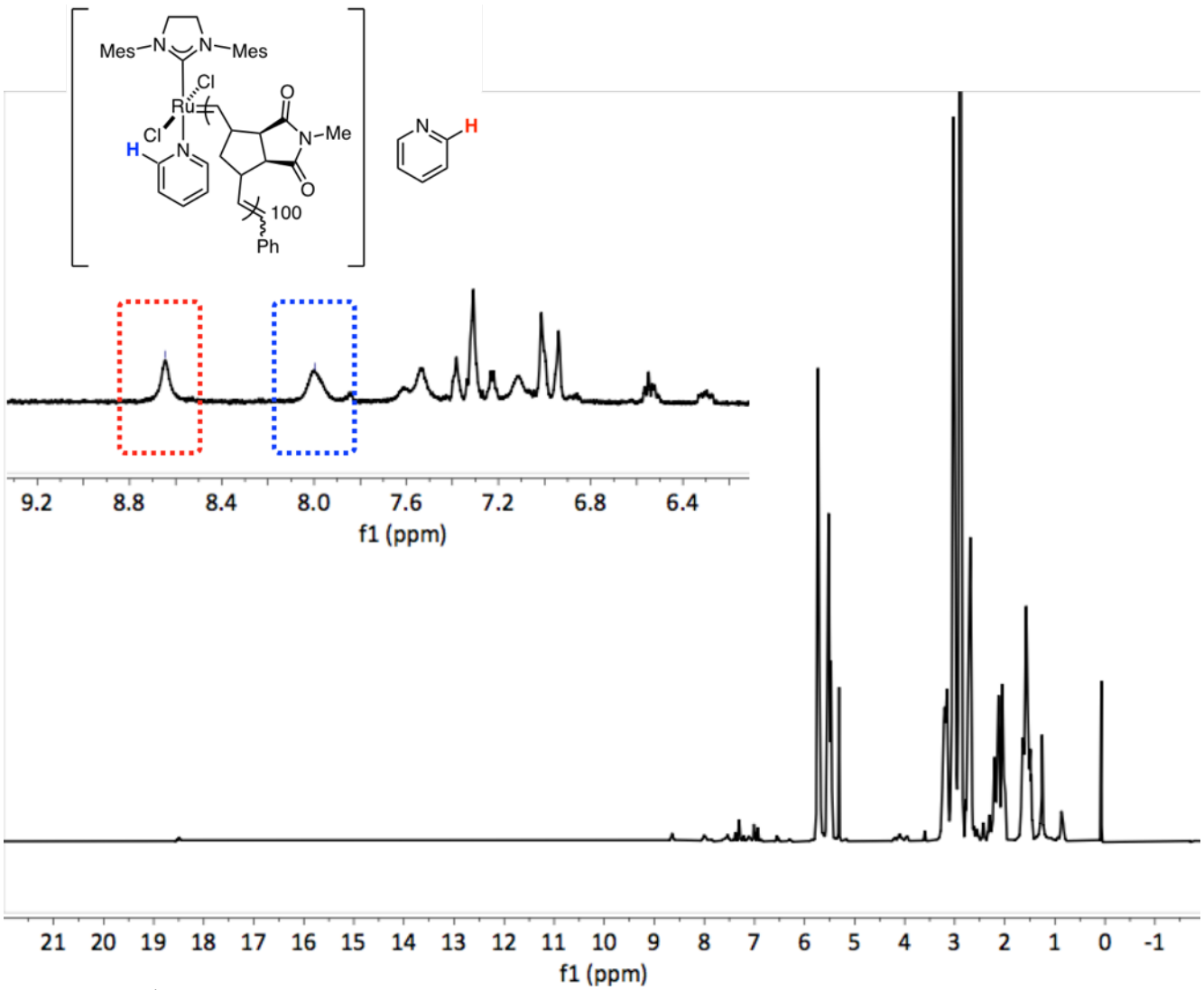

Figure S25. ^{1}H NMR spectrum of *poly-xx*-NMI bound Ru alkylidene ([Ru] = 0.05 mM) showing the pyridine bound resting state.

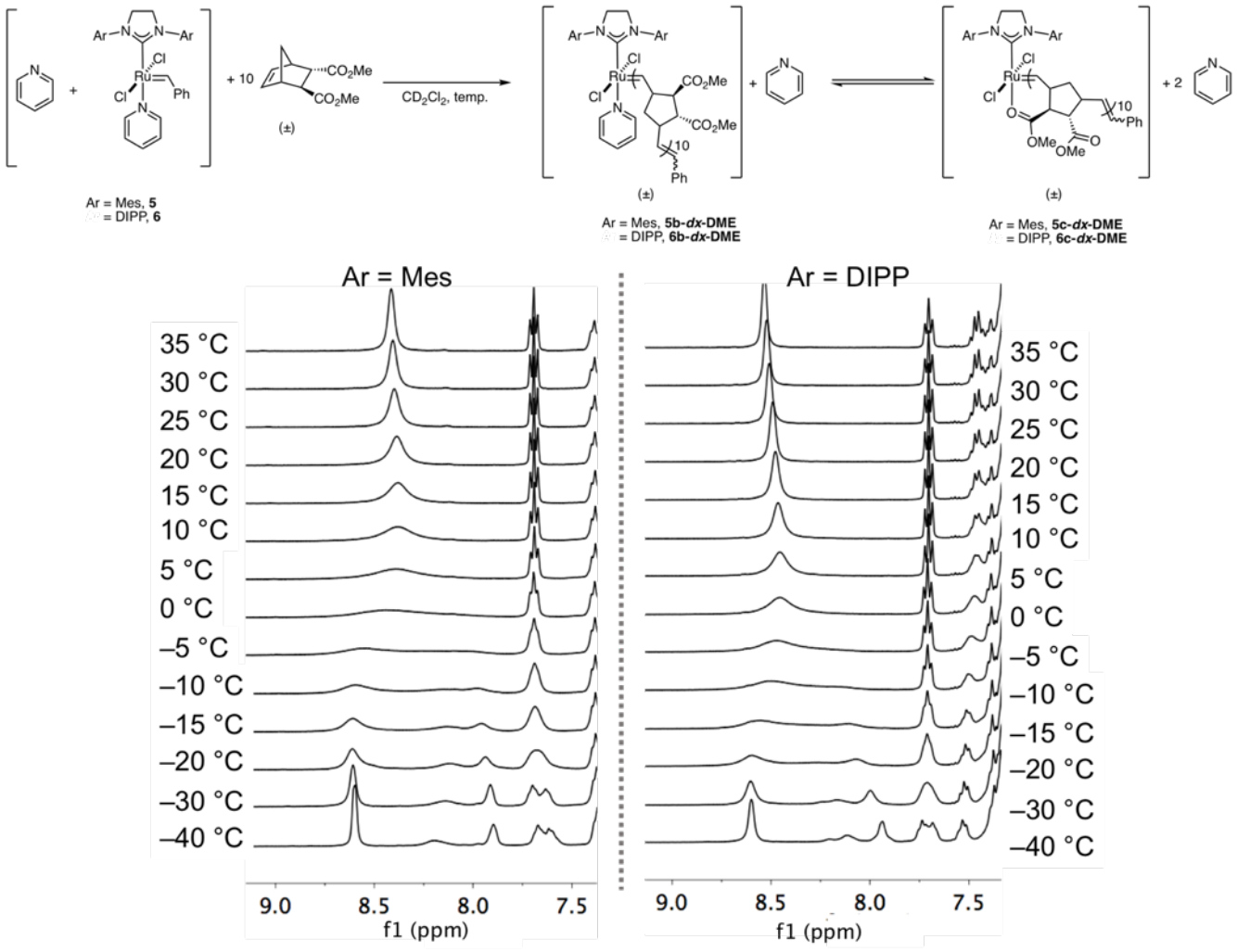

Figure S26. Variable Temperature NMR array (400 MHz) showing the coalescence of free (8.6 ppm) and bound (8.2–7.9 ppm) pyridine signals for **5-*dx*-DME** (left) and **6-*dx*-DME** (right). Each Ru complex exists as a pair of isomers as the Ru center can be adjacent to the *exo* or the *endo* ester.

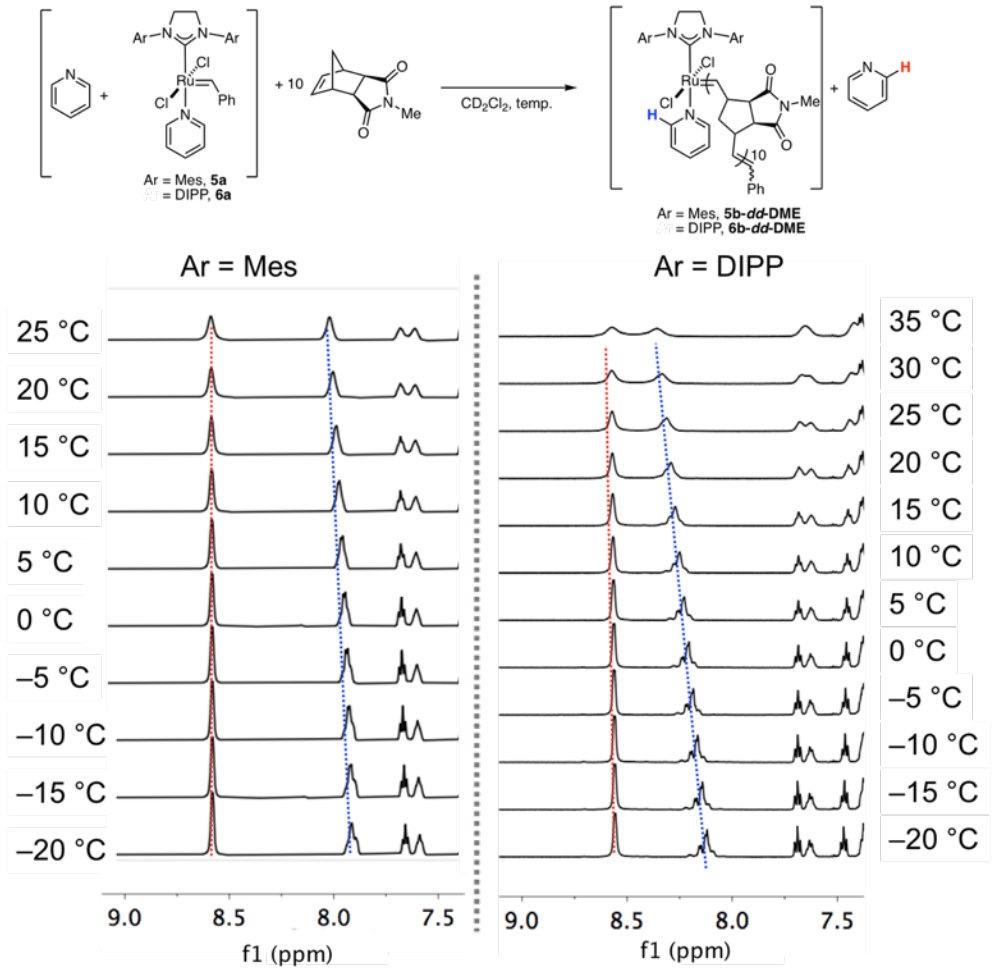

Figure S27. Variable Temperature NMR (600 MHz) array showing the free (8.6 ppm) and bound (8.2–7.9 ppm) pyridine signals for **5-*xx*-NMI** (left) and **6-*xx*-NMI** (right).

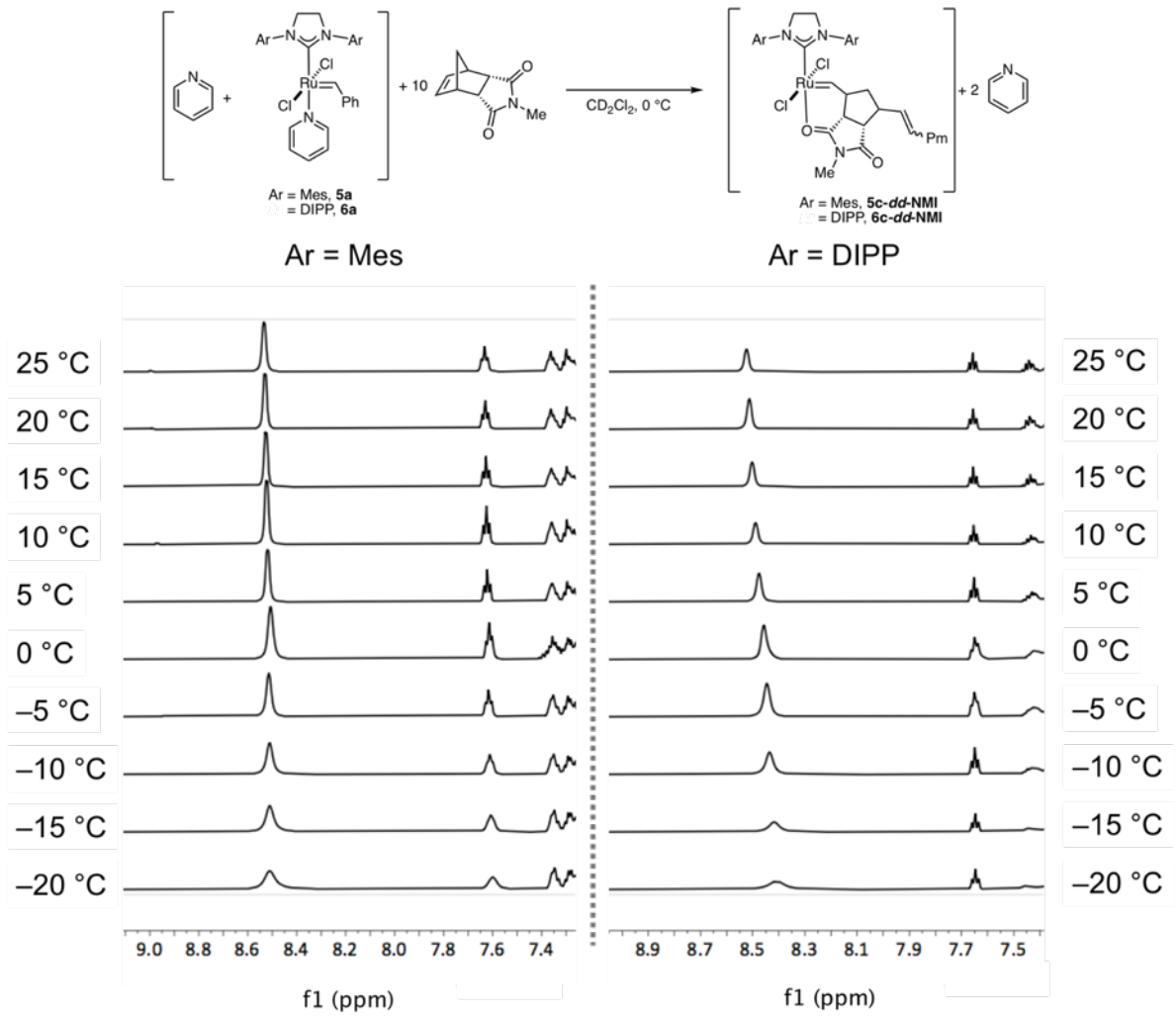

Figure S28. Variable Temperature NMR array (600 MHz) showing the free (8.6 ppm) pyridine signal for **5-*dd*-NMI** (left) and **6-*dd*-NMI** (right).

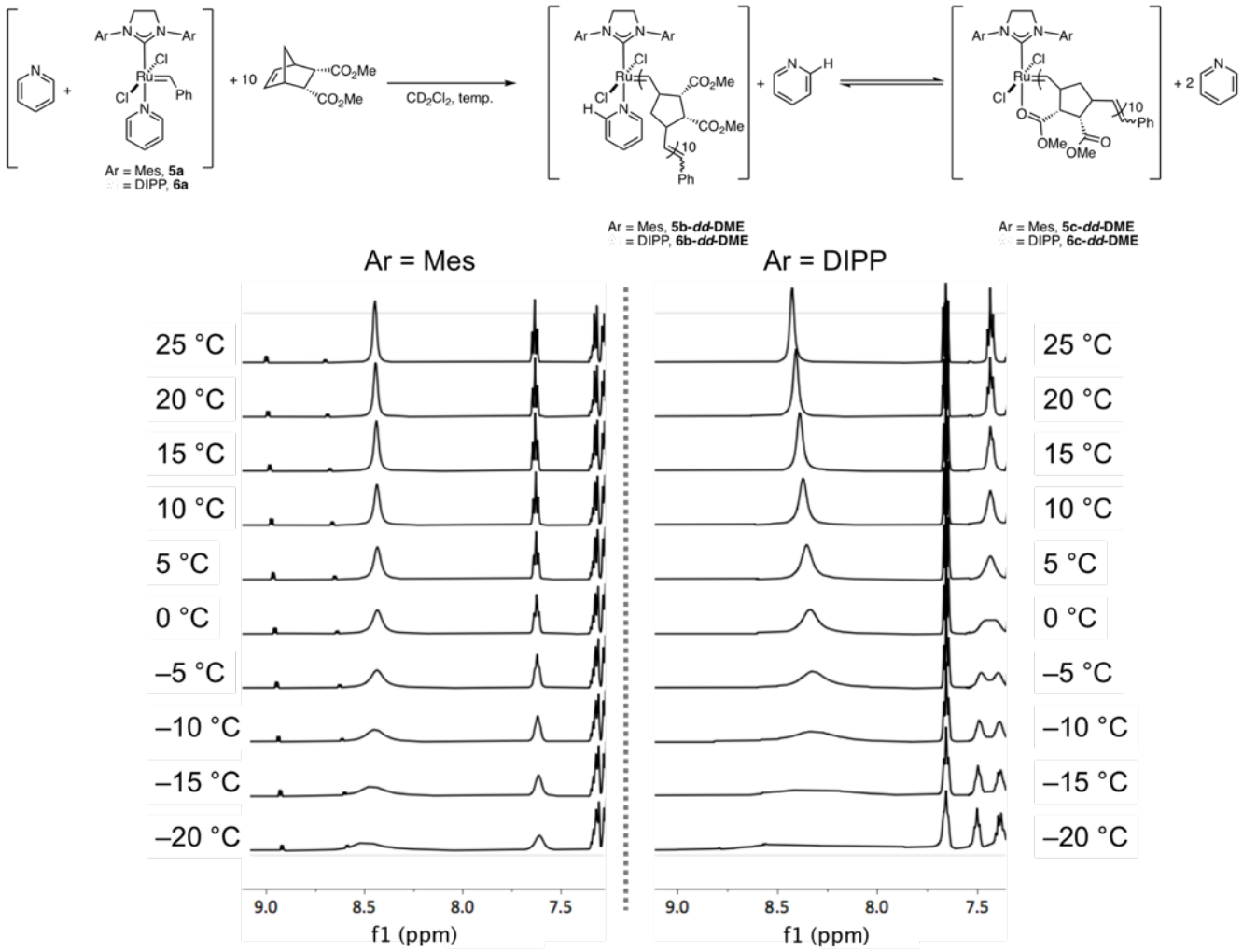

Figure S29. Variable Temperature NMR array (600 MHz) showing the free (8.6 ppm) pyridine signal for **5-dd-DME** (left) and **6-dd-DME** (right).

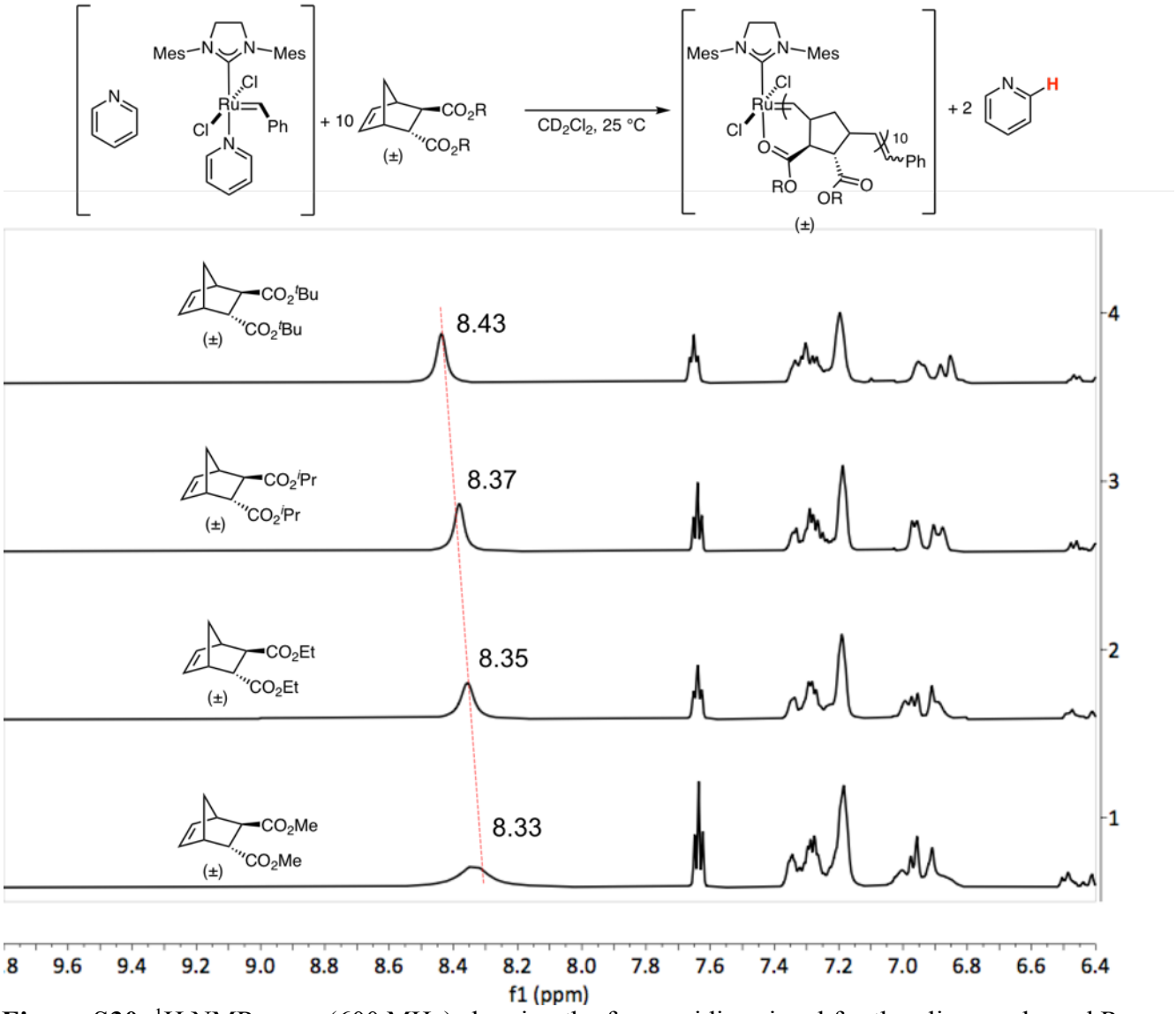

Figure S30. ^{1}H NMR array (600 MHz) showing the free pyridine signal for the oligomer bound Ru catalyst with SIMes as a function of the structure of the ester group. The larger group (Me < Et < *i*-Pr < *t*-Bu) causes the chemical shift of the pyridine resonance to increase.

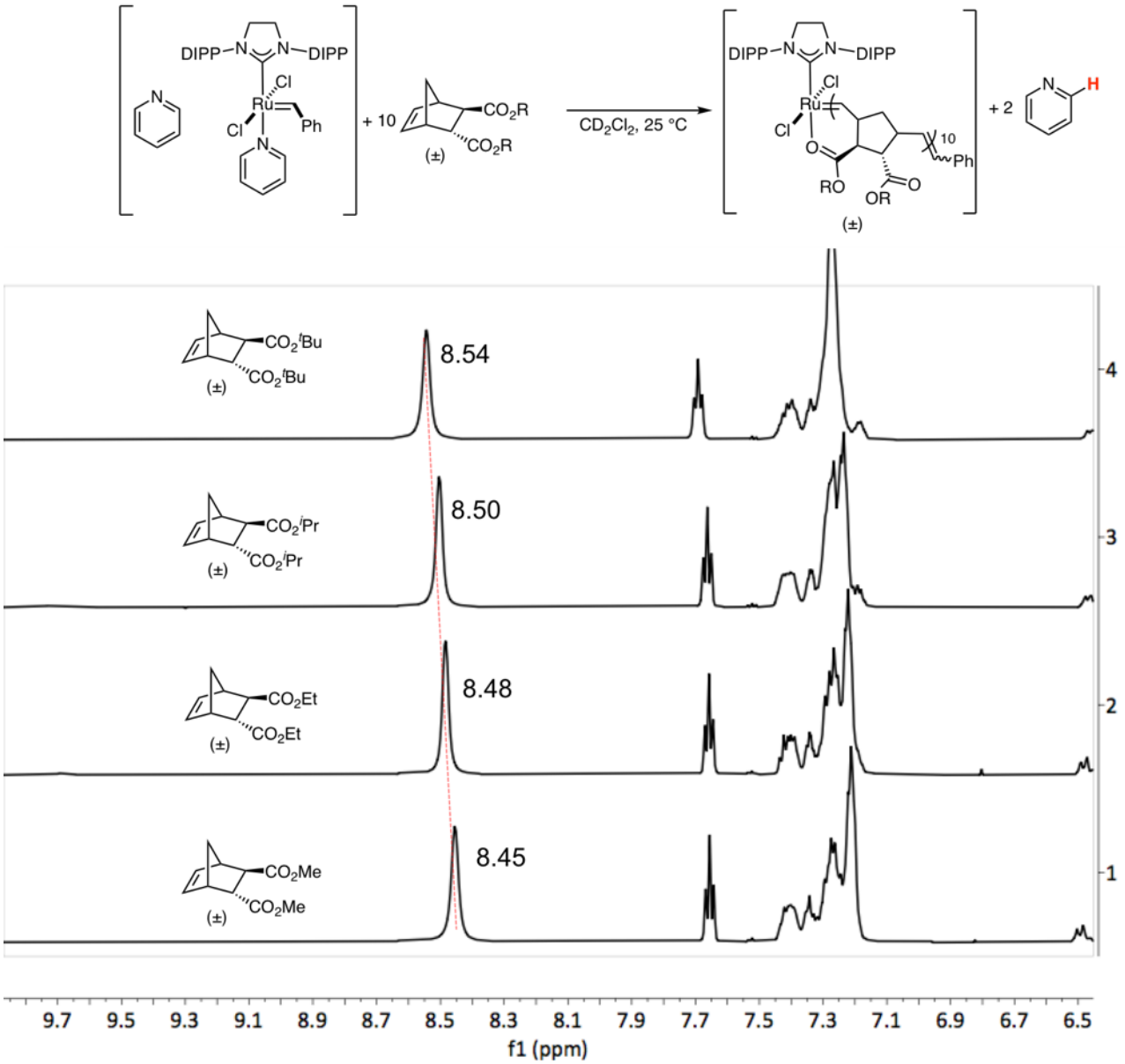

Figure S31. ^{1}H NMR array (600 MHz) showing the free pyridine signal for the oligomer bound Ru catalyst with SIPr as a function of the structure of the ester group. The larger group (Me < Et < *i*-Pr < *t*-Bu) causes the chemical shift of the pyridine resonance to increase. The absolute chemical shift is larger for the SIPr ligand than for the SIMes ligand due to increased steric repulsion between the larger aryl rings of the SIPr ligand.

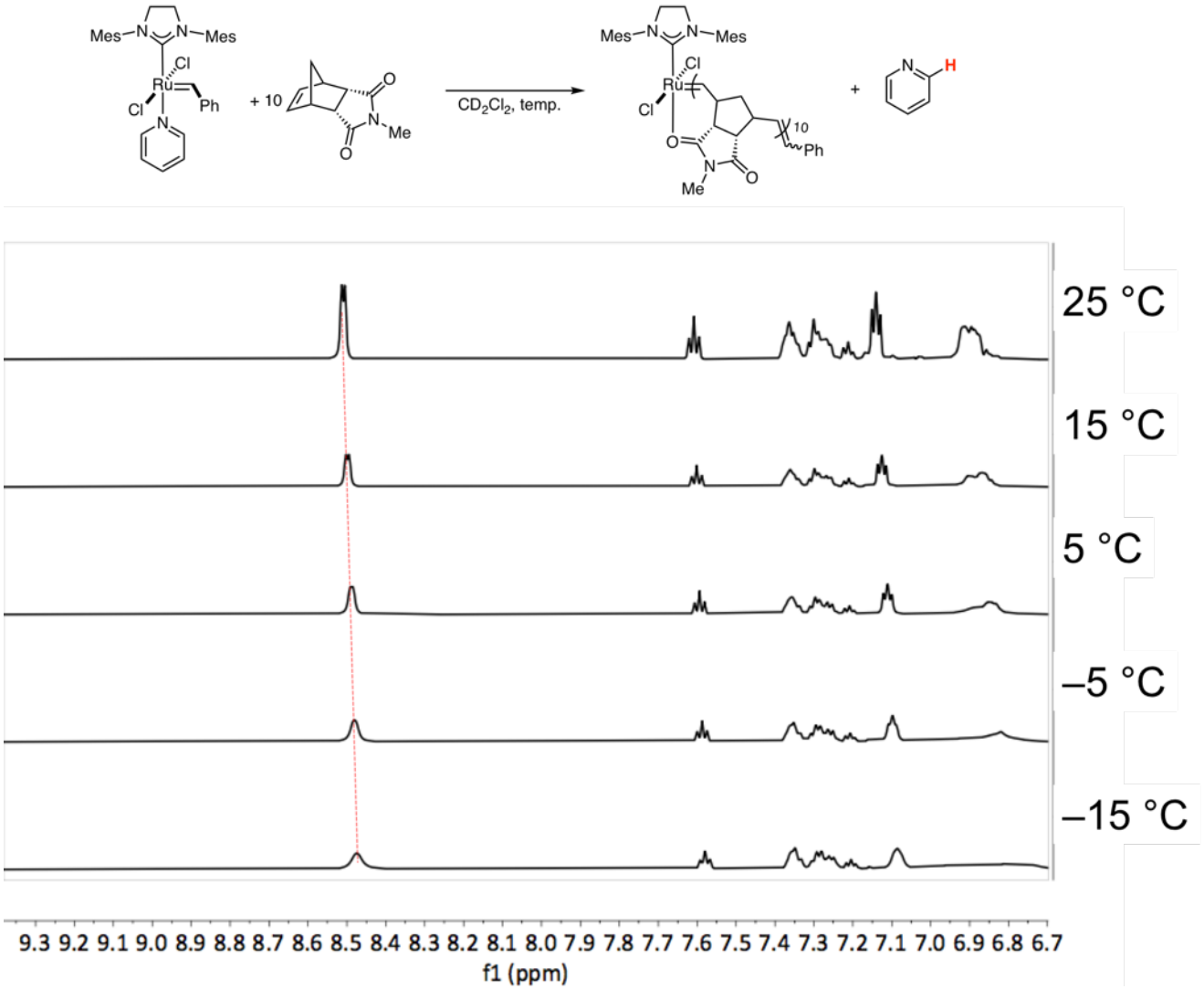

Figure S32. Variable temperature ^{1}H NMR array (600 MHz) showing the free pyridine signal for the oligo-(*dd*-NMI) bound **5a** with one equivalent of pyridine.

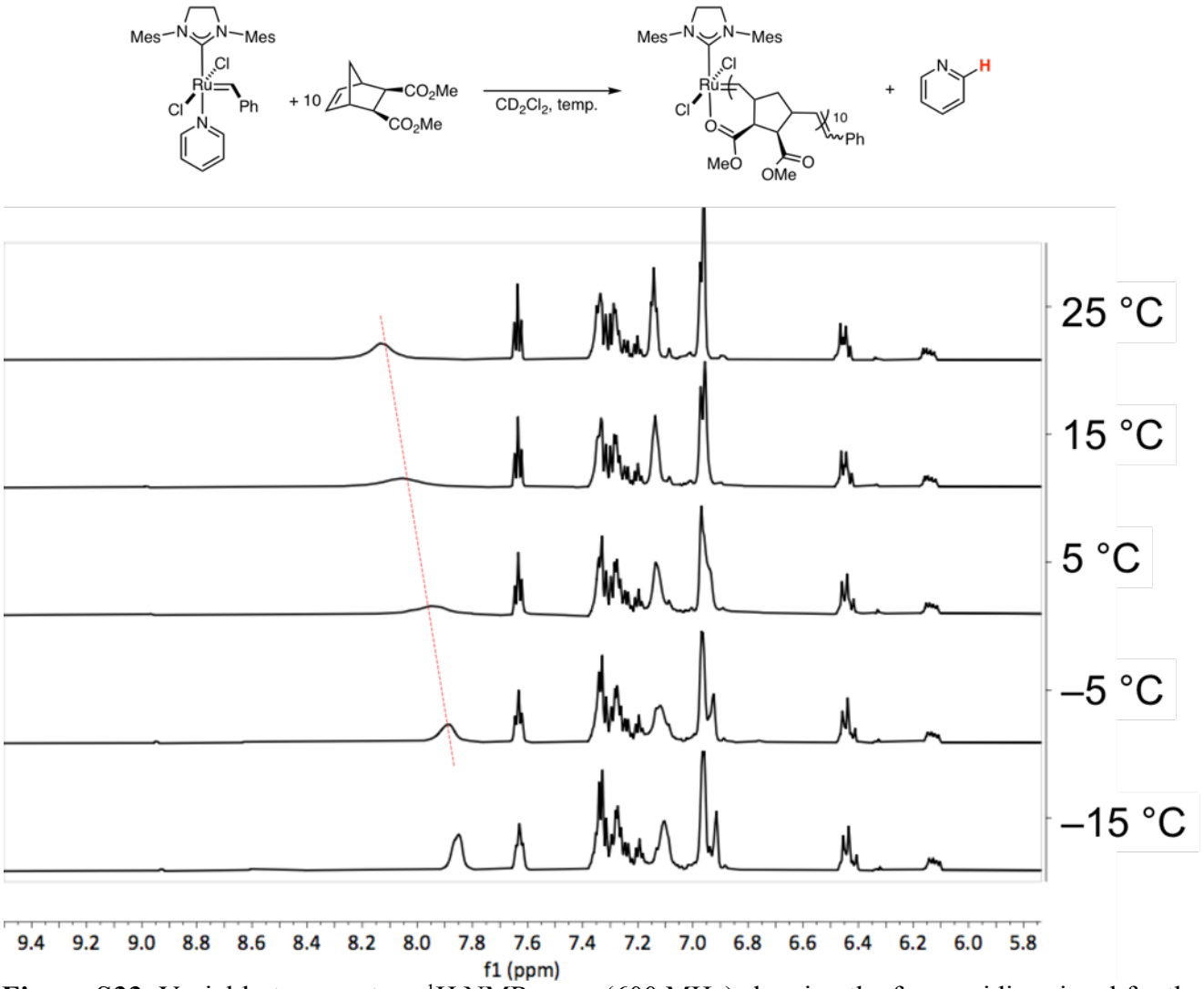

Figure S33. Variable temperature ^{1}H NMR array (600 MHz) showing the free pyridine signal for the oligo-(*xx*-DME) bound **5a** with one equivalent of pyridine.

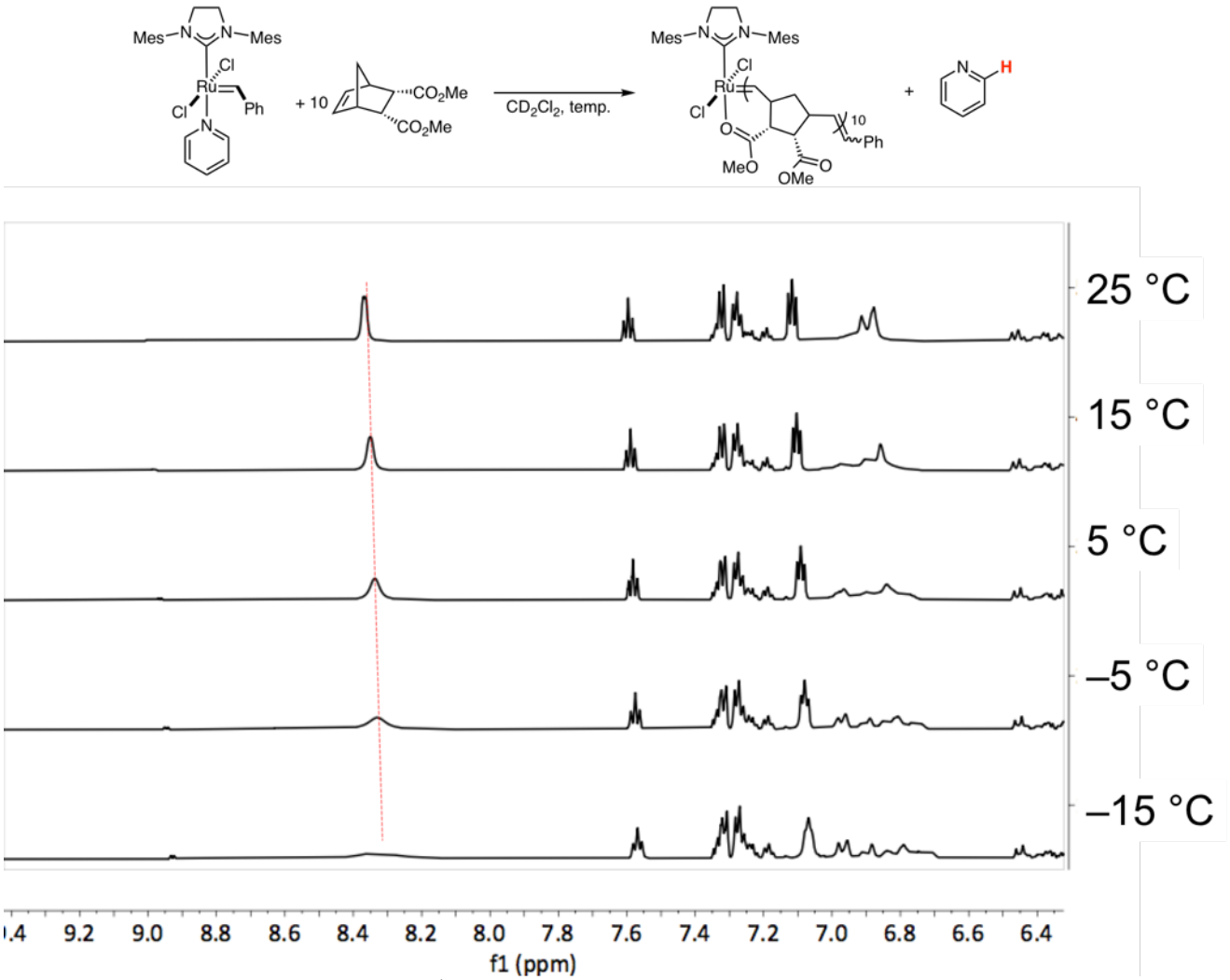

Figure S34. Variable temperature ^{1}H NMR array (600 MHz) showing the free pyridine signal for the oligo-(*dd*-DME) bound **5a** with one equivalent of pyridine.

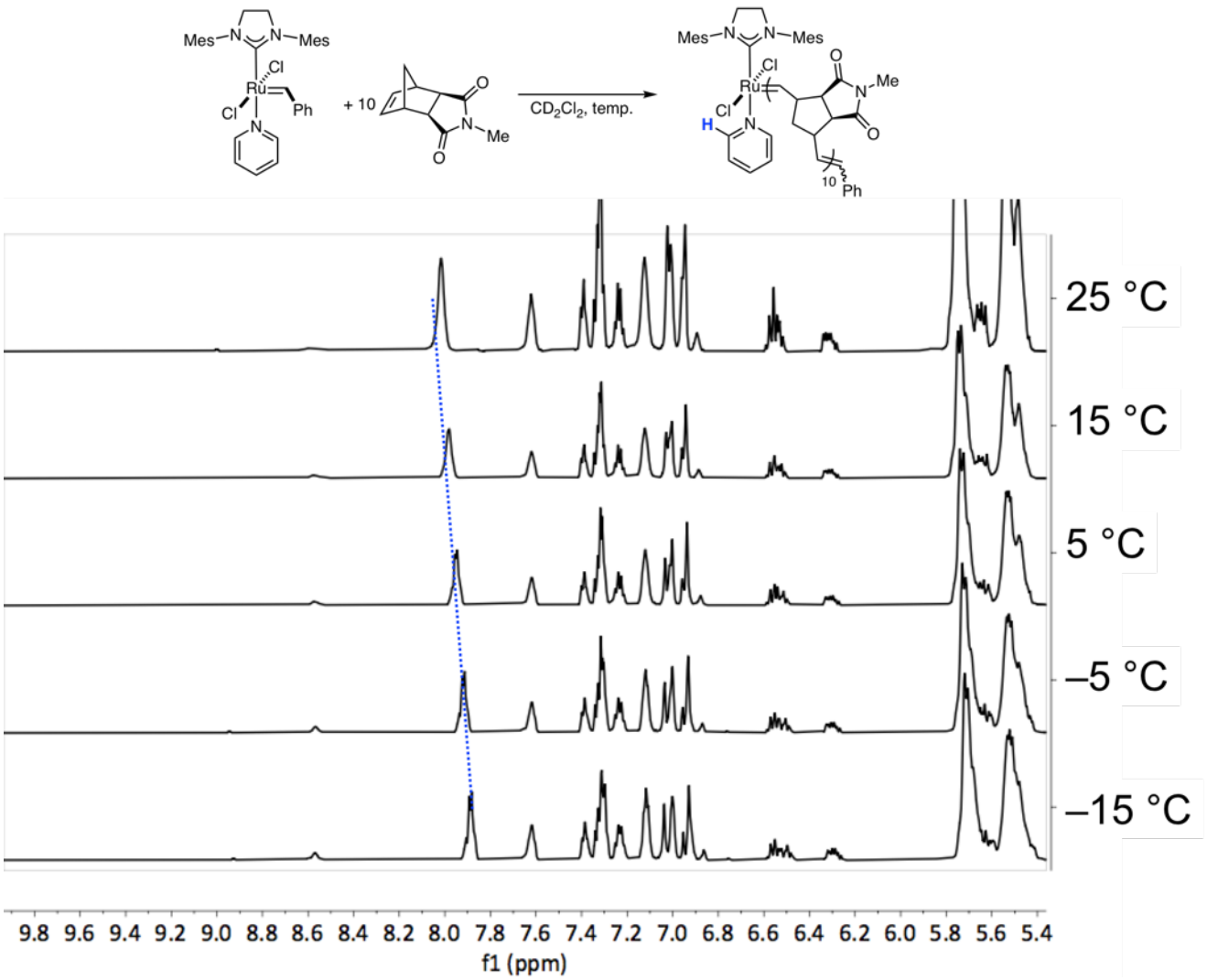

Figure S35. Variable temperature ^{1}H NMR array (600 MHz) showing the free pyridine signal for the oligo-(*xx*-NMI) bound **5a** with one equivalent of pyridine.

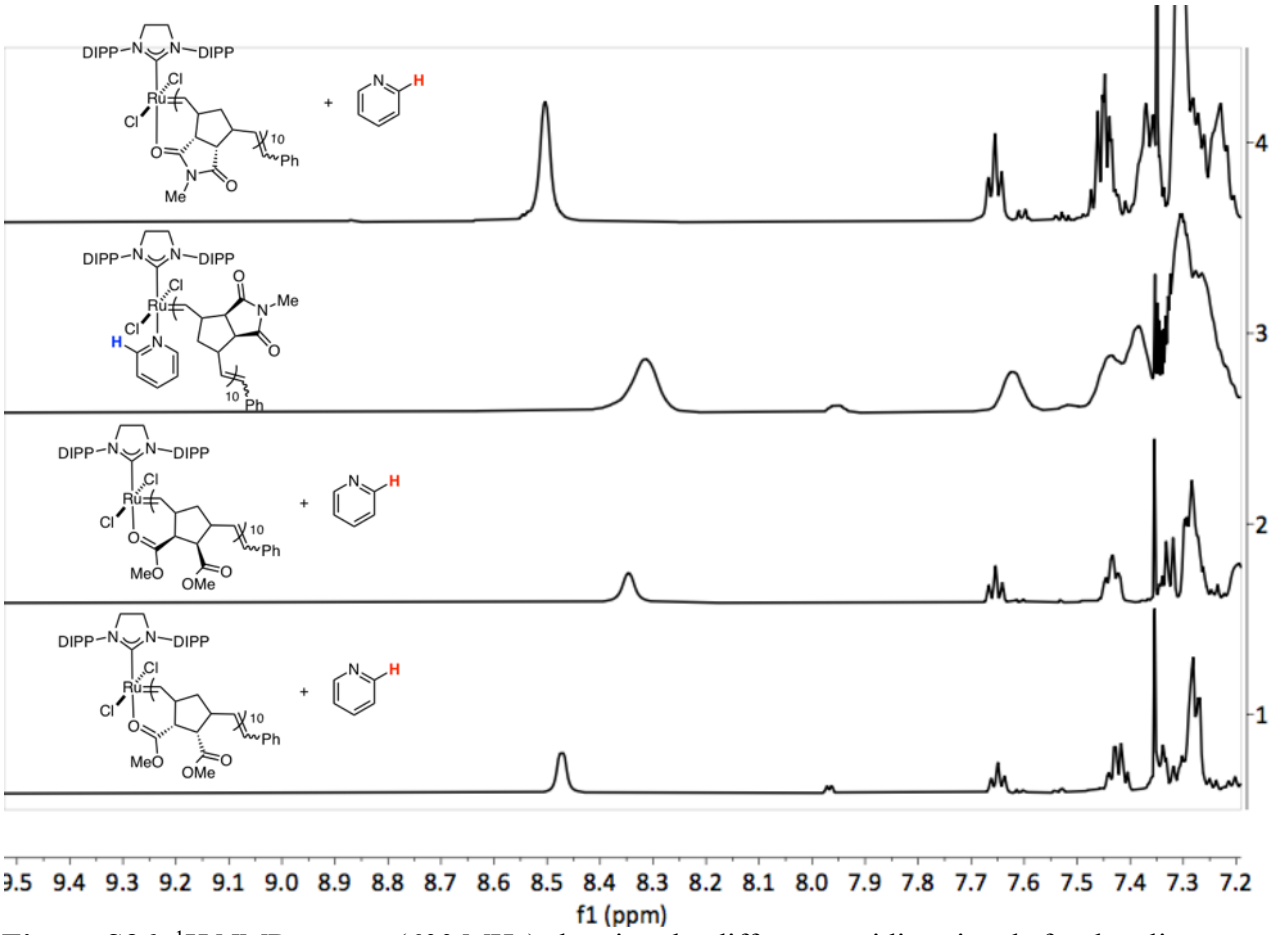

Figure S36. ^{1}H NMR spectra (600 MHz) showing the different pyridine signals for the oligomer bound **6a** with one equivalent of pyridine. The *endo* substituted monomers show a significant shift in the pyridine resonace towards it free value (8.59 ppm) indicating chelation.

Dynamic NMR analysis

Dynamic NMR lineshape analysis was performed using the DNMR application in TopSpin 4.0.6. The bound and the free pyridine molecules were simulated as a single spin system consisting of two molecules each with three resonances. Line broadening was fixed to 2 Hz, as determined by fitting the spectrum of the unbound pyridine at –40 °C.

Molecule 1		Molecule 2	
Nuc1	Pseudospin = 1.0	Nuc4	Pseudospin = 1.0
Nuc2	Pseudospin = 0.5	Nuc5	Pseudospin = 0.5
	J1 = 5.5 Hz		J4 = 5.5 Hz
Nuc3	Pseudospin = 1.0	Nuc6	Pseudospin = 1.0
	J1 = 1.9 Hz		J4 = 1.9 Hz
	J2 = 7.6 Hz		J5 = 7.6 Hz

The program was allowed to optimize the line fitting (Best Overlap >90%) by scanning the frequency of exchange (*k* under 'Reaction') and the equilibrium (*K*, parameter *X* under 'Molecule' tab). The calculated values for *k* (in Hz) and *X* are shown in the table below.

Table S4. Calculated frequencies of pyridine exchange for **5-*xx*-DME** and **6-*xx*-DME** and equilibrium constants favoring the chelated Ru complex**.**

	k (Hz)		*X*	
Temp (K)	**5**	**6**	**5**	**6**
268	98	160.7	0.528	0.543
273	169	255	0.535	0.600
278	247	334	0.541	0.620
283	351	610	0.558	0.690
288	497	787	0.565	0.697
293	707	1103	0.583	0.728
298	1021	1361	0.605	0.770
303	1494	2067	0.622	0.810
308	2100	2604	0.639	0.840

The parameter *X* is the mole fraction of the free pyridine compared to the total (free+bound) pyridine:

$$X = \frac{free}{total}$$
$$(free) + (bound) = 1$$

Simulated Spectra for **6-*xx*-DME** (green line) overlayed with experimental spectra (blue line).

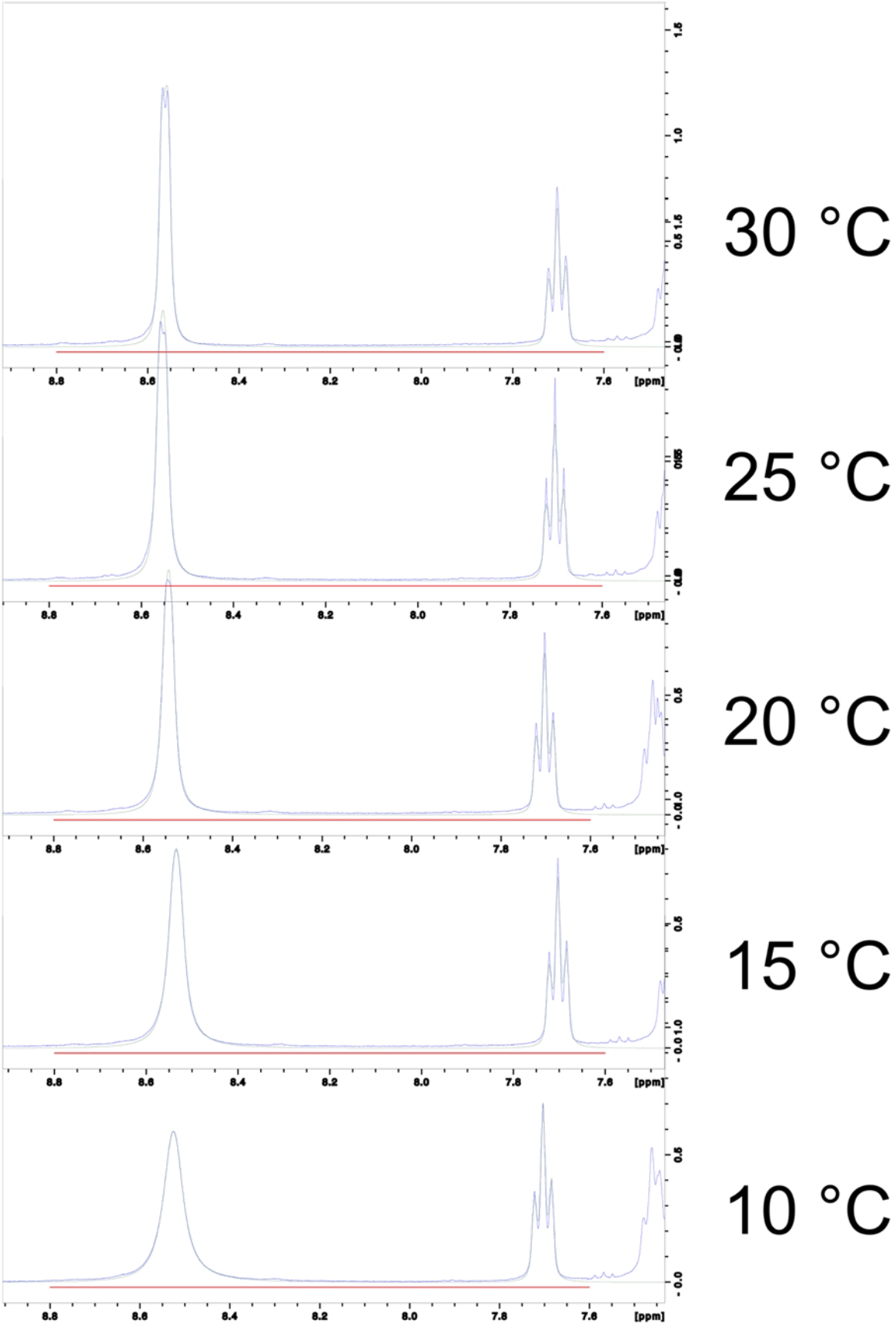

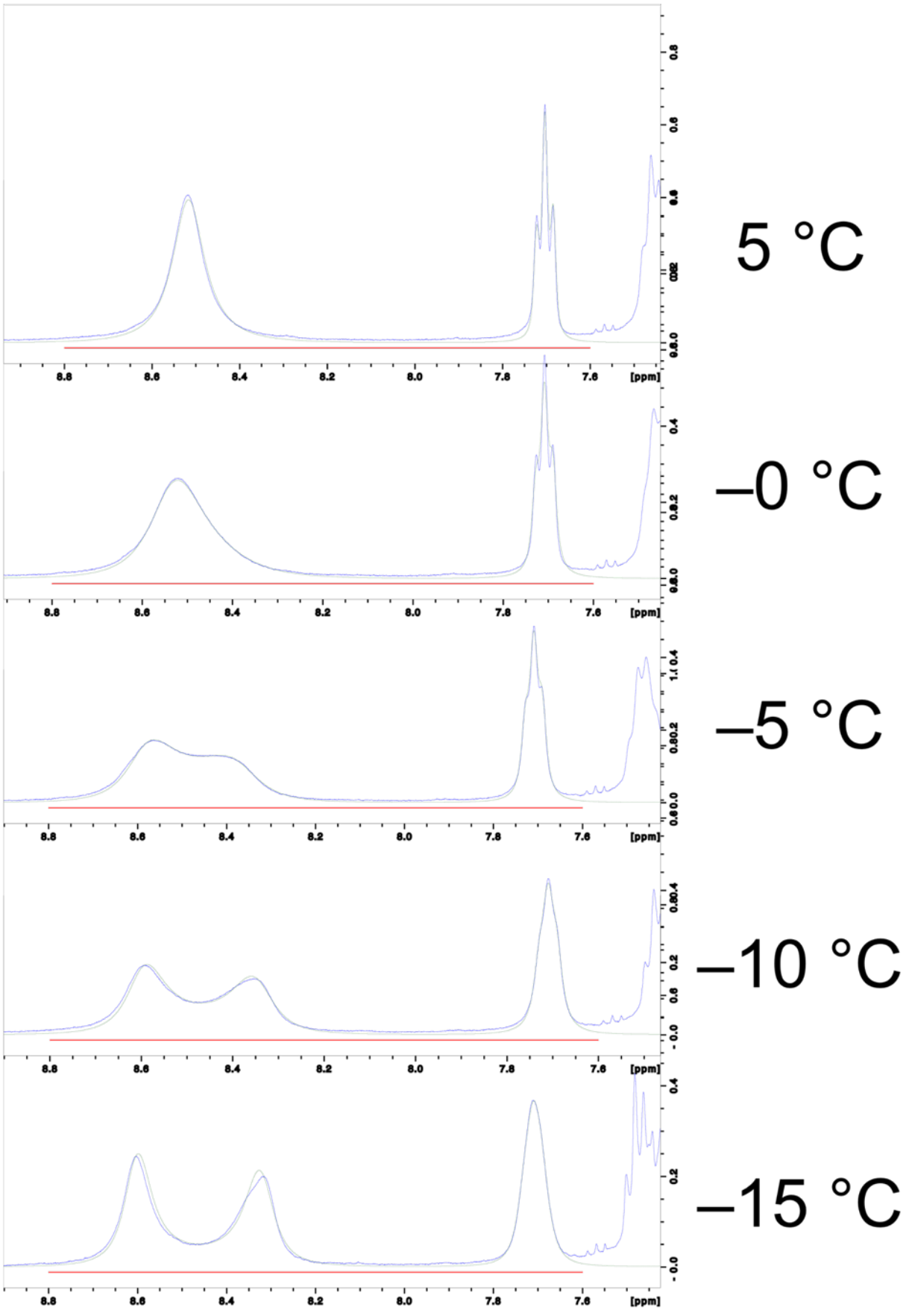
5 °C
–0 °C
–5 °C
–10 °C
–15 °C
8.8
8.6
8.4
8.2
8.0
7.8
7.6
[ppm]

Simulated Spectra for **5-*xx*-DME** (green line) overlayed with experimental spectra (blue line).

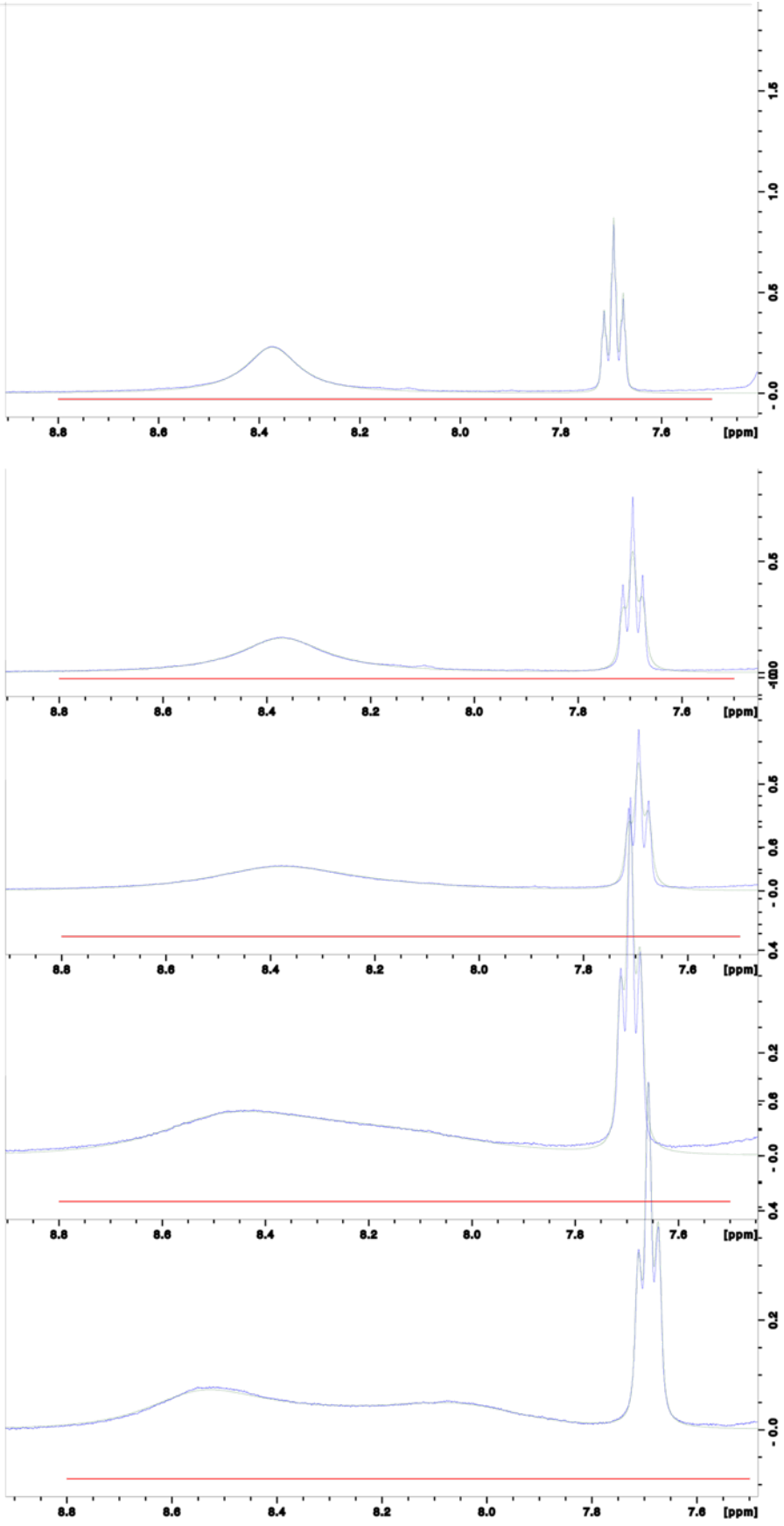

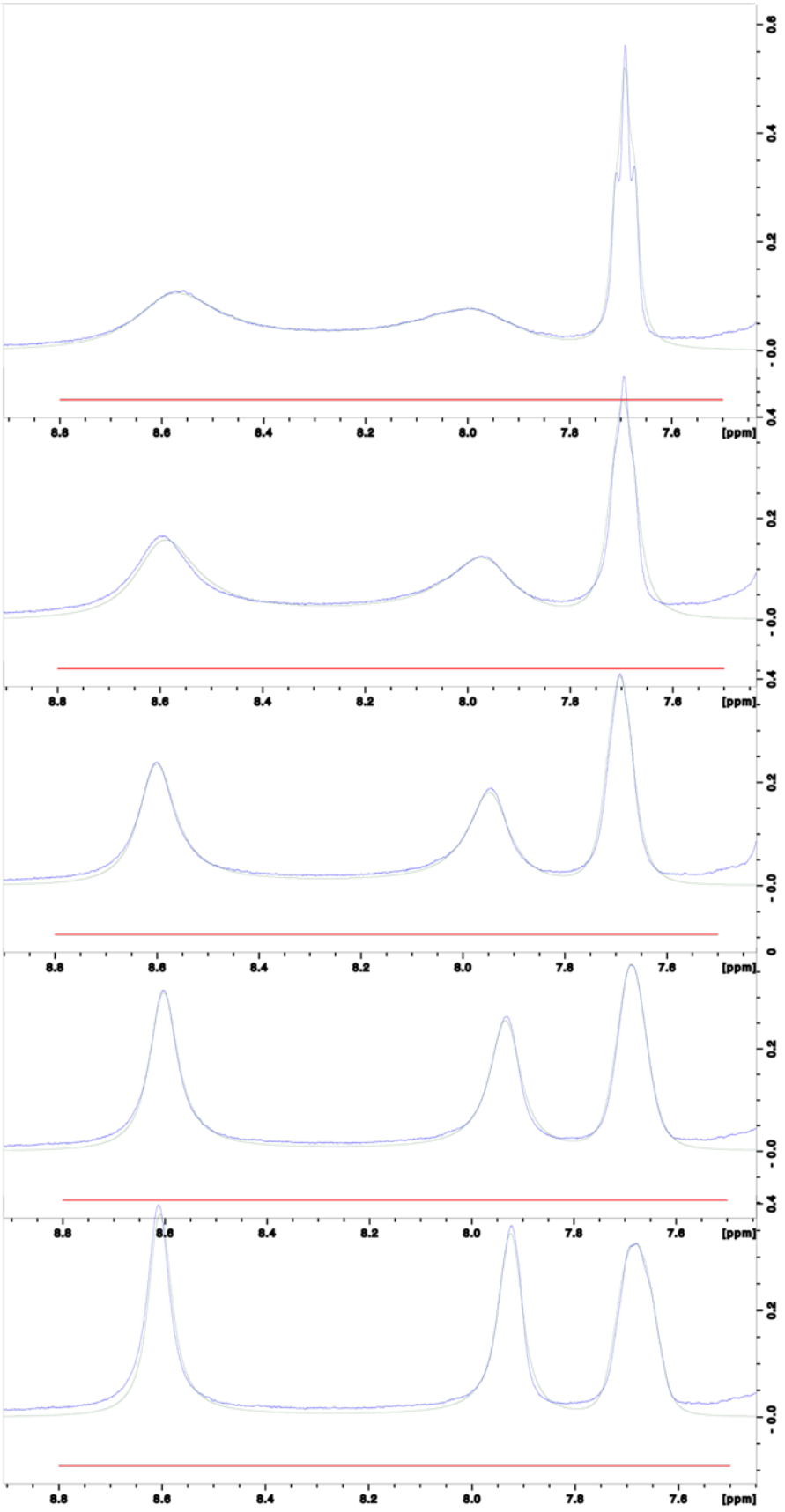

5 °C

–0 °C

–5 °C

–10 °C

–15 °C

Polymer Characterization

Macromonomers and small molecules monomers were characterized by GPC.

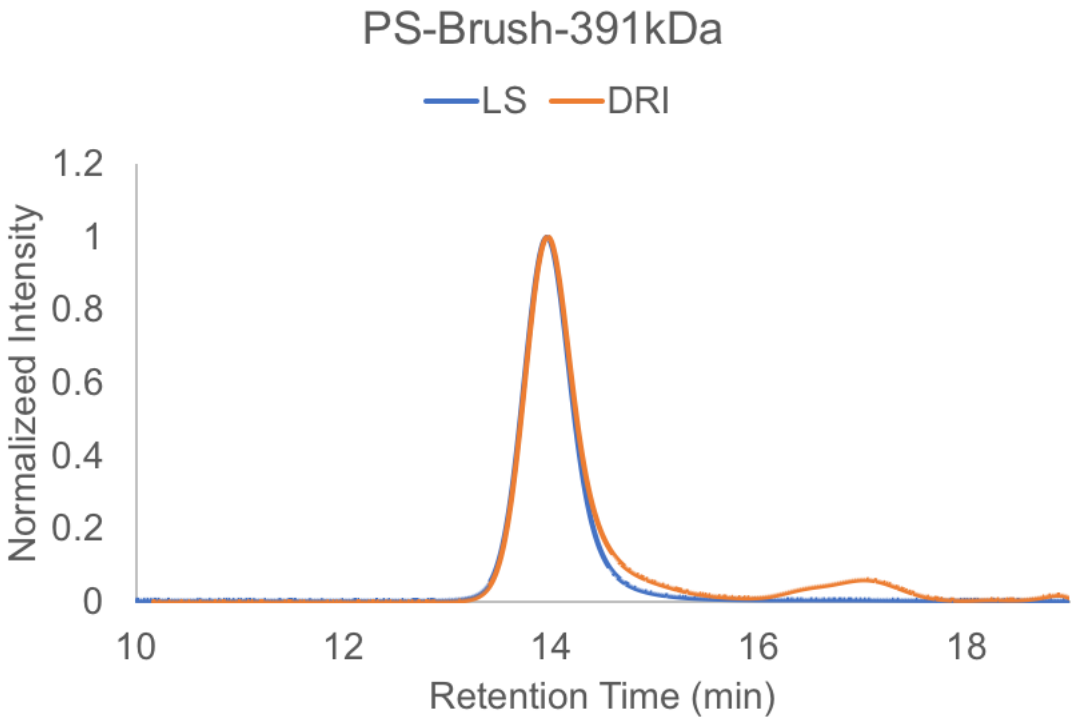

Figure S37. GPC trace for the ROMP of PS-MM with **6**.

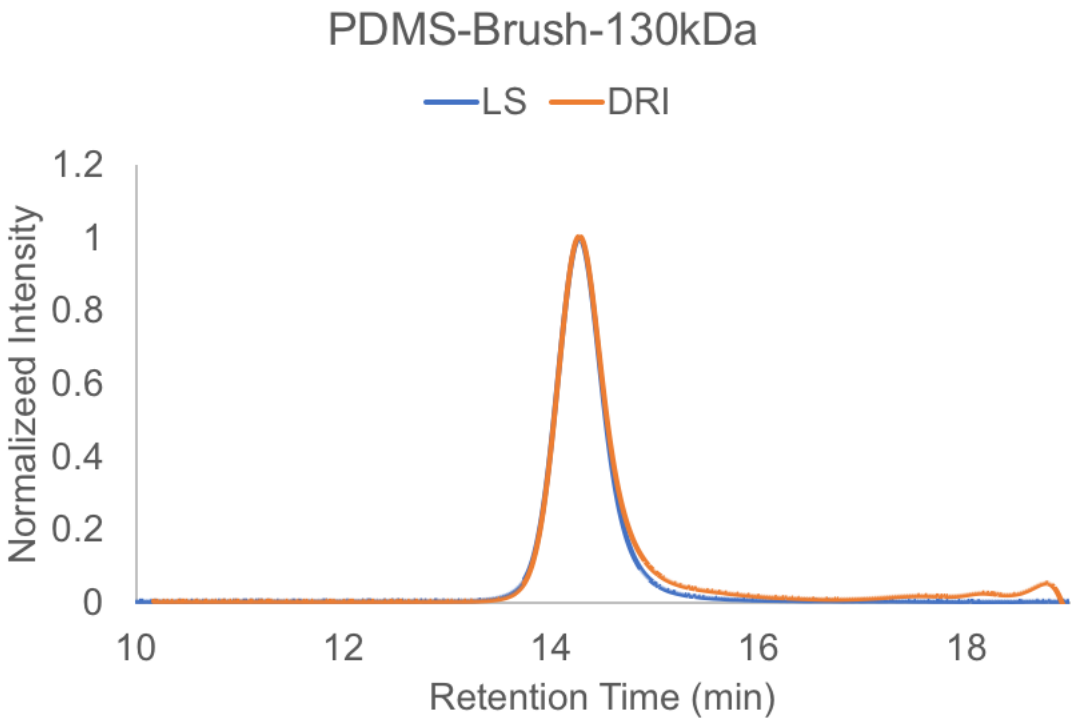

Figure S38. GPC trace for the ROMP of PDMS-MM with **6**.

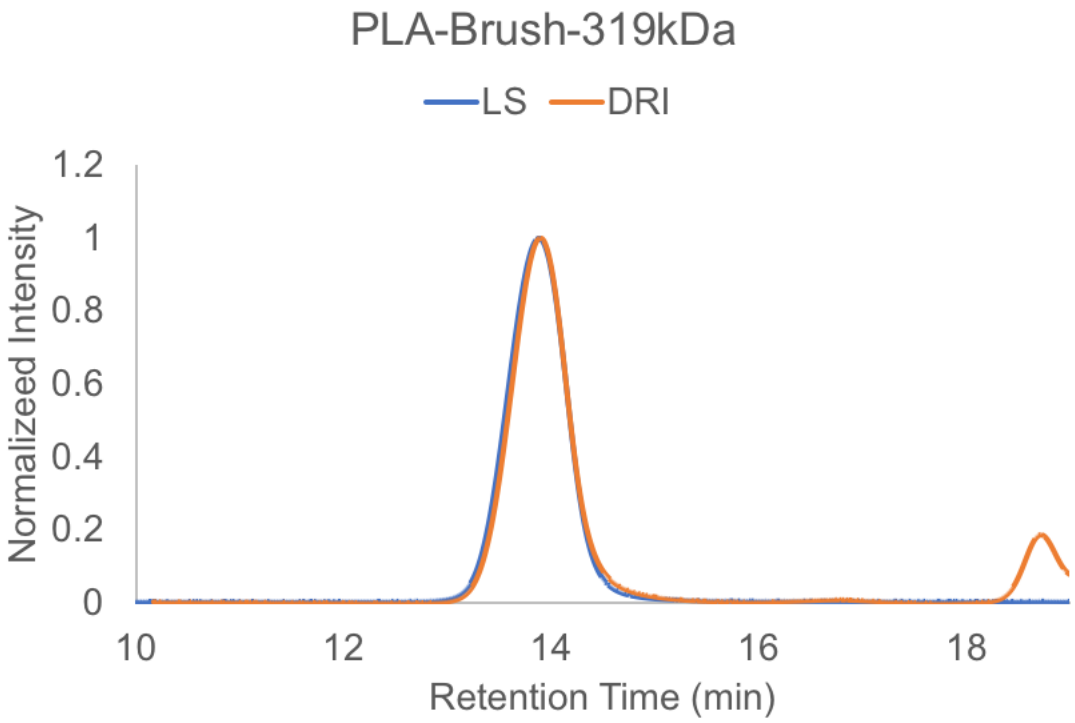

Figure S39. GPC trace for the ROMP of PLA-MM with **6**.

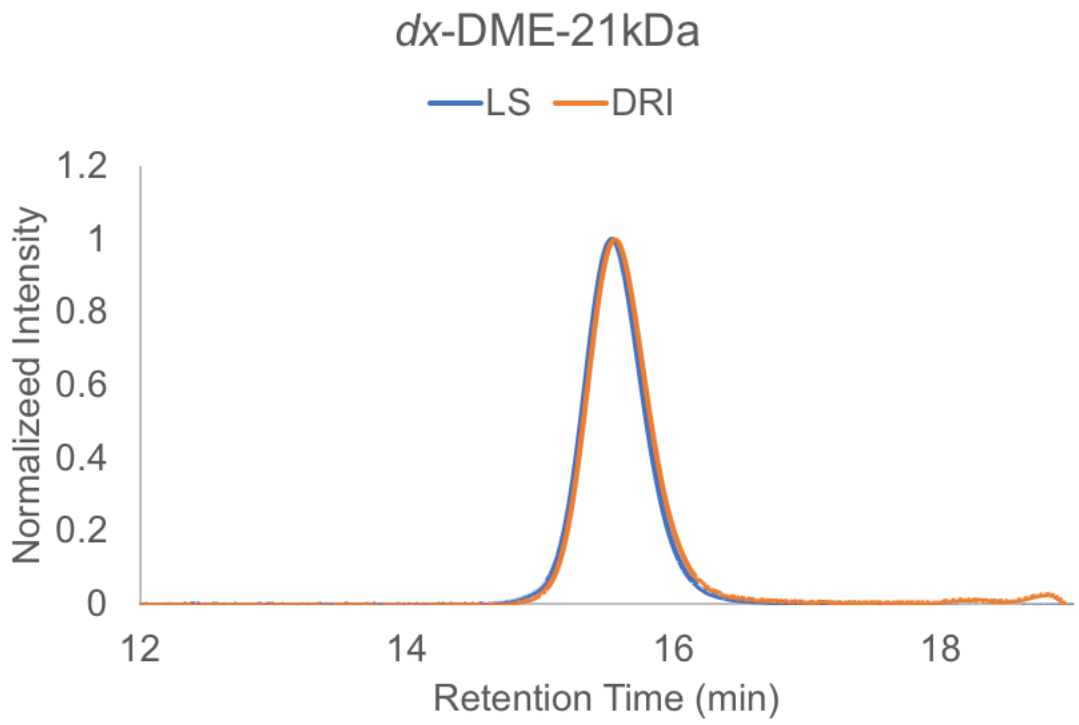

Figure S40. GPC trace for the ROMP of ***dx*-DME** with **6**.

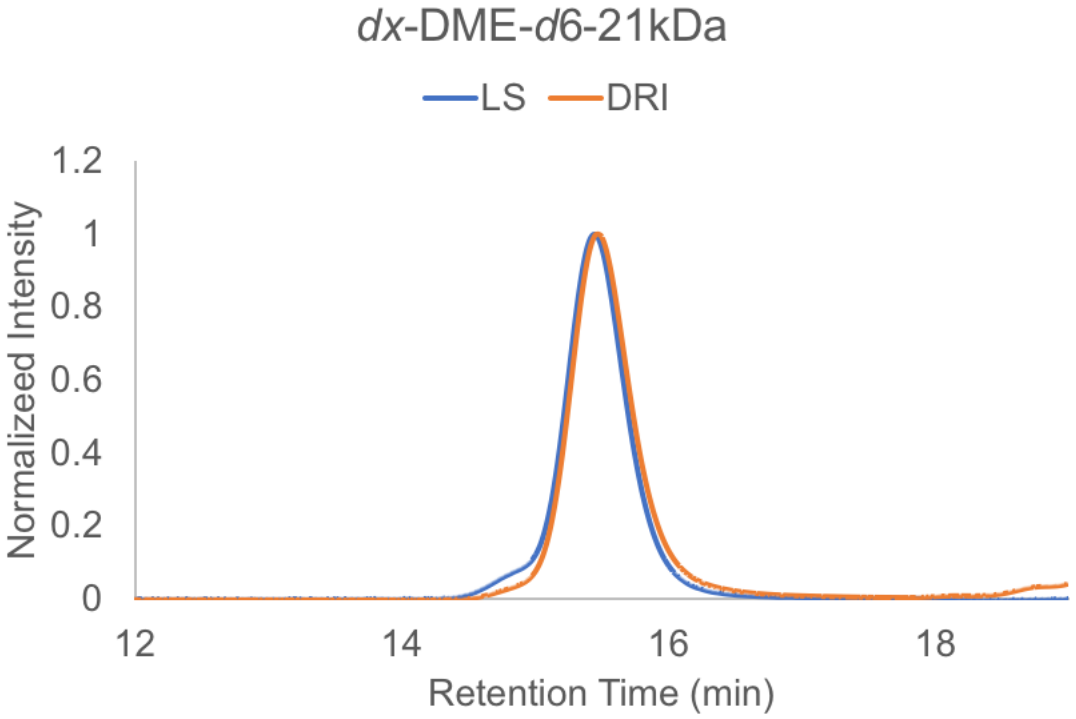

Figure S41. GPC trace for the ROMP of ***dx*-DME-d_6** with **6**.

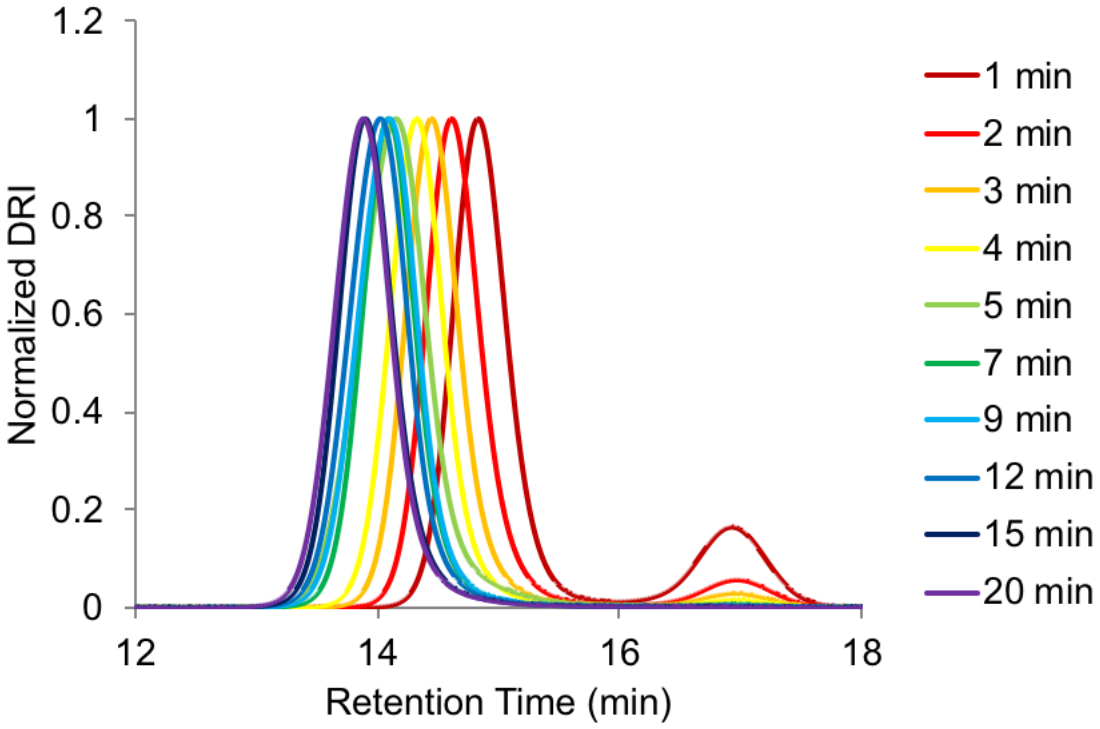

Figure S42. GPC analysis of the polymerization of PS-MM using **6**.

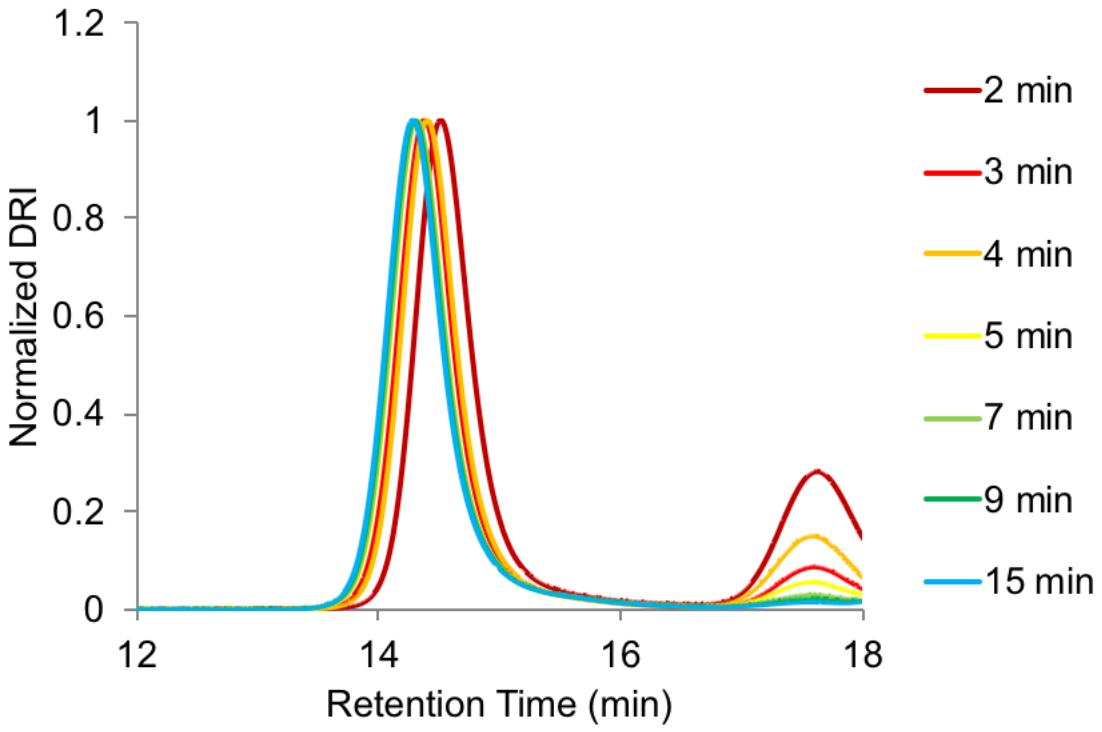

Figure S43. GPC analysis of the polymerization of PDMS-MM using **6**.

Table S5. GPC data collected for norbornene monomers polymerized using **6** in CH_2Cl_2.

Monomer	Target Mn	DP	Measured Mn	Measured Mw	Đ (Mw/Mn)
dx-DME	21.0 kDa	100	21.6 kDa	21.9 kDa	1.02
xx-DME	21.0 kDa	100	22.1 kDa	22.3 kDa	1.01
dd-DME	21.0 kDa	100	21.1 kDa	21.5 kDa	1.02
xx-NMI	17.7 kDa	100	17.2 kDa	17.4 kDa	1.01
dd-NMI	17.7 kDa	100	18.2 kDa	18.4 kDa	1.01
xx-NPI	23.9 kDa	100	24.5 kDa	24.7 kDa	1.02
x-ME	15.2 kDa	100	15.8 kDa	16.3 kDa	1.03
x-MOM	13.8 kDa	100	14.1 kDa	14.5 kDa	1.03
dx-D^{t}BE	29.4 kDa	100	30.0 kDa	30.6 kDa	1.02
dd-DMN	12.2 kDa	100	12.2 kDa	12.4 kDa	1.02
PS (3.91 kDa)	391 kDa	100	305 kDa	334 kDa	1.10
PLA (3.16 kDa)	316 kDa	100	274 kDa	281 kDa	1.03
PDMS (1.3 kDa)	130 kDa	100	121 kDa	127 kDa	1.05

Kinetic Data

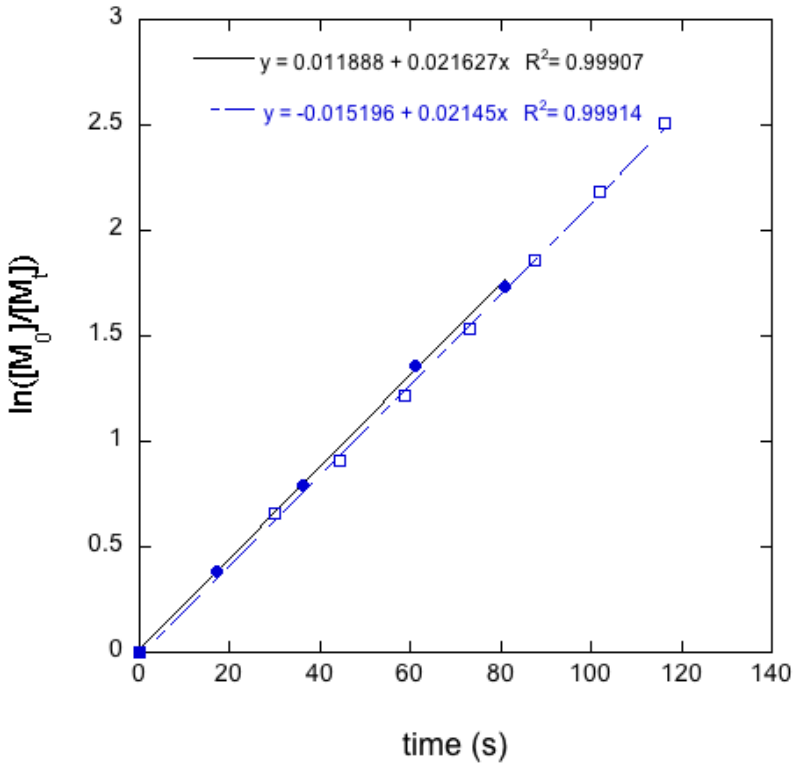

Figure S44. Plot of ln([M0]/[Mt]) against time for the polymerization of ***xx*-NMI** with **6** as monitored by NMR (□) or by taking aliquots from a batch reaction (•).

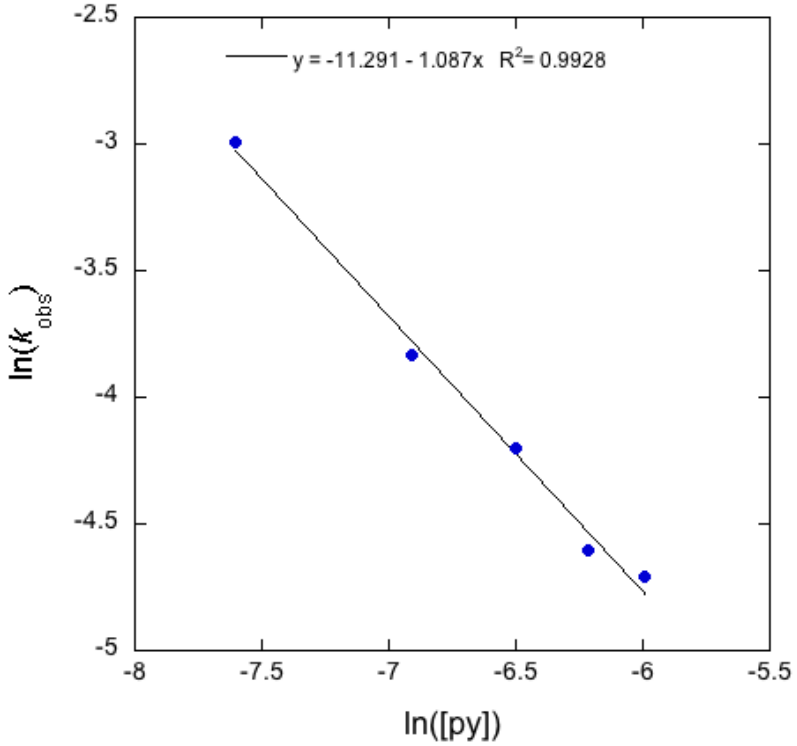

Figure S45. Plot of ln[py] against lnk_{obs} for the polymerization of ***xx*-NMI** with **6** showing inverse first-order dependence on [py].

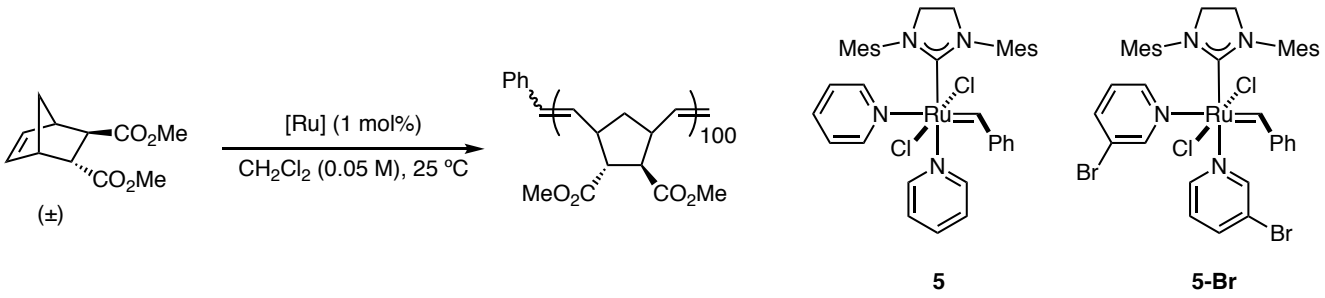

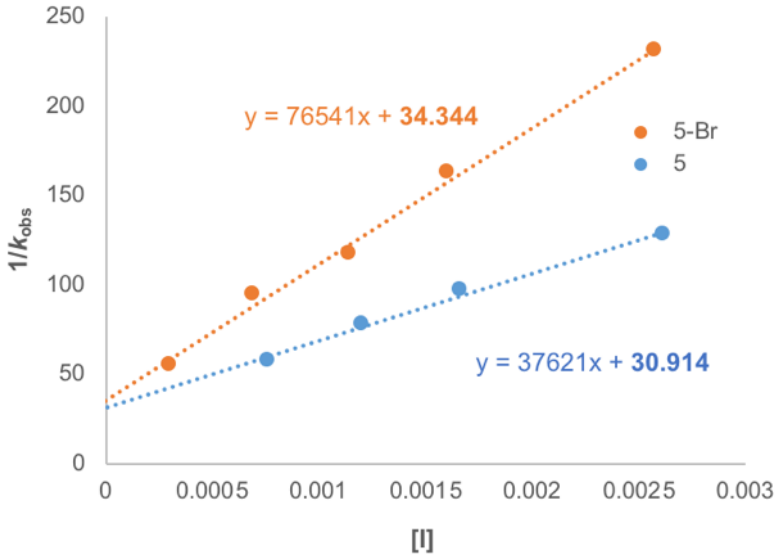

Figure S46. Plot of $1/k_{obs}$ against [I] (I = pyridine, 3-bromopyridine) for polymerization of *dx*-DME with **5** and **5-Br**. The non-zero y-intercept supports the intermediacy of the chelated Ru species in the absence of any ligand.

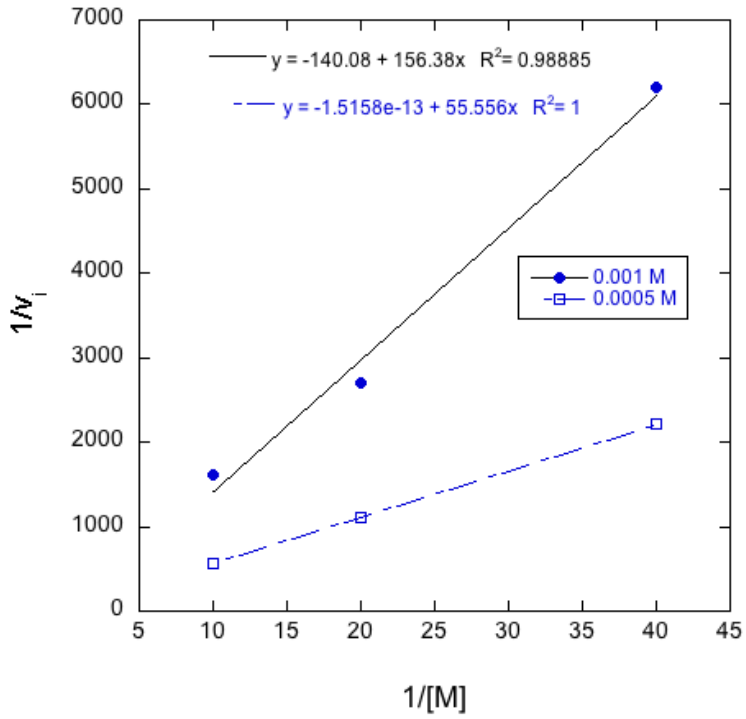

Figure S47. Double reciprocal plot for the polymerization of ***xx*-NMI** with **5**.

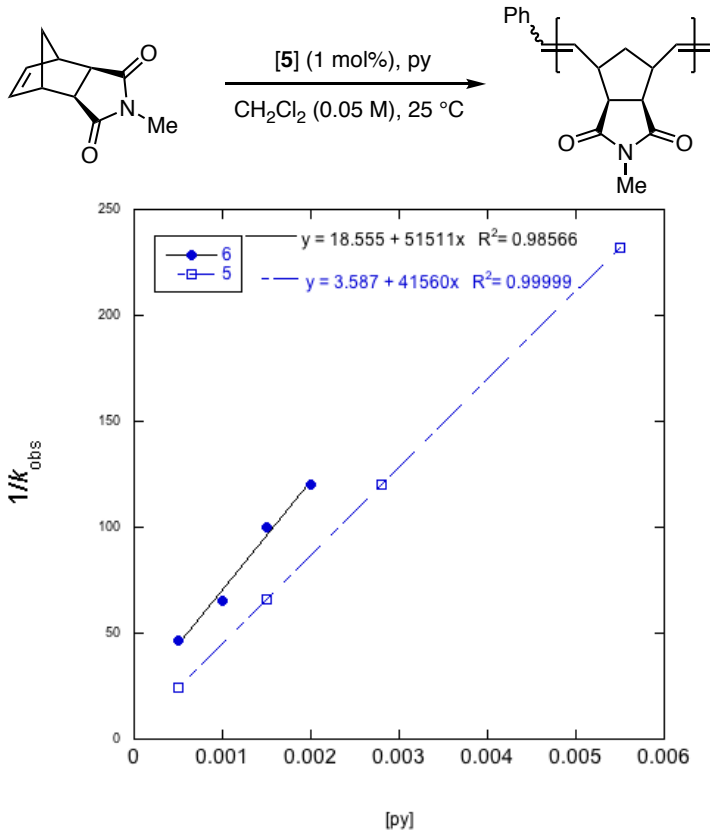

Figure S48. Plot of $1/k_{obs}$ against [py] for the polymerization of *xx*-NMI with **5** or **6** in the presence of pyridine. The y-intercept is near zero, implicating the lack of a chelated Ru state.

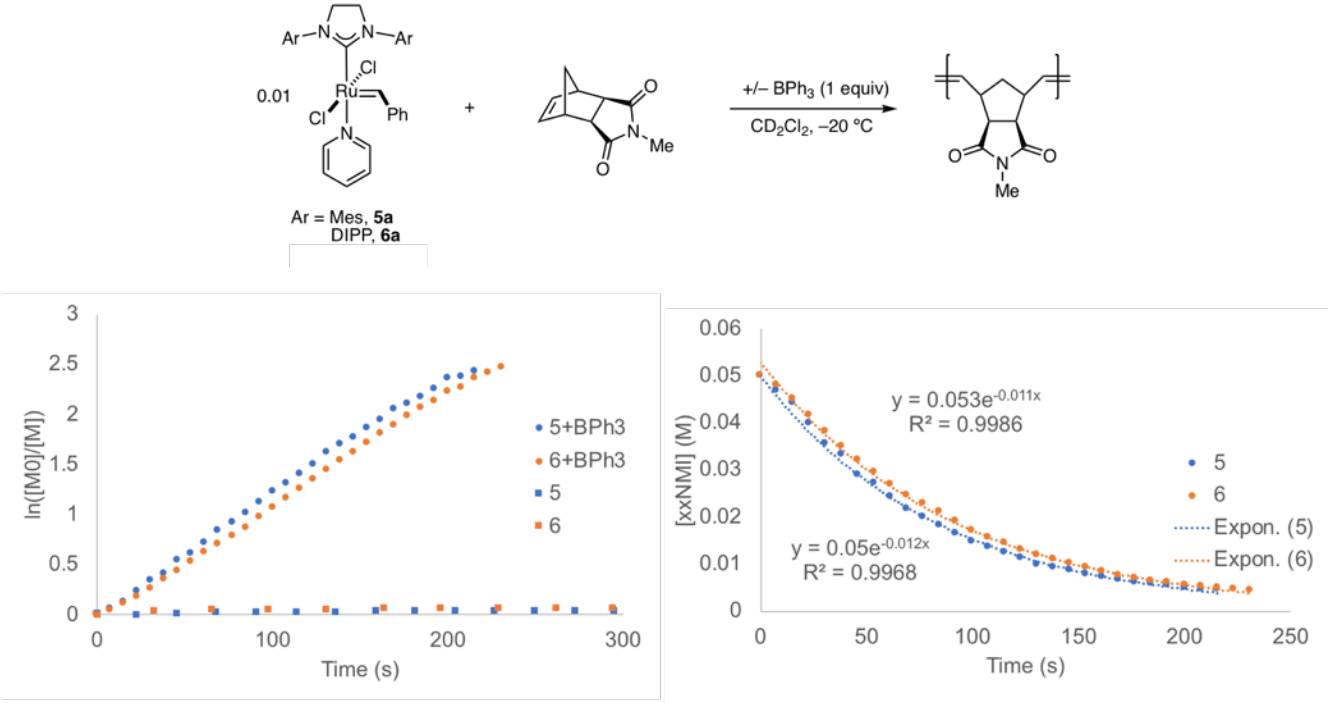

Figure S49. Polymerization of ***xx*-NMI** with **5a** or **6a** at –20 °C in the presence or absence of BPh_3 to trap the pyridine ligand. The observed rate constants for polymerization were identical for both catalysts.

Initiation Rates at 0 °C

A solution of Ru catalyst (45mM, 0.2 mL) was added to an oven dried NMR tube, sealed with a rubber septum and secured with vinyl tape. The tube was cooled to –78 °C in a dry ice/acetone bath and a solution of the desired monomer (333 mM, 0.3 mL) was added by syringe. The tube was quickly inverted to mix and inserted into the NMR spectrometer. An automated data acquisition program collected ^{1}H spectra at regular intervals. The consumption of the Ru catalysts was monitored by integrating the benzylidene signal and fit to a first-order function.

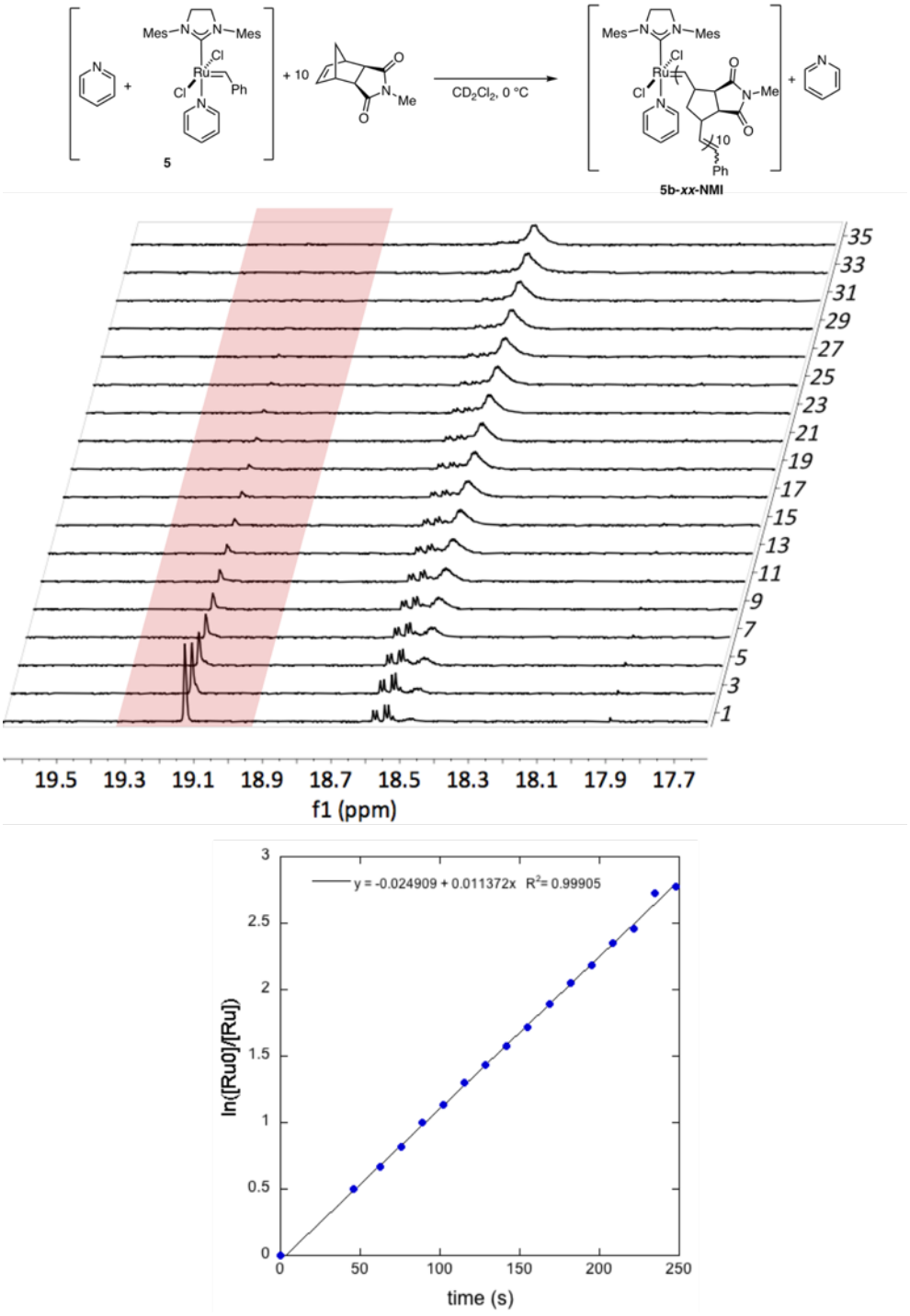

Figure S50. Initiation of **5** with *xx*-NMI in CD_2Cl_2 at 0 °C.

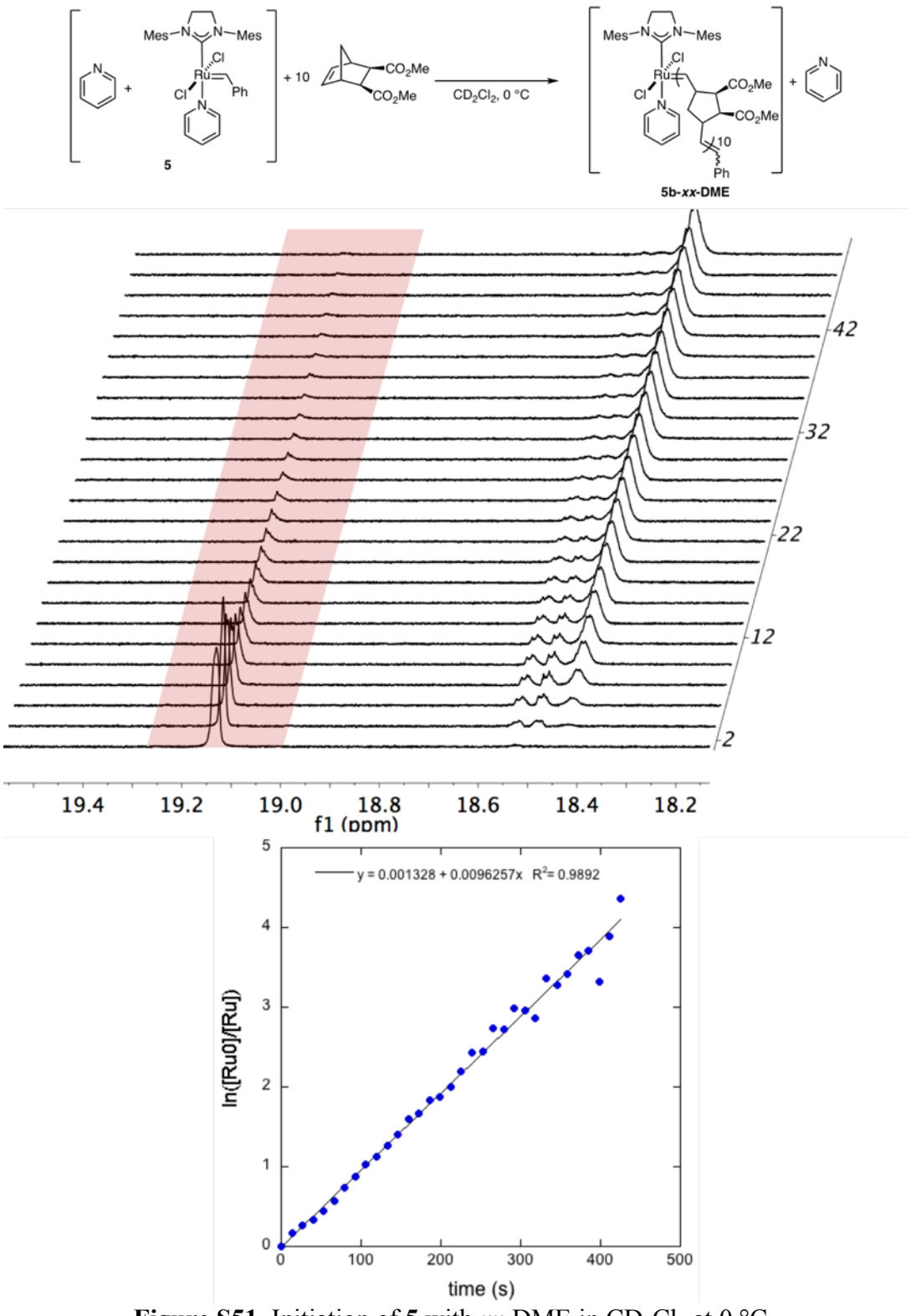

Figure S51. Initiation of **5** with *xx*-DME in CD_2Cl_2 at 0 °C.

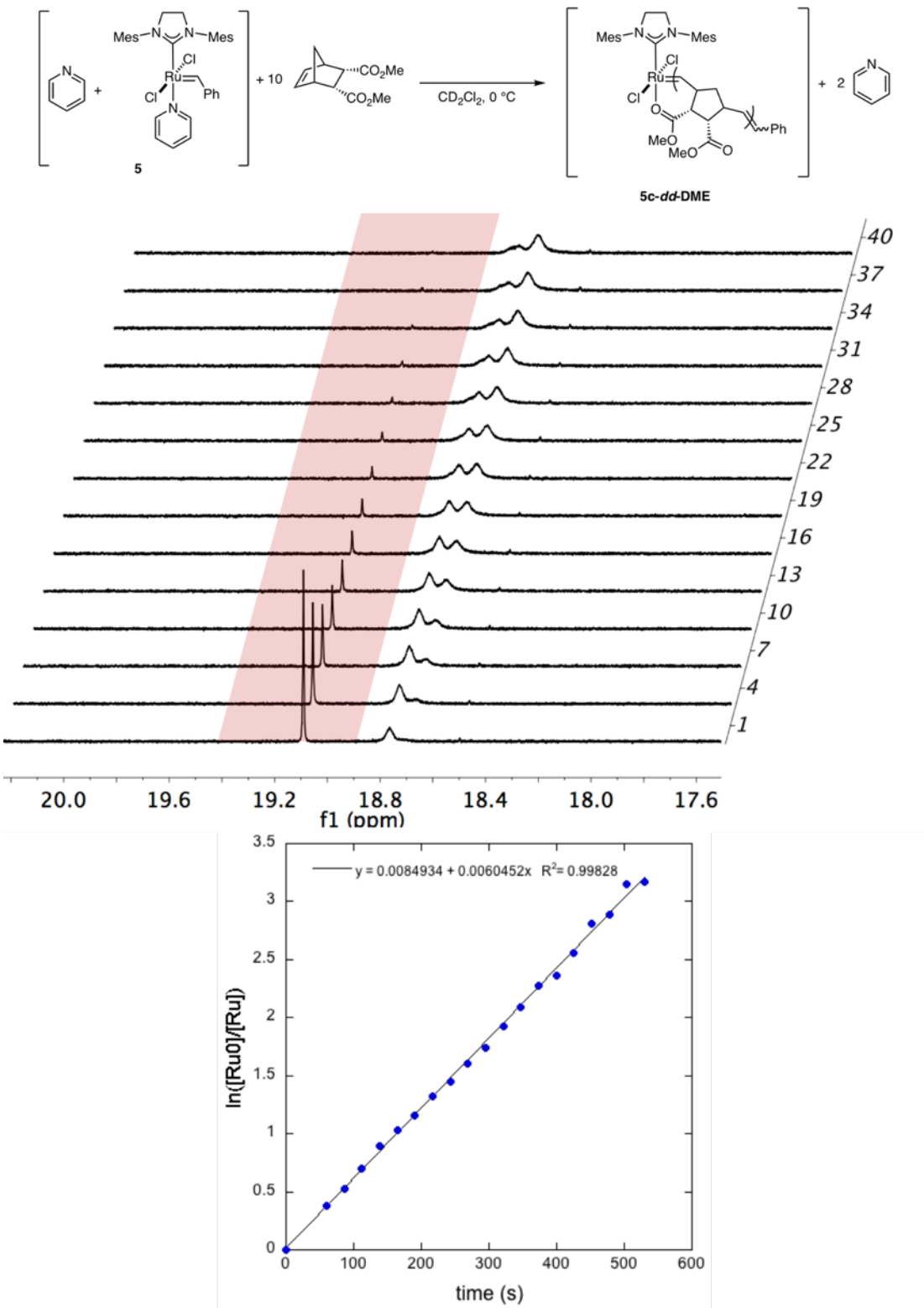

Figure S52. Initiation of **5** with *dd*-DME in CD_2Cl_2 at 0 °C.

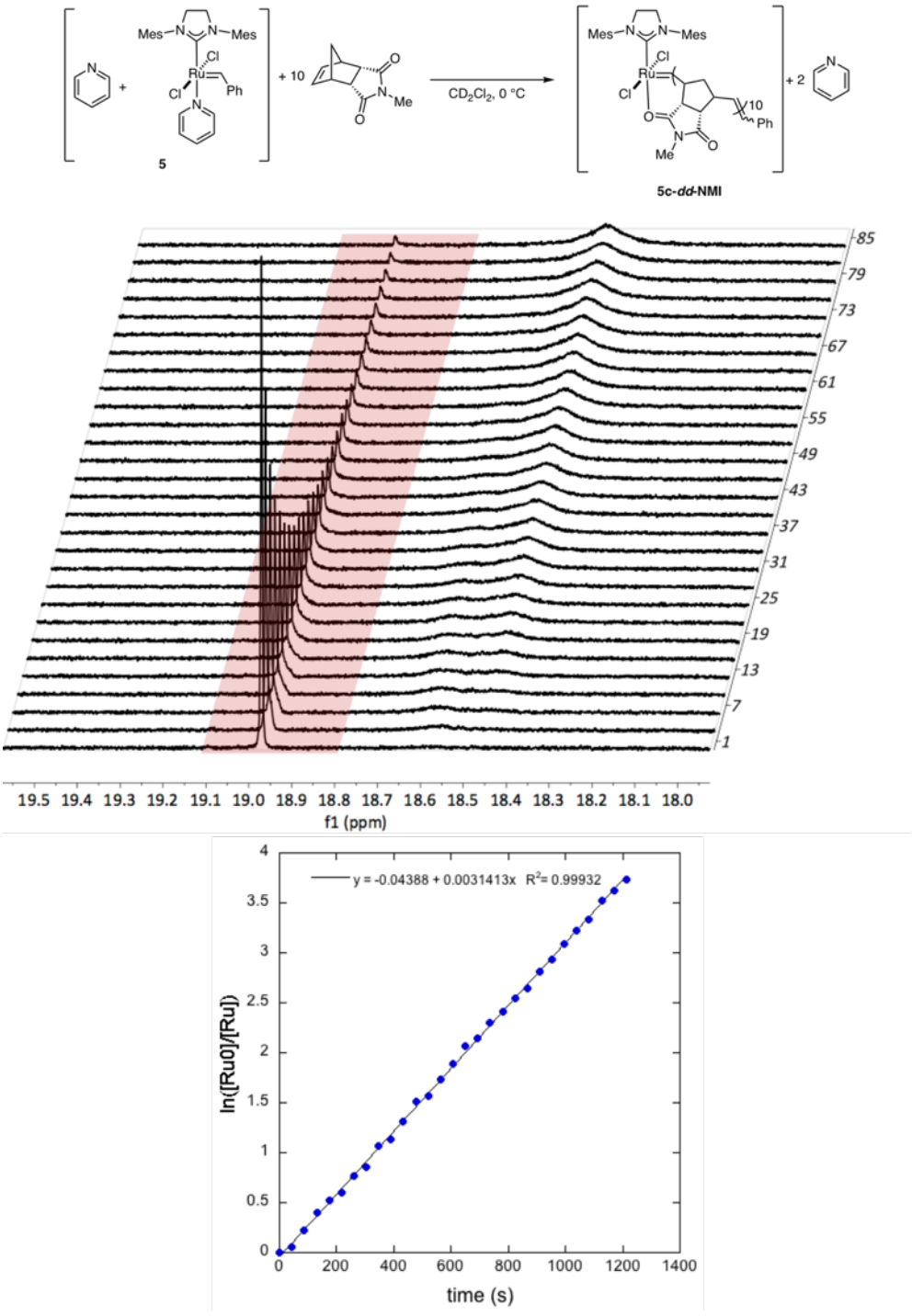

Figure S53. Initiation of **5** with *dd*-NMI in CD_2Cl_2 at 0 °C.

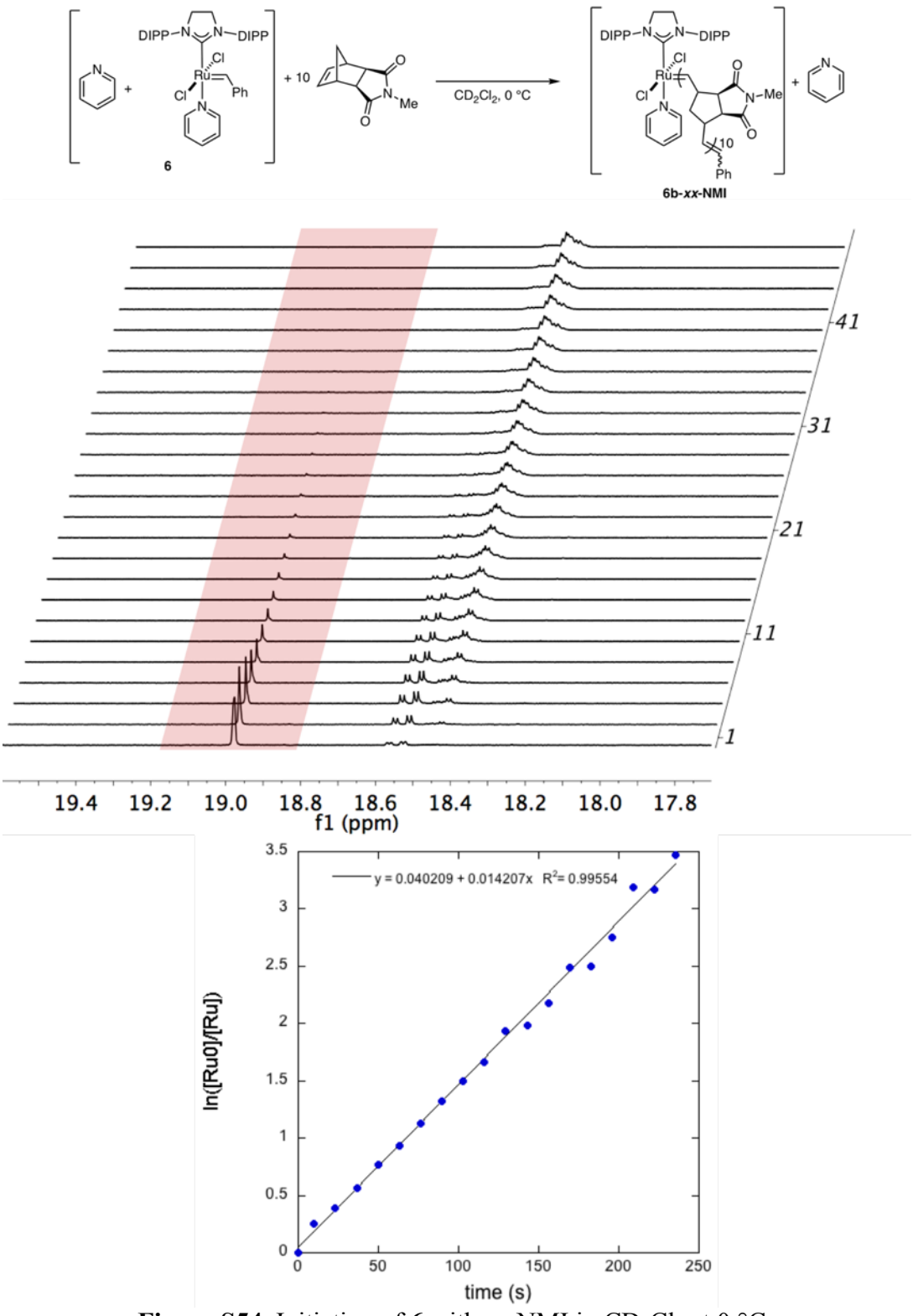

Figure S54. Initiation of **6** with *xx*-NMI in CD_2Cl_2 at 0 °C.

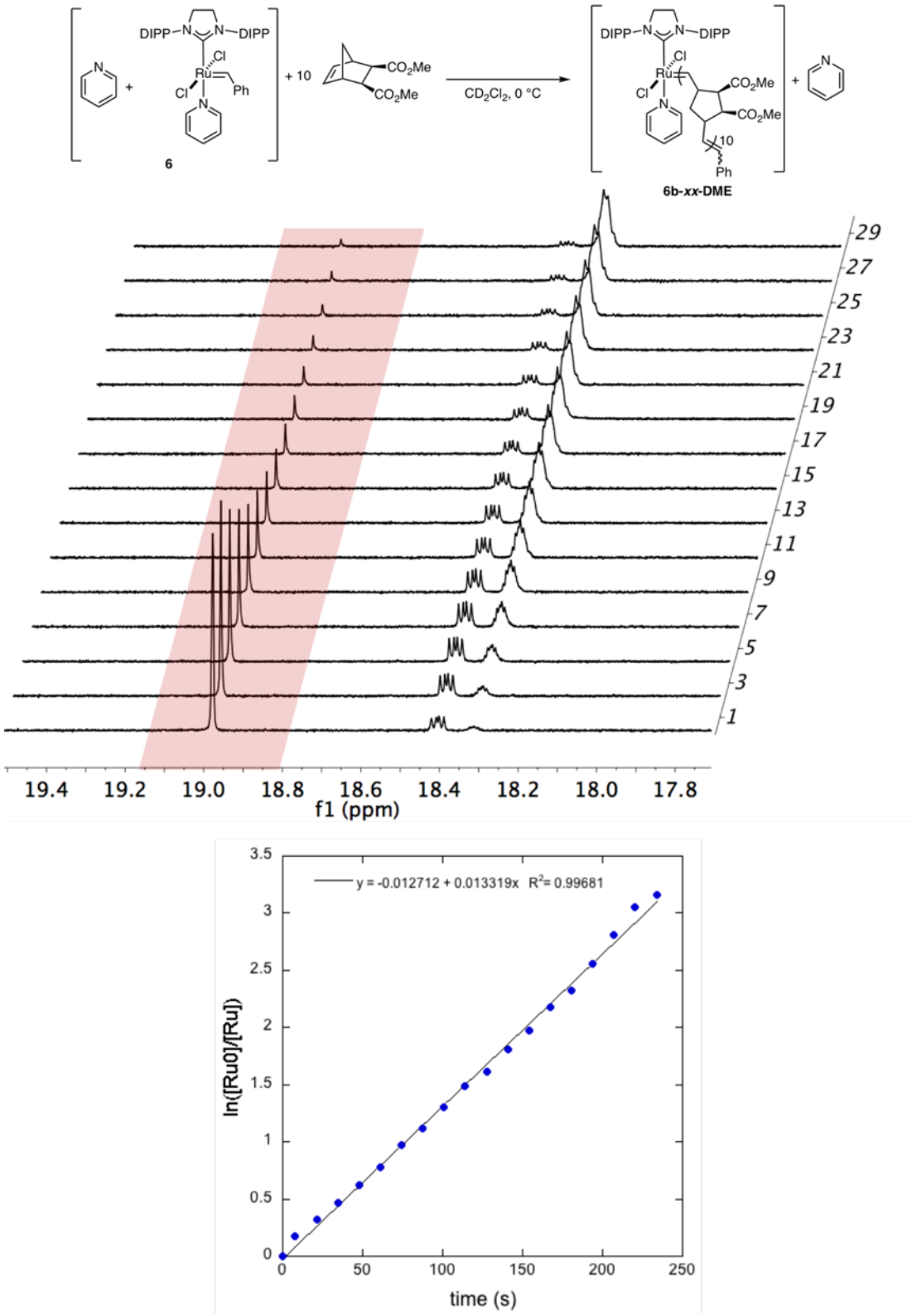

Figure S55. Initiation of **6** with *xx*-DME in CD_2Cl_2 at 0 °C.

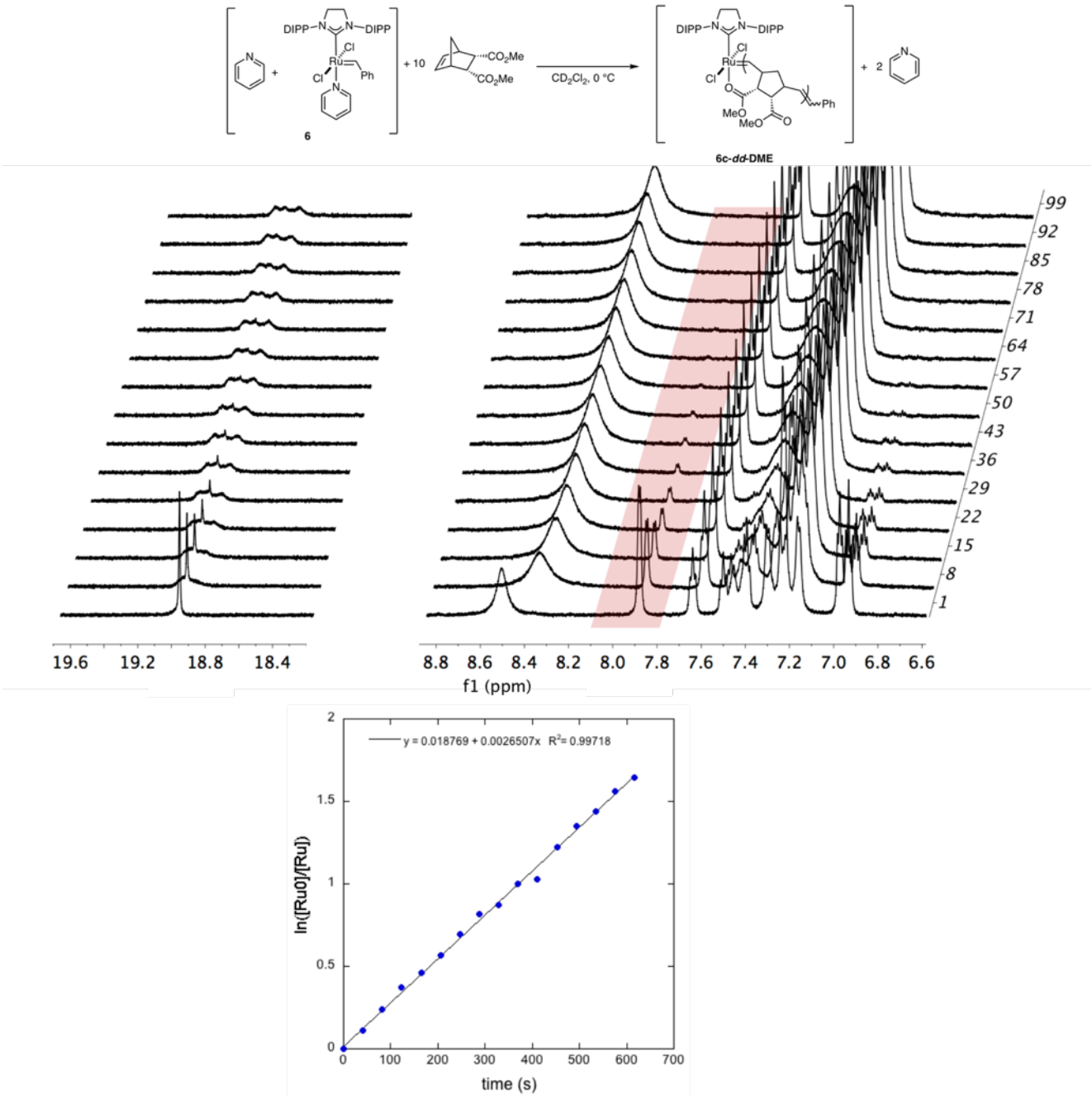

Figure S56. Initiation of **6** with *dd*-DME in CD_2Cl_2 at 0 °C. The signal for the benzylidene of **6** (19 ppm) overlapped with the signal of the alkylidene of **6c-*dd*-DME** (19 ppm) and so the consumption of **6** was monitored by using the signal for the bound pyridine ligand (7.9 ppm).

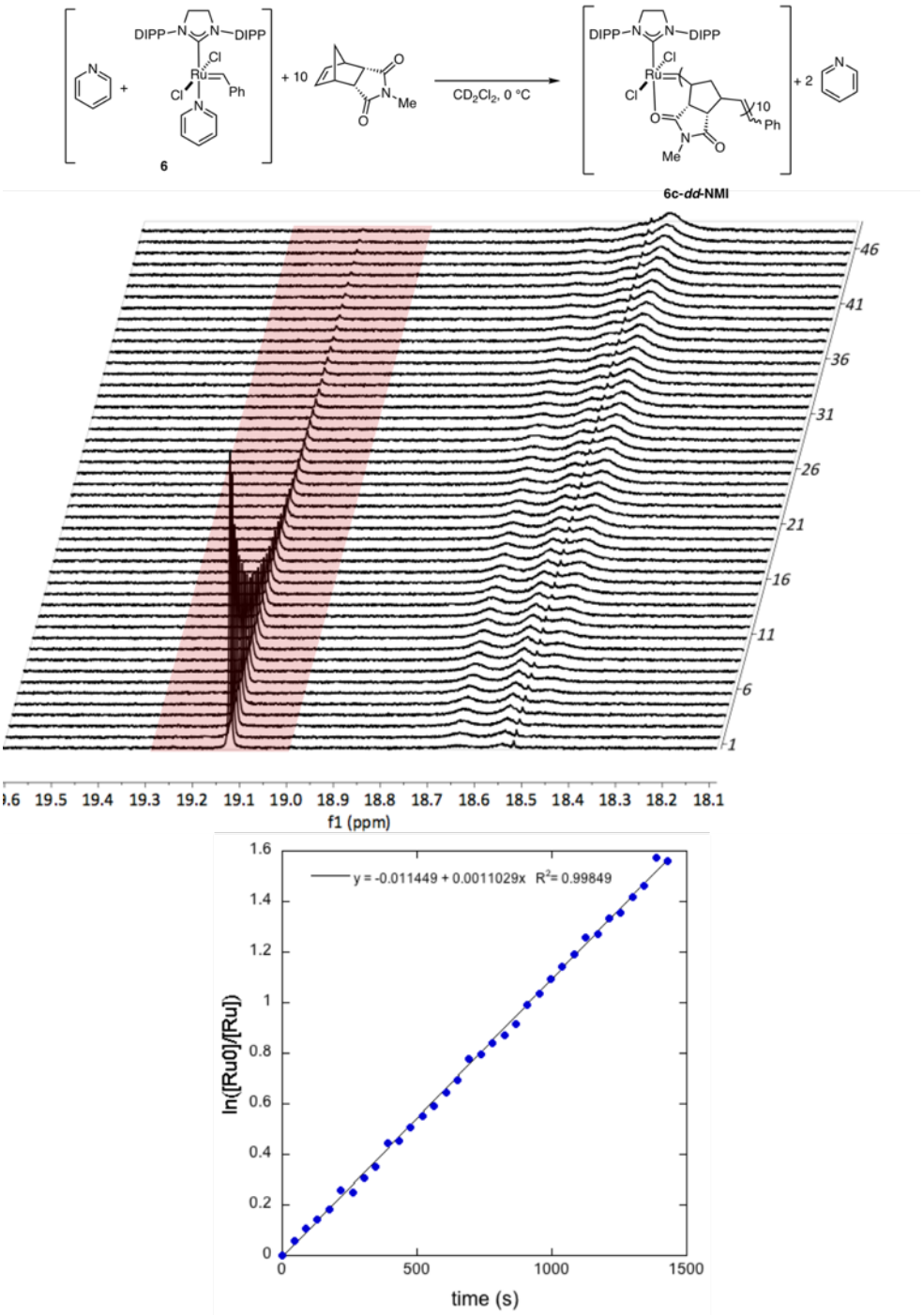

Figure S57. Initiation of **6** with *dd*-NMI in CD_2Cl_2 at 0 °C.

Cross-over experiments

A solution of Ru catalyst (45mM, 0.5 mL) was added to vial containing the first monomer (225 mmol) and shaken to mix. The reaction mixture was transferred to an oven dried NMR tube (0.2 mL), sealed with a rubber septum and secured with vinyl tape. The tube was cooled to –78 °C in a dry ice/acetone bath and a solution of the second monomer (333 mM, 0.3 mL, final volume 0.5 mL, [Ru] = 18 mM) was added by syringe. The tube was quickly inverted to mix and inserted into the NMR spectrometer. An automated data acquisition program collected ^{1}H spectra at regular intervals.

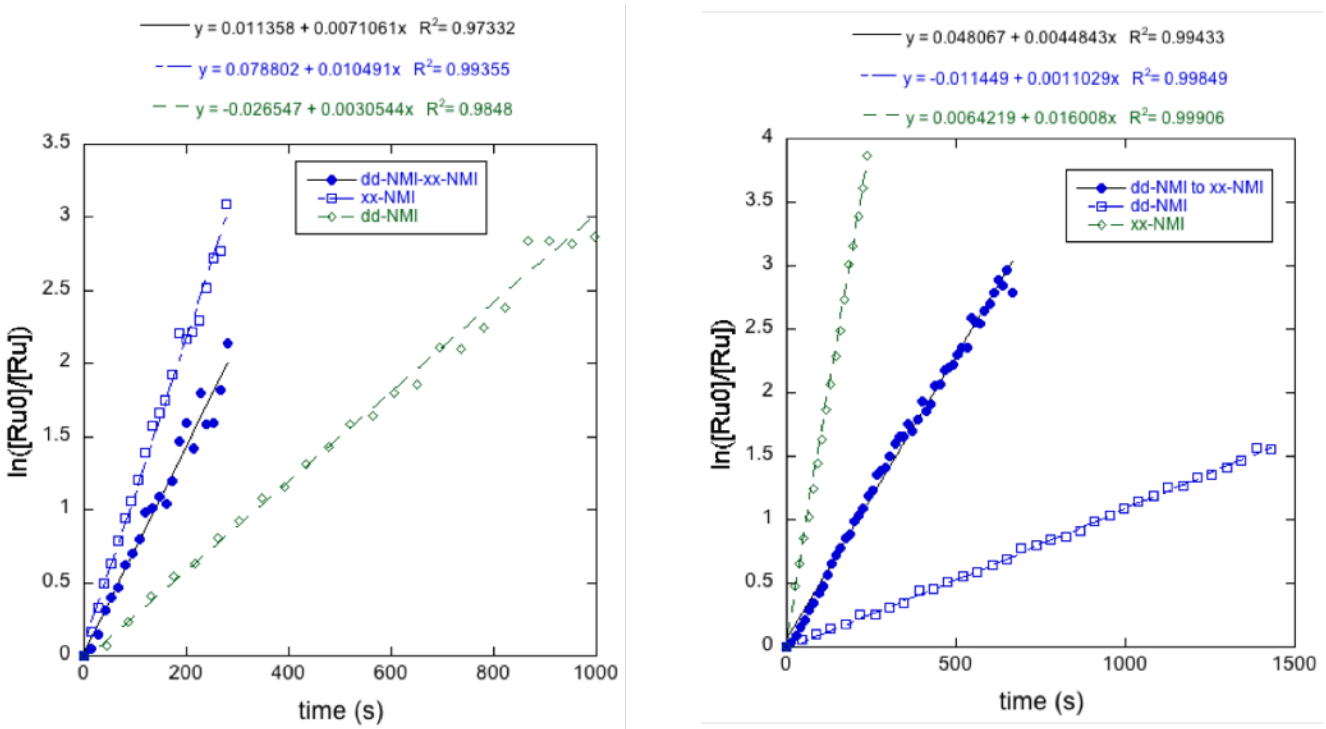

Figure S58. Plots of ln([Ru$_0$]/[Ru$_t$]) versus T for **5** (left) and **6** (right) showing relative rates for the initiation of each catalyst with *xx*-NMI (steeper line), *dd*-NMI (shallower line), and the reaction between **5-*dd*-NMI** or **6-*dd*-NMI** and *xx*-NMI (middle line).

Eyring Analysis

The rate of polymerization of *xx*-NMI was measured according to the methods for kinetic measurements by ^{1}H NMR. The Ru catalysts were injected at low temperature using a dry-ice acetone bath, and the NMR tubes were quickly transferred to the precooled NMR probe and monitored using an automated data acquisition sequence to record ^{1}H NMR spectra at regular intervals. The ROMP in the presence of acid was conducted with 10 equiv of acid relative to [**5**].

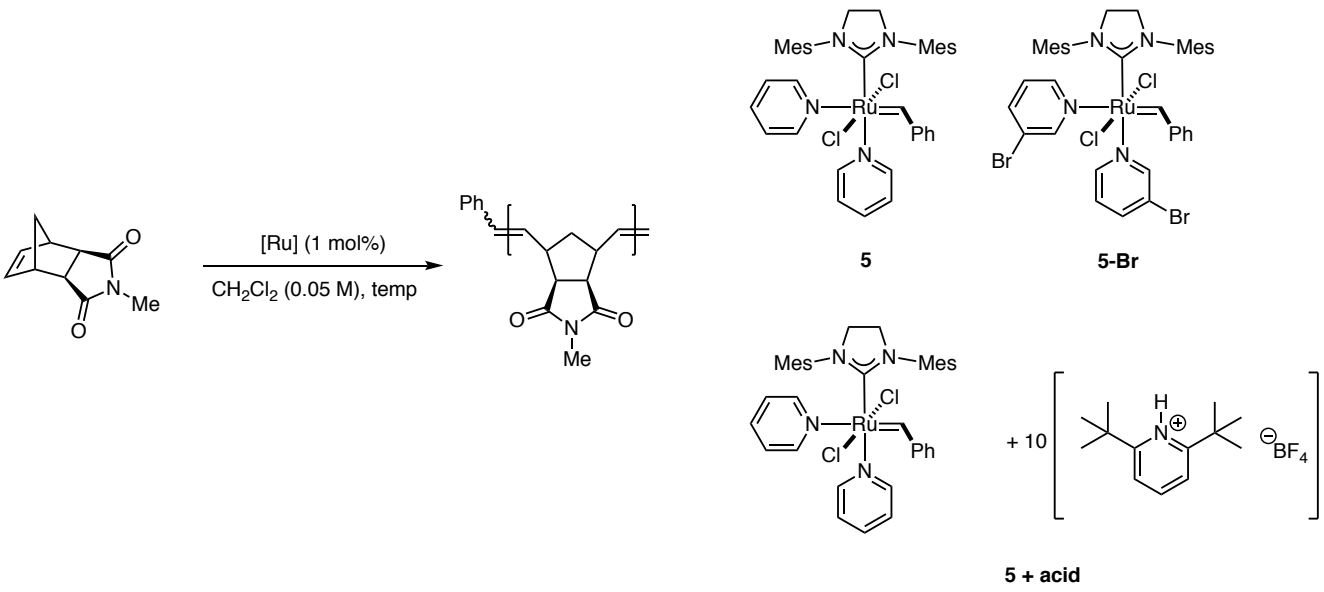

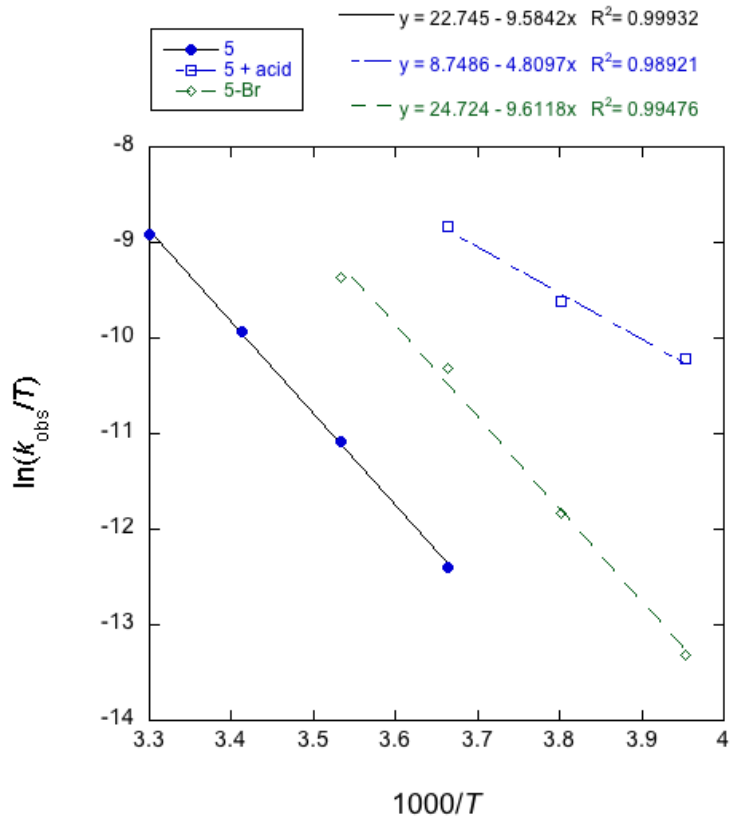

Figure S59. Temperature profiles for the polymerization of *xx*-NMI with **5** (•), **5** in the presence of 2,6-di*tert*butylpyridium tetrafluoroborate (□) and **5-Br** (◇).

Table S6

	5	**5-Br**	**5** + acid
Delta H	19.0 ± 0.4kcal/mol	19.0 ± 1 kcal/mol	9.5 ± 1 kcal/mol
Delta S	–8 ± 5 J/mol•K	8 ± 15 J/mol•K	–124 ±15 J/mol•K

Eyring analysis determined activation parameters for the ROMP of ***xx*-NMI**. The calculated values are composites that reflect every step of the reaction coordinate. For **5-Br** and **5**, the activation parameters are nearly identical, with entropies of activation near zero, consistent with a more favorable ligand dissociation step, prior to olefin binding and cycloaddition. When ***xx*-NMI** is polymerized with **5** in the presence of acid, the pyridine ligands are protonated and so the mechanism simplifies to an associative monomer coordination step and subsequent cycloaddition (K_3 and k_4 in the cycle below): the resulting entropy of activation is much more negative, reflecting this truncated mechanism. For the chelating monomer ***xx*-DME**, the activation entropies reflect the opening of the chelate ring and the monomer association and cycloaddition steps. The opening of the chelate ring is expected to have a much smaller entropic contribution compared to dissociation of pyridine, and so the composite values are more negative and more strongly reflect the monomer association step.

For the polymerization of ***xx*-DME** with **6**, the entropy of activation is smaller than that of **5**: the opening of the chelate ring is more costly since the polymer chain must rotate up into the bulkier aryl rings of **6**.

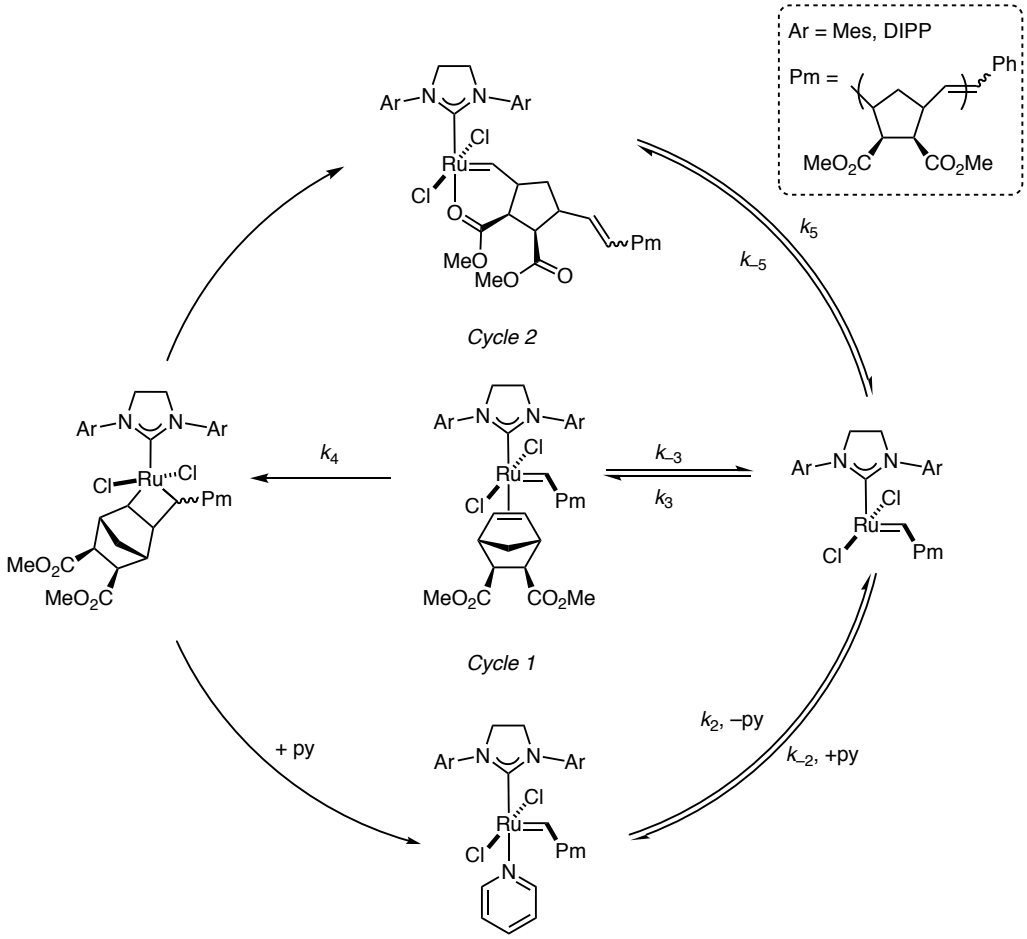

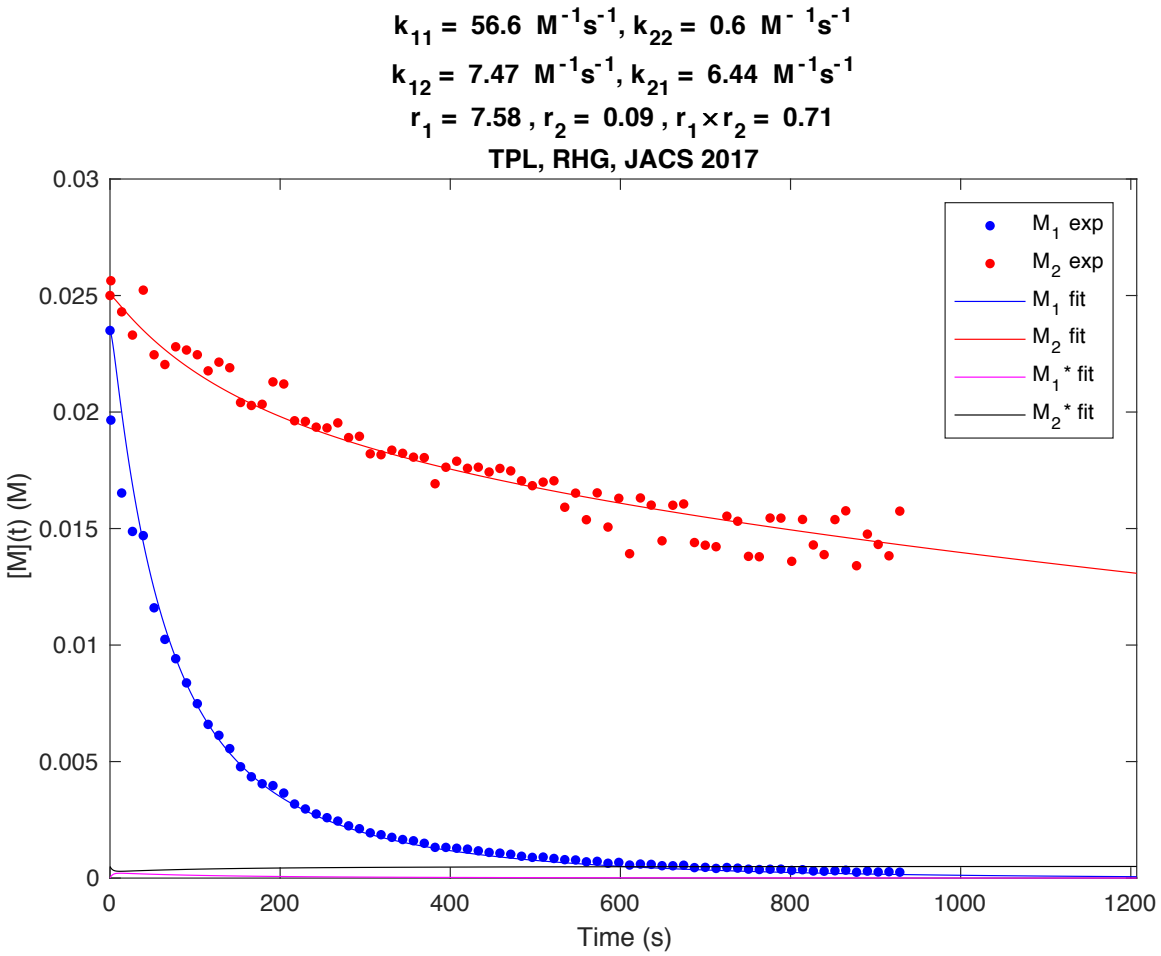

Figure S60. Non-linear least squares fitting to the copolymerization of ***xx*-NMI** and ***dd*-NMI** using **5**, fit using the MATLAB protocol outline by our group.[5]

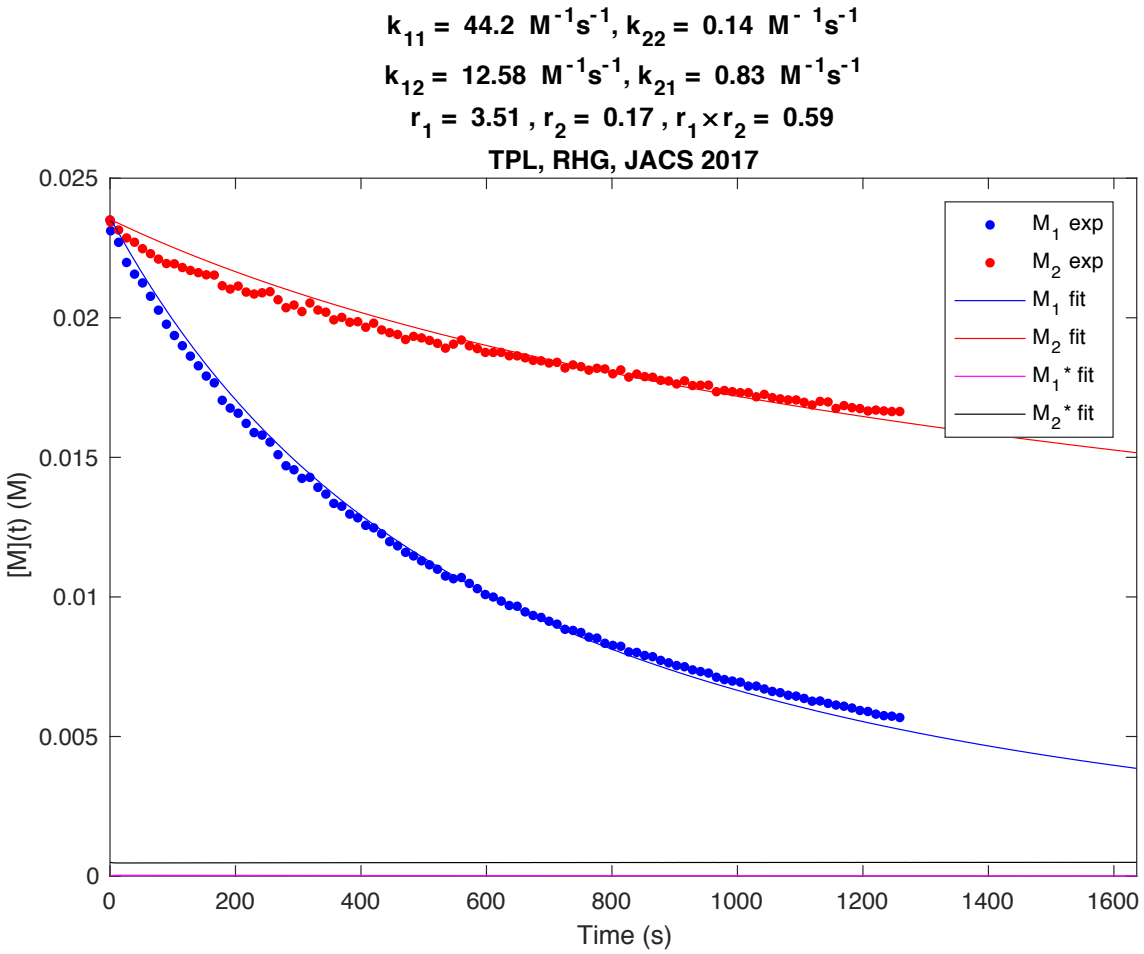

Figure S61. Non-linear least squares fitting to the copolymerization of ***xx*-NMI** and ***dd*-NMI** using **6**, fit using the MATLAB protocol outline by our group.[5]

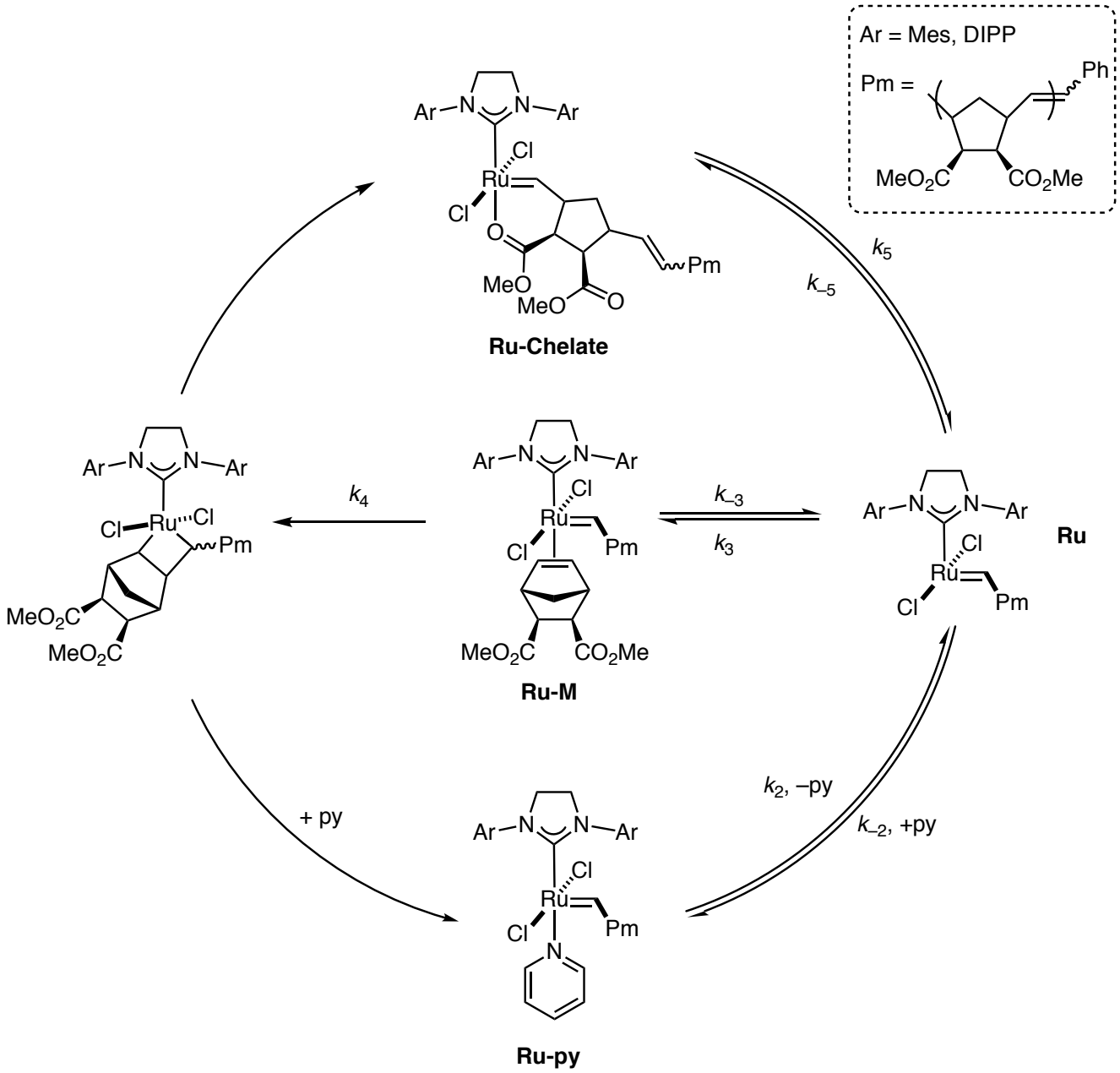

(1)

$$[Ru]_0 = [Ru\text{-}py] + [Ru\text{-}chelate] + [Ru] + [Ru\text{-}M]$$

(2)

$$\frac{-d[Ru]}{dt} = k_2[Ru\text{-}py] - k_{-2}[Ru][py] + k_5[Ru\text{-}chelate] - k_{-5}[Ru] - k_3[Ru][M] + k_{-3}[Ru\text{-}M] = 0$$

(3)

$$\frac{-d[Ru\text{-}py]}{dt} = -k_2[Ru\text{-}py] + k_{-2}[Ru][py] = 0$$

(4)

$$\frac{-d[Ru\text{-}Che]}{dt} = -k_5[Ru\text{-}che] + k_{-5}[Ru] = 0$$

(5)

$$\frac{-d[\text{Ru-M}]}{dt} = -k_4[\text{Ru-M}] + k_3[\text{Ru}][\text{M}] - k_{-3}[\text{Ru-M}] = 0$$

Solving for [Ru] in (5) and using the Michealis-Menten constant K_m:

(6)

$$[\text{Ru}] = \frac{k_4 + k_{-3}[\text{Ru-M}]}{k_3[\text{M}]} = \frac{K_m[\text{Ru-M}]}{[\text{M}]}$$

Combining (6) with (3) and (4) and solving for [Ru-py] and [Ru-Che] respectively:

$$\frac{-d[\text{Ru-py}]}{dt} = -k_2[\text{Ru-py}] + k_{-2}[\text{Ru}][\text{py}] = -k_2[\text{Ru-py}] + k_{-2}[\text{py}]\left(\frac{K_m[\text{Ru-M}]}{[\text{M}]}\right) = 0$$

$$[\text{Ru-py}] = \frac{k_{-2}}{k_2}\left(\frac{K_m[\text{Ru-M}]}{[\text{M}]}\right)[\text{py}] = \left(\frac{K_m[\text{Ru-M}]}{K_2[\text{M}]}\right)[\text{py}]$$

$$\frac{-d[\text{Ru-Che}]}{dt} = -k_5[\text{Ru-che}] + k_{-5}[\text{Ru}] = -k_5[\text{Ru-che}] + k_{-5}\left(\frac{K_m[\text{Ru-M}]}{[\text{M}]}\right) = 0$$

$$[\text{Ru-che}] = \frac{k_{-5}}{k_5}\left(\frac{K_m[\text{Ru-M}]}{[\text{M}]}\right) = \left(\frac{K_m[\text{Ru-M}]}{K_5[\text{M}]}\right)$$

Combining the terms for [Ru], [Ru-py], and [Ru-Che] into (1) so that everything is defined by [Ru-M]:

$$[\text{Ru}]_0 = [\text{Ru-py}] + [\text{Ru-chelate}] + [\text{Ru}] + [\text{Ru-M}]$$

$$[\text{Ru}]_0 = \left(\frac{K_m[\text{Ru-M}]}{K_2[\text{M}]}\right)[\text{py}] + \left(\frac{K_m[\text{Ru-M}]}{K_5[\text{M}]}\right) + \frac{K_m[\text{Ru-M}]}{[\text{M}]} + [\text{Ru-M}]$$

Factor [Ru-M]:

$$[\text{Ru}]_0 = \left(\frac{K_m[\text{py}]}{K_2[\text{M}]} + \frac{K_m}{K_5[\text{M}]} + \frac{K_m}{[\text{M}]} + 1\right)[\text{Ru-M}]$$

The common denominator is K_2K_5[M]:

$$[\text{Ru}]_0 = \left(\frac{K_m K_5[\text{py}]}{K_2 K_5[\text{M}]} + \frac{K_2 K_m}{K_2 K_5[\text{M}]} + \frac{K_2 K_5 K_m}{K_2 K_5[\text{M}]} + \frac{K_2 K_5[\text{M}]}{K_2 K_5[\text{M}]} \right) [\text{Ru-M}]$$

$$[\text{Ru}]_0 = \left(\frac{K_m K_5[\text{py}] + K_2 K_m + K_2 K_5 K_m + K_2 K_5[\text{M}]}{K_2 K_5[\text{M}]} \right) [\text{Ru-M}]$$

Rearranging to solve for [Ru-M]:

$$[\text{Ru-M}] = \left(\frac{K_2 K_5[\text{M}]}{K_m K_5[\text{py}] + K_2 K_m + K_2 K_5 K_m + K_2 K_5[\text{M}]} \right) [\text{Ru}]_0$$

The rate limiting step is k_4[Ru-M] so the rate law is then:

$$\frac{-\text{d}[\text{M}]}{\text{dt}} = \frac{k_4 K_2 K_5 [\text{Ru}]_0 [\text{M}]}{K_m K_5[\text{py}] + K_2 K_m + K_2 K_5 K_m + K_2 K_5[\text{M}]}$$

NMR spectra

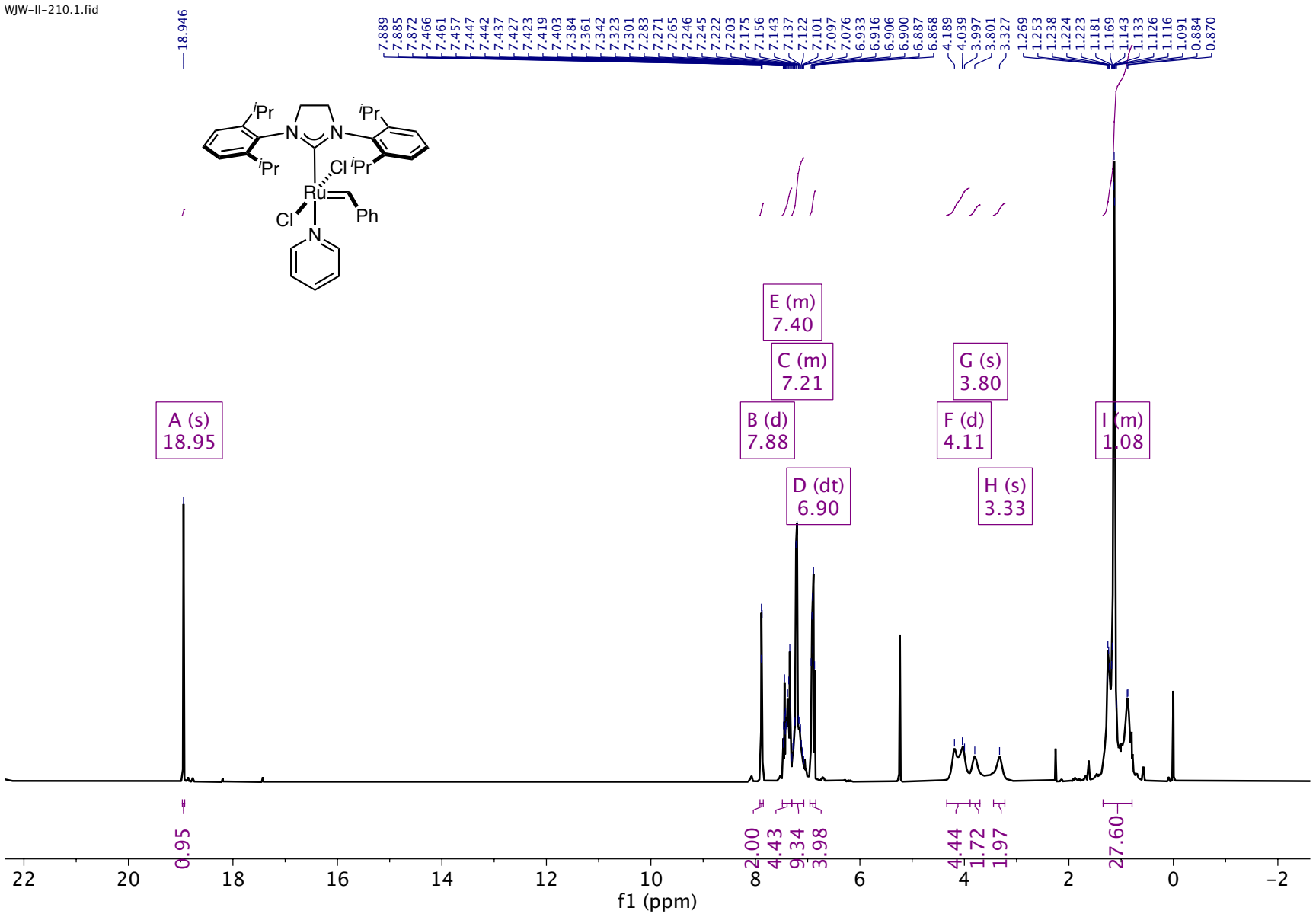
WJW-II-210.1.fid
18.946
7.889
7.885
7.872
7.466
7.461
7.457
7.447
7.442
7.437
7.427
7.423
7.419
7.403
7.384
7.361
7.342
7.323
7.301
7.283
7.271
7.265
7.246
7.245
7.222
7.203
7.175
7.156
7.143
7.137
7.122
7.101
7.097
7.076
6.933
6.916
6.906
6.900
6.887
6.868
4.189
4.039
3.997
3.801
3.327
1.269
1.253
1.238
1.224
1.223
1.181
1.169
1.143
1.133
1.126
1.116
1.091
0.884
0.870
iPr
iPr
iPr
Cl iPr
Ru
Cl
Ph
N
N
N
A (s)
18.95
B (d)
7.88
C (m)
7.21
D (dt)
6.90
E (m)
7.40
F (d)
4.11
G (s)
3.80
H (s)
3.33
I (m)
1.08
0.95
2.00
4.43
9.34
3.98
4.44
1.72
1.97
27.60
22
20
18
16
14
12
10
8
6
4
2
0
−2
f1 (ppm)

^{13}C NMR:

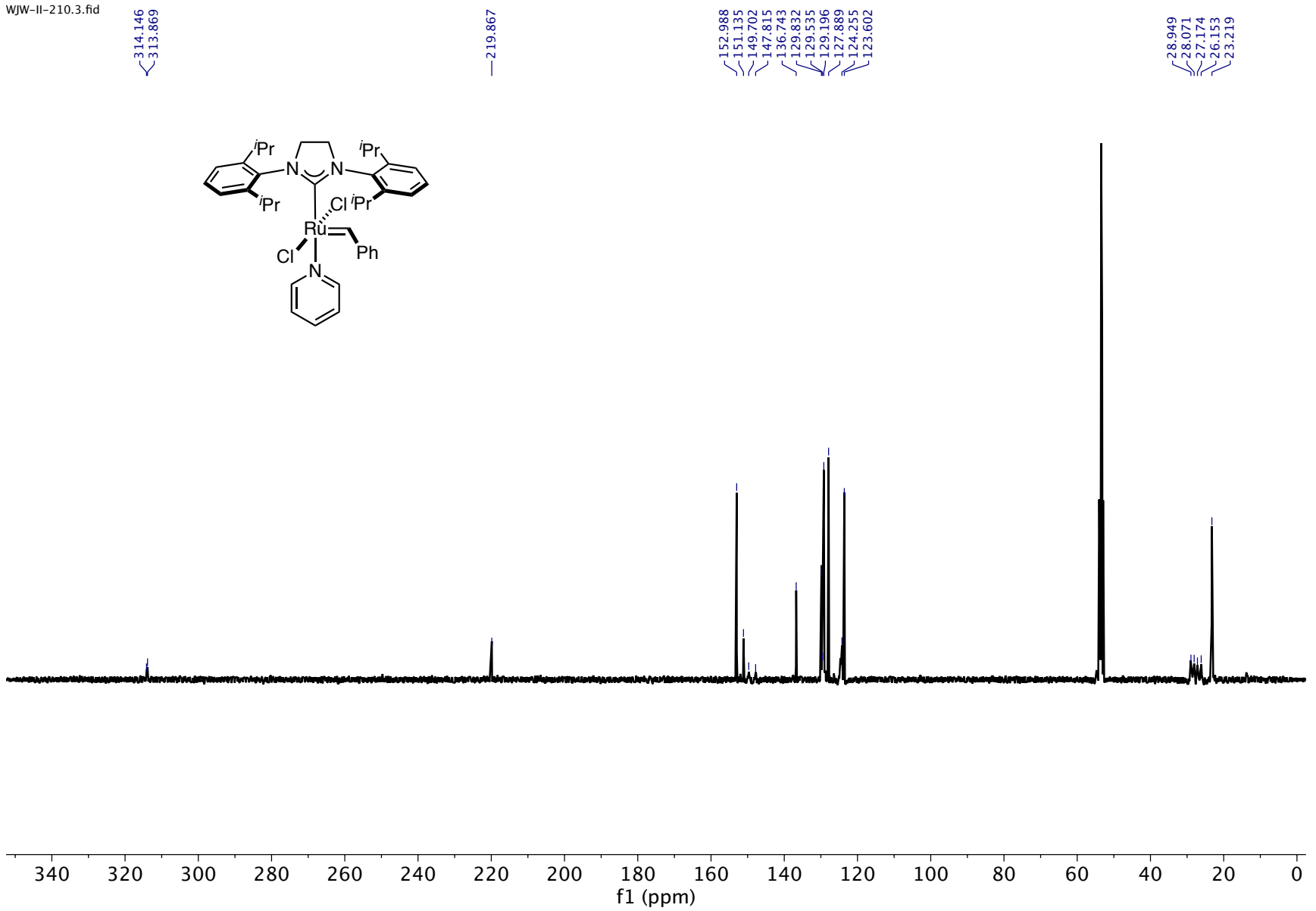
WJW-II-210.3.fid
314.146
313.869
219.867
152.988
151.135
149.702
147.815
136.743
129.832
129.535
129.196
127.889
124.255
123.602
28.949
28.071
27.174
26.153
23.219
iPr
iPr
iPr
iPr
N
N
Cl
Ru
Cl
Ph
N
340
320
300
280
260
240
220
200
180
160
140
120
100
80
60
40
20
0
f1 (ppm)

^{1}H NMR:

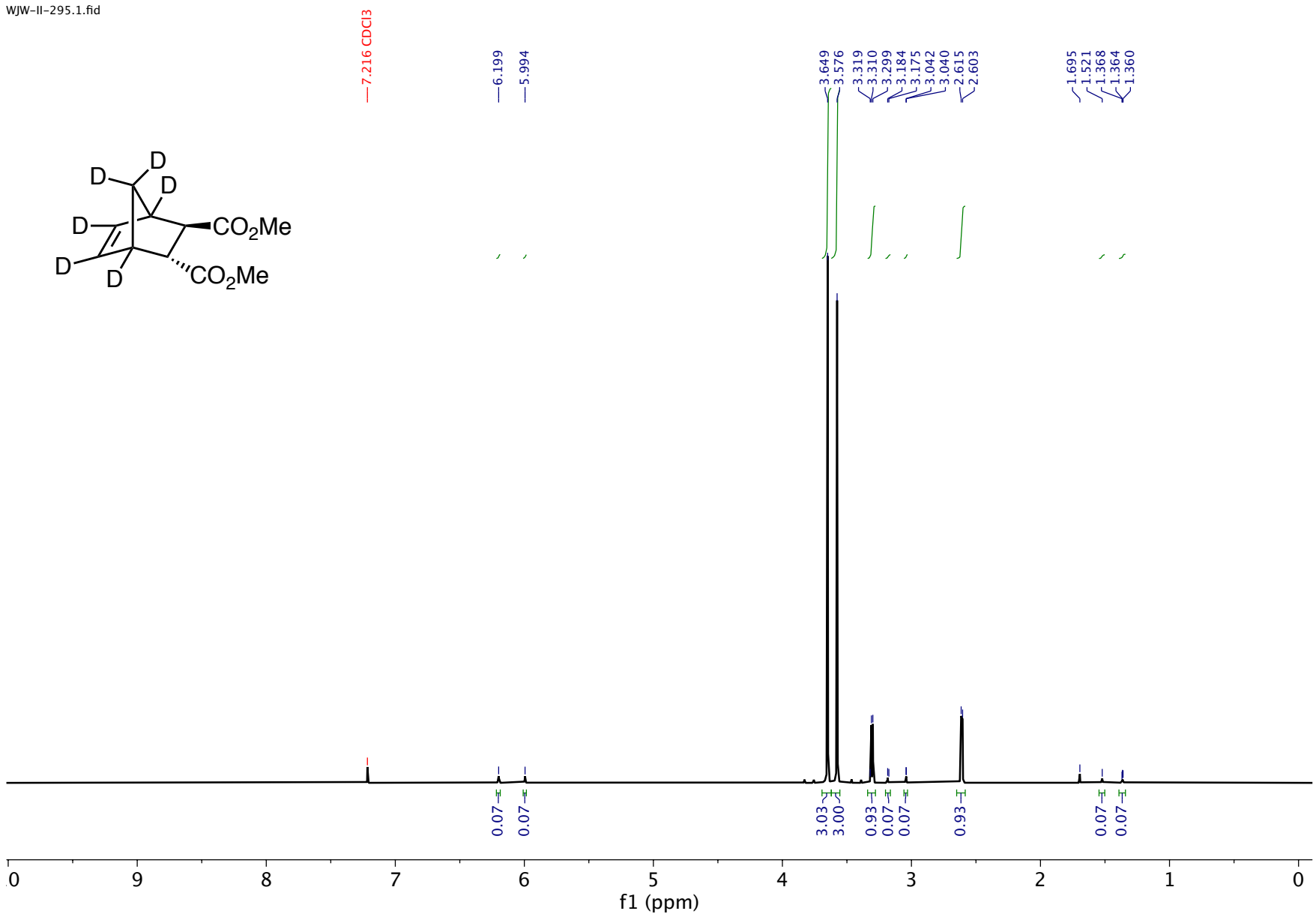
WJW-II-295.1.fid
7.216 CDCl3
6.199
5.994
3.649
3.576
3.319
3.310
3.299
3.184
3.175
3.042
3.040
2.615
2.603
1.695
1.521
1.368
1.364
1.360
D
D
D
D
D
D
CO2Me
CO2Me
0.07
0.07
3.03
3.00
0.93
0.07
0.07
0.93
0.07
0.07
0
9
8
7
6
5
4
3
2
1
0
f1 (ppm)

^{13}C NMR:

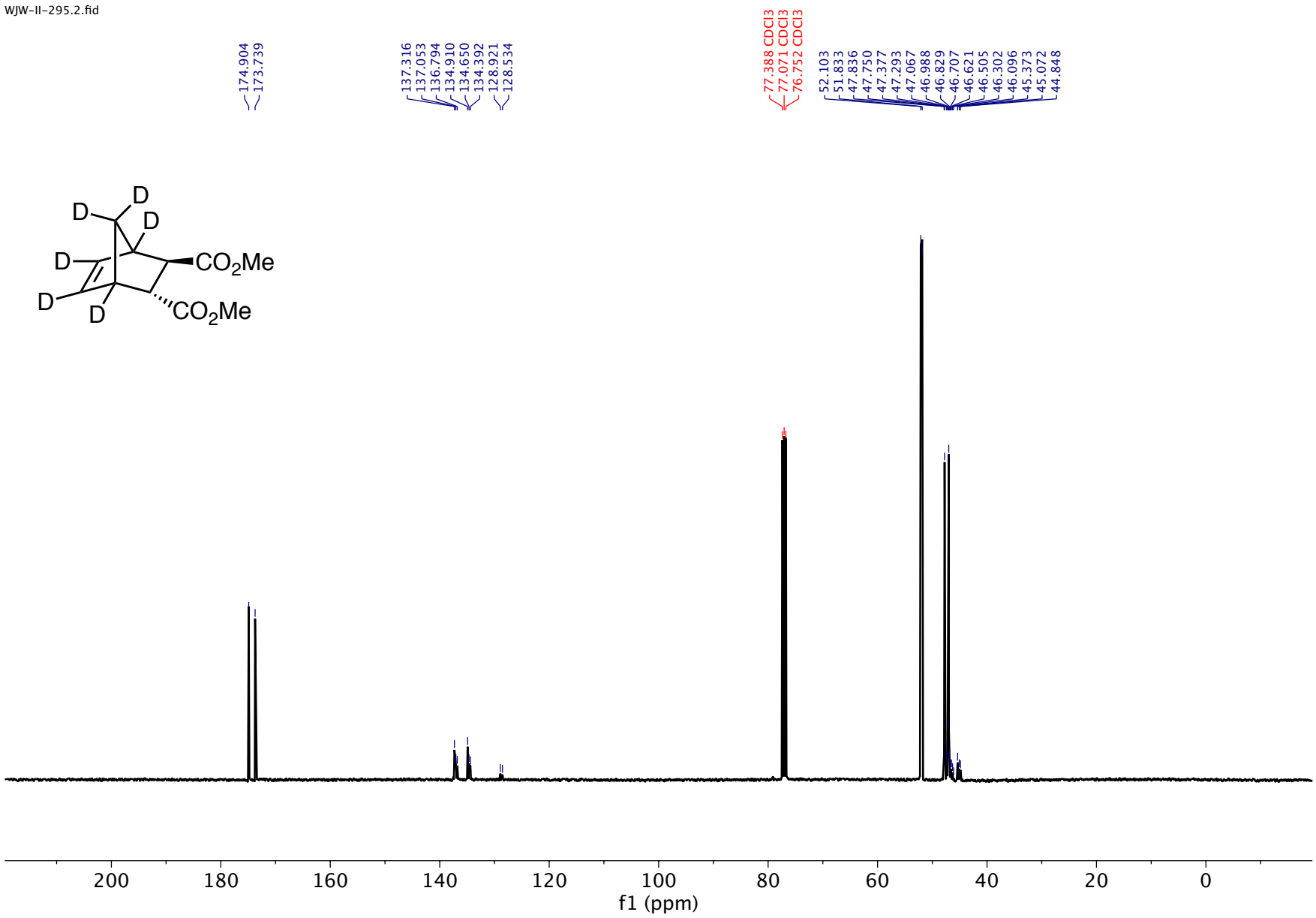
WJW-II-295.2.fid
174.904
173.739
137.316
137.053
136.794
134.910
134.650
134.392
128.921
128.534
77.388 CDCl3
77.071 CDCl3
76.752 CDCl3
52.103
51.833
47.836
47.750
47.377
47.293
47.067
46.988
46.829
46.707
46.621
46.505
46.302
46.096
45.373
45.072
44.848
D
D
D
D
D
D
CO2Me
CO2Me
200
180
160
140
120
100
80
60
40
20
0
f1 (ppm)

^{1}H NMR

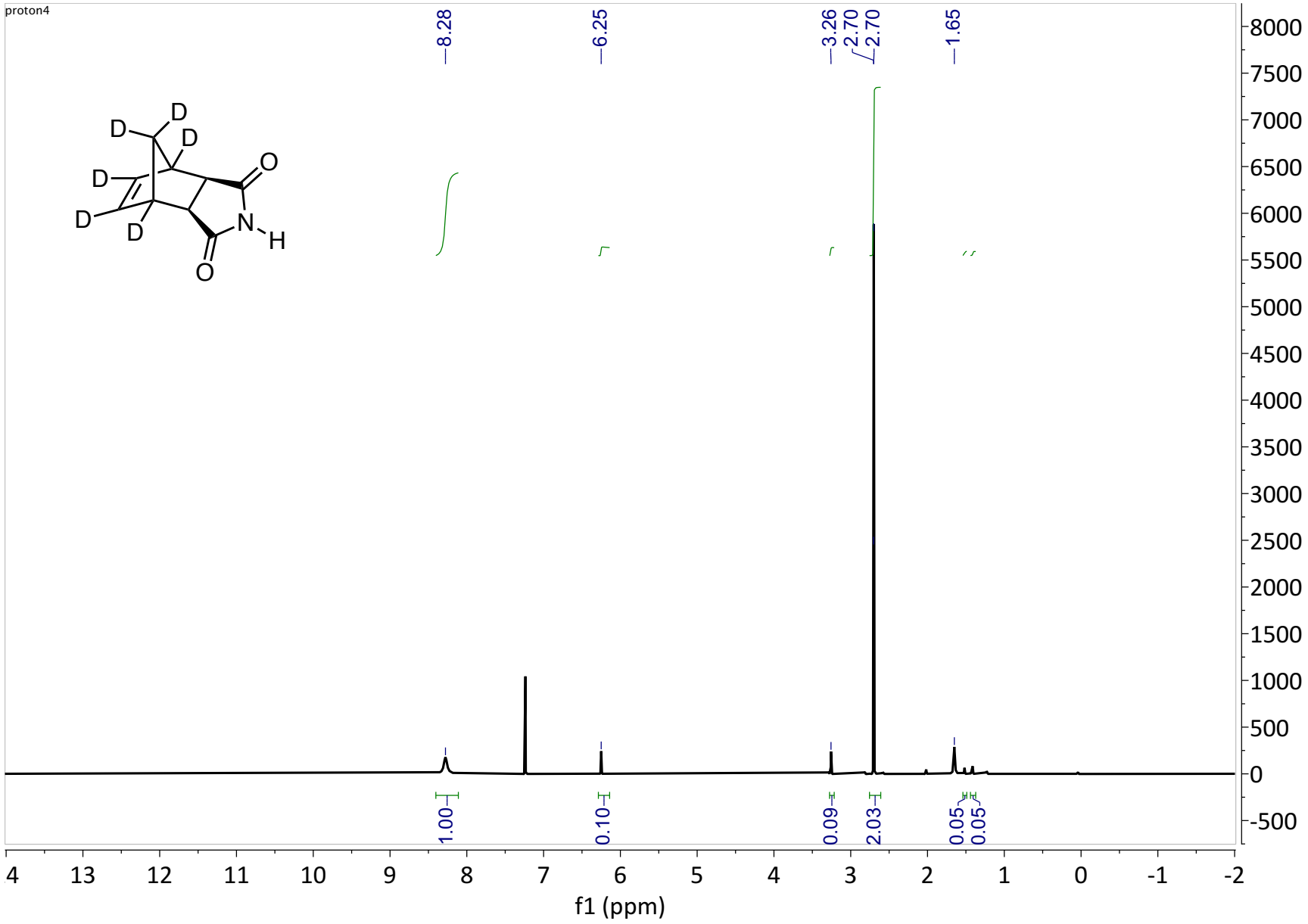
proton4
8.28
6.25
3.26
2.70
2.70
1.65
D
D
D
D
D
D
O
N
H
O
1.00
0.10
0.09
2.03
0.05
0.05
f1 (ppm)

^{2}H NMR:

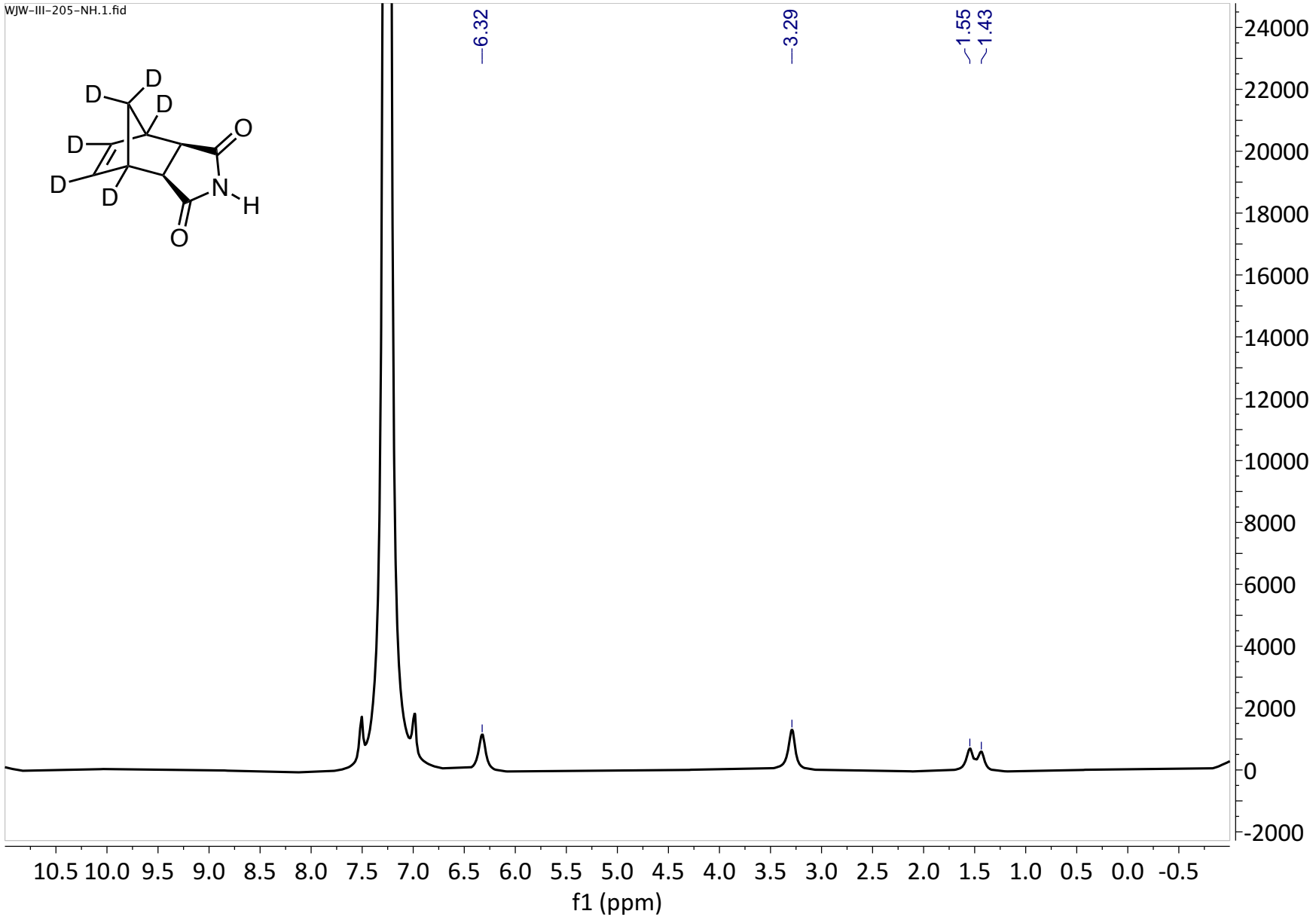
WJW-III-205-NH.1.fid
6.32
3.29
1.55
1.43
D
D
D
D
D
D
O
N
H
O
24000
22000
20000
18000
16000
14000
12000
10000
8000
6000
4000
2000
0
-2000
10.5 10.0 9.5 9.0 8.5 8.0 7.5 7.0 6.5 6.0 5.5 5.0 4.5 4.0 3.5 3.0 2.5 2.0 1.5 1.0 0.5 0.0 -0.5
f1 (ppm)

^{13}C NMR:

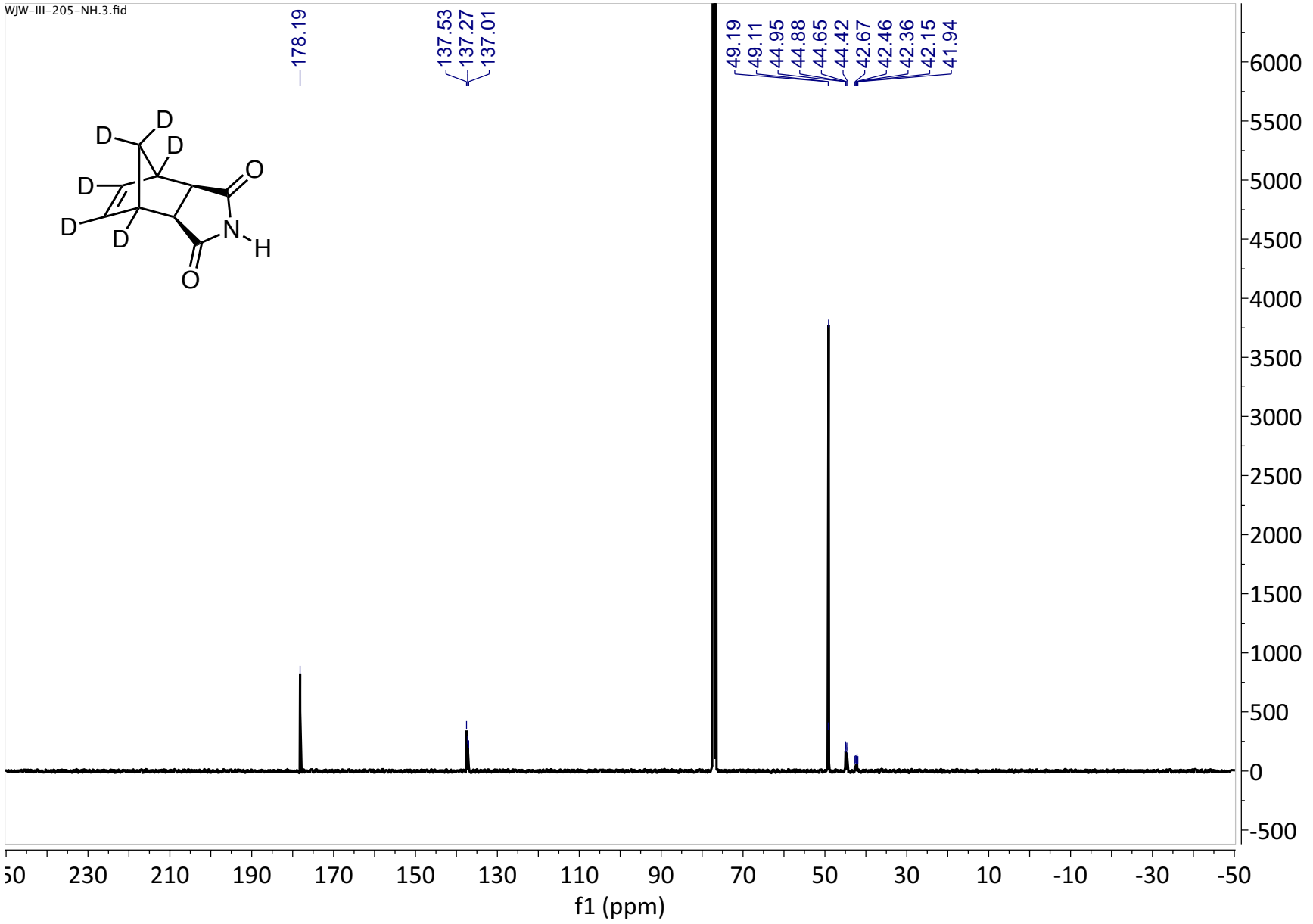
WJW-III-205-NH.3.fid
178.19
137.53
137.27
137.01
49.19
49.11
44.95
44.88
44.65
44.42
42.67
42.46
42.36
42.15
41.94
D
D
D
D
D
D
O
N
H
O
6000
5500
5000
4500
4000
3500
3000
2500
2000
1500
1000
500
0
-500
230
210
190
170
150
130
110
90
70
50
30
10
-10
-30
-50
f1 (ppm)

^{1}H NMR:

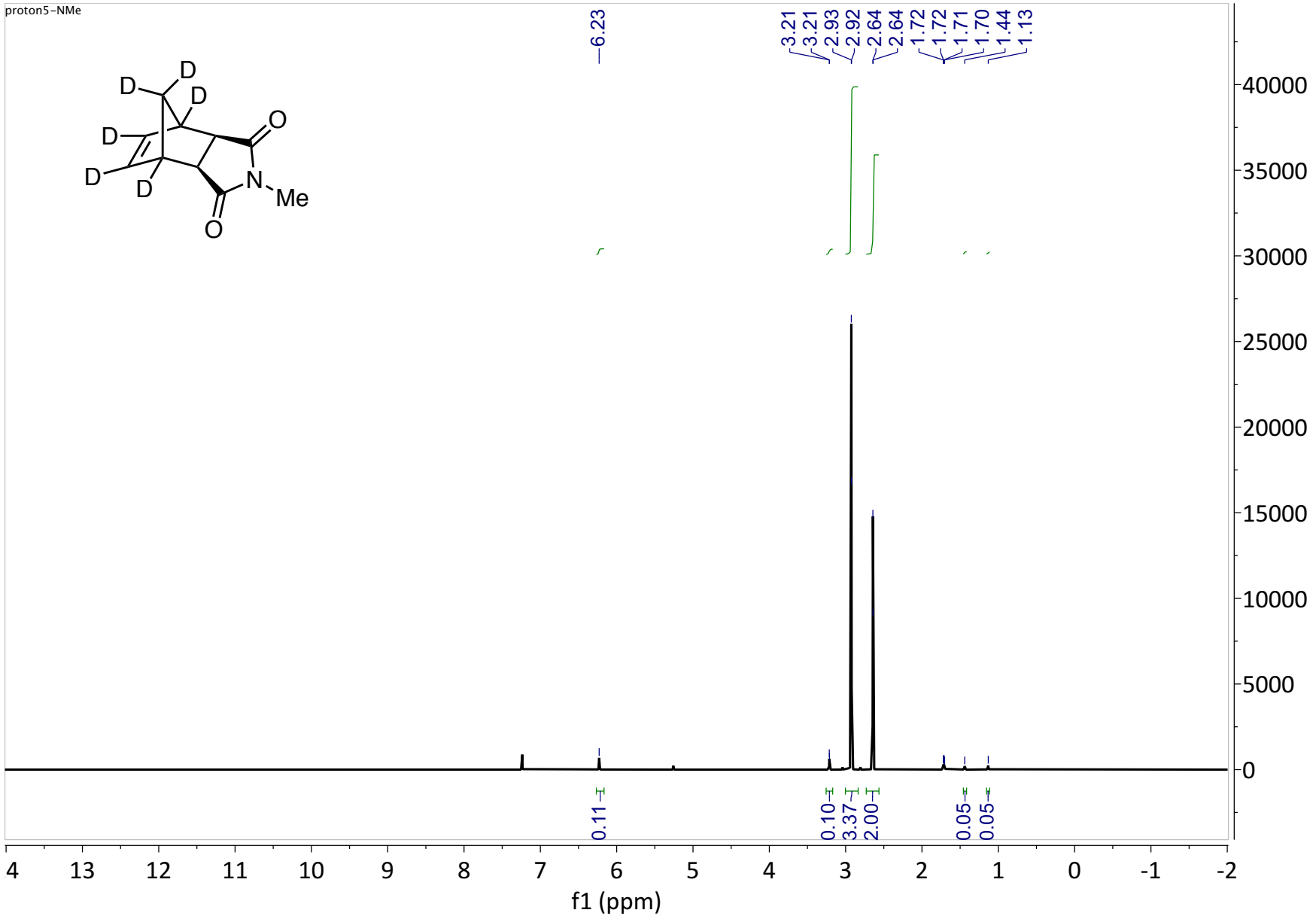
proton5-NMe
6.23
3.21
3.21
2.93
2.92
2.64
2.64
1.72
1.72
1.71
1.70
1.44
1.13
D
D
D
D
D
D
O
N
Me
O
40000
35000
30000
25000
20000
15000
10000
5000
0
0.11
0.10
3.37
2.00
0.05
0.05
4
13
12
11
10
9
8
7
6
5
4
3
2
1
0
-1
-2
f1 (ppm)

^{2}H NMR:

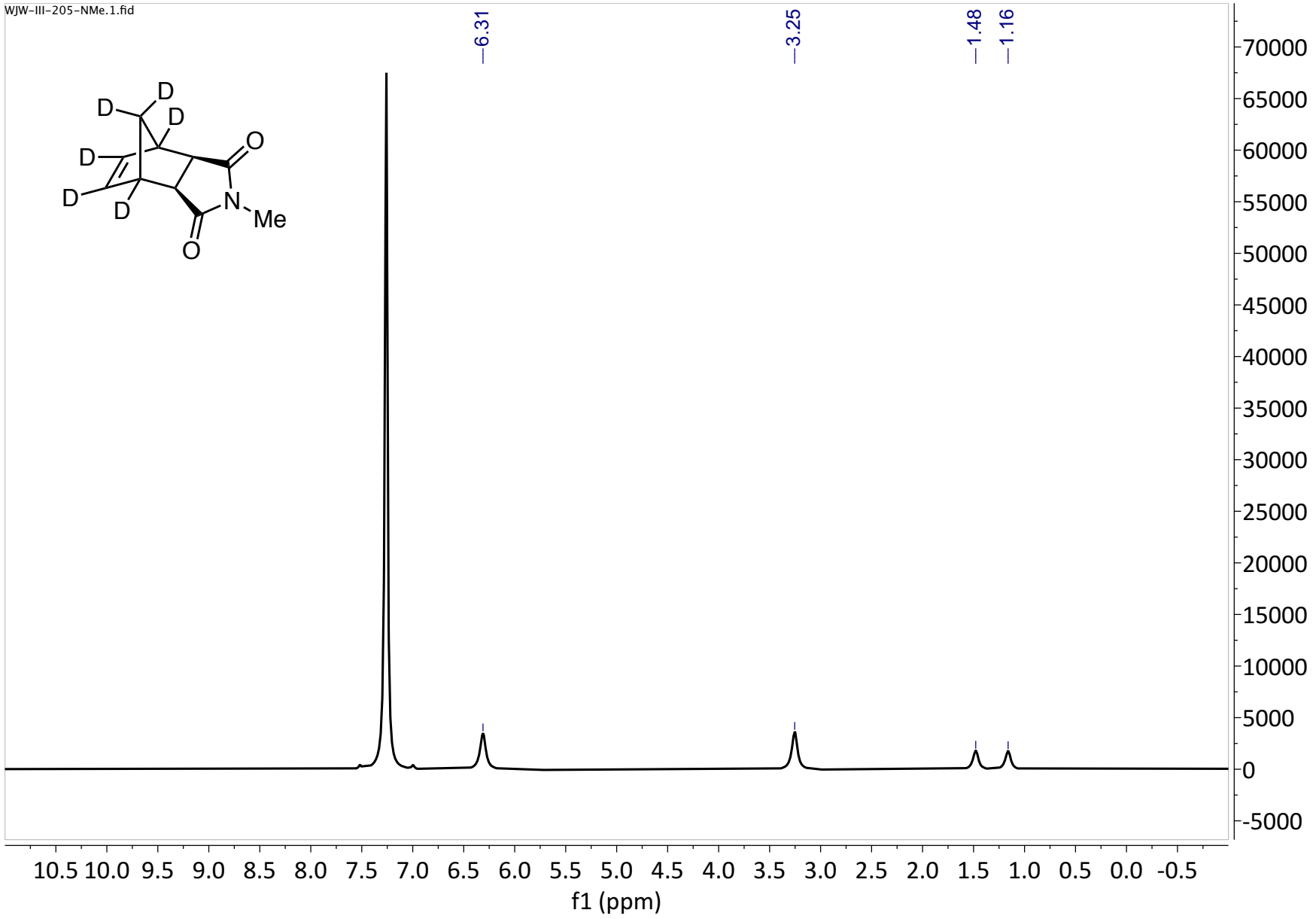
WJW-III-205-NMe.1.fid
6.31
3.25
1.48
1.16
D
D
D
D
D
D
O
O
N
Me
70000
65000
60000
55000
50000
45000
40000
35000
30000
25000
20000
15000
10000
5000
0
-5000
10.5 10.0 9.5 9.0 8.5 8.0 7.5 7.0 6.5 6.0 5.5 5.0 4.5 4.0 3.5 3.0 2.5 2.0 1.5 1.0 0.5 0.0 -0.5
f1 (ppm)

^{13}C NMR:

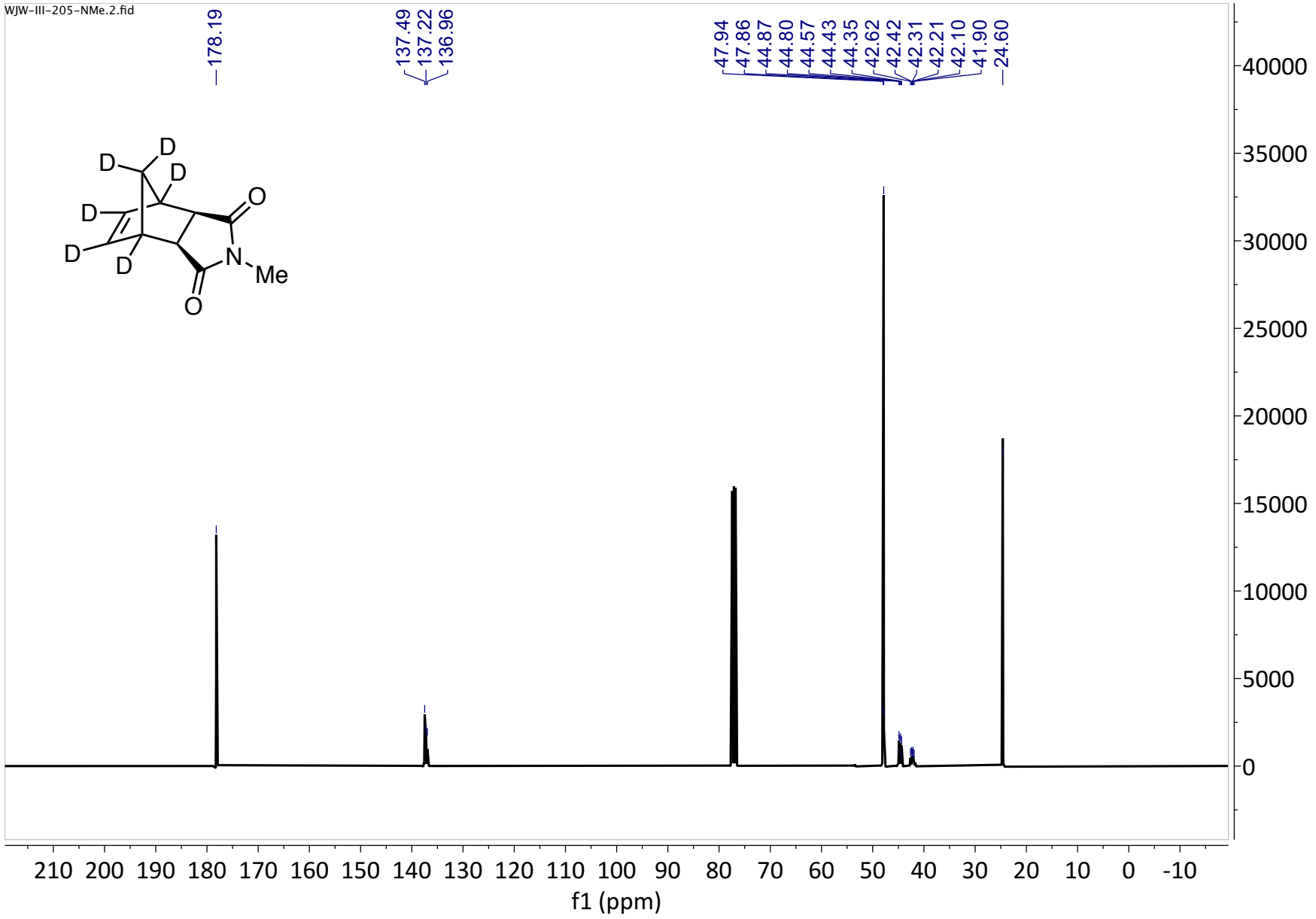
WJW-III-205-NMe.2.fid
178.19
137.49
137.22
136.96
47.94
47.86
44.87
44.80
44.57
44.43
44.35
42.62
42.42
42.31
42.21
42.10
41.90
24.60
D
D
D
D
D
D
O
N
Me
O
40000
35000
30000
25000
20000
15000
10000
5000
0
210 200 190 180 170 160 150 140 130 120 110 100 90 80 70 60 50 40 30 20 10 0 -10
f1 (ppm)

^{1}H NMR:

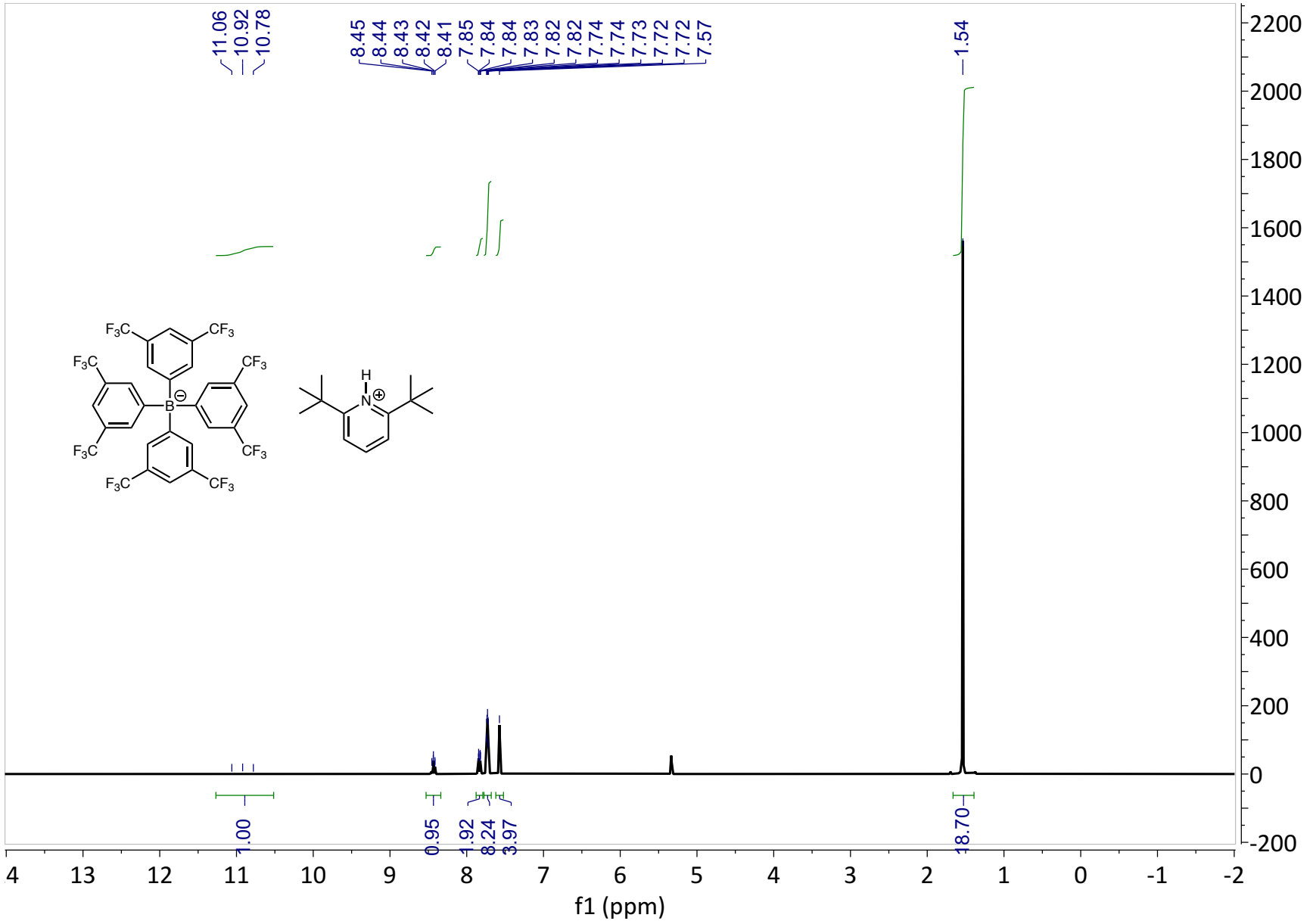
11.06
10.92
10.78
8.45
8.44
8.43
8.42
8.41
7.85
7.84
7.84
7.83
7.82
7.82
7.74
7.74
7.73
7.72
7.72
7.57
1.54
F3C
CF3
B
H
N
1.00
0.95
1.92
8.24
3.97
18.70
f1 (ppm)

^{13}C NMR:

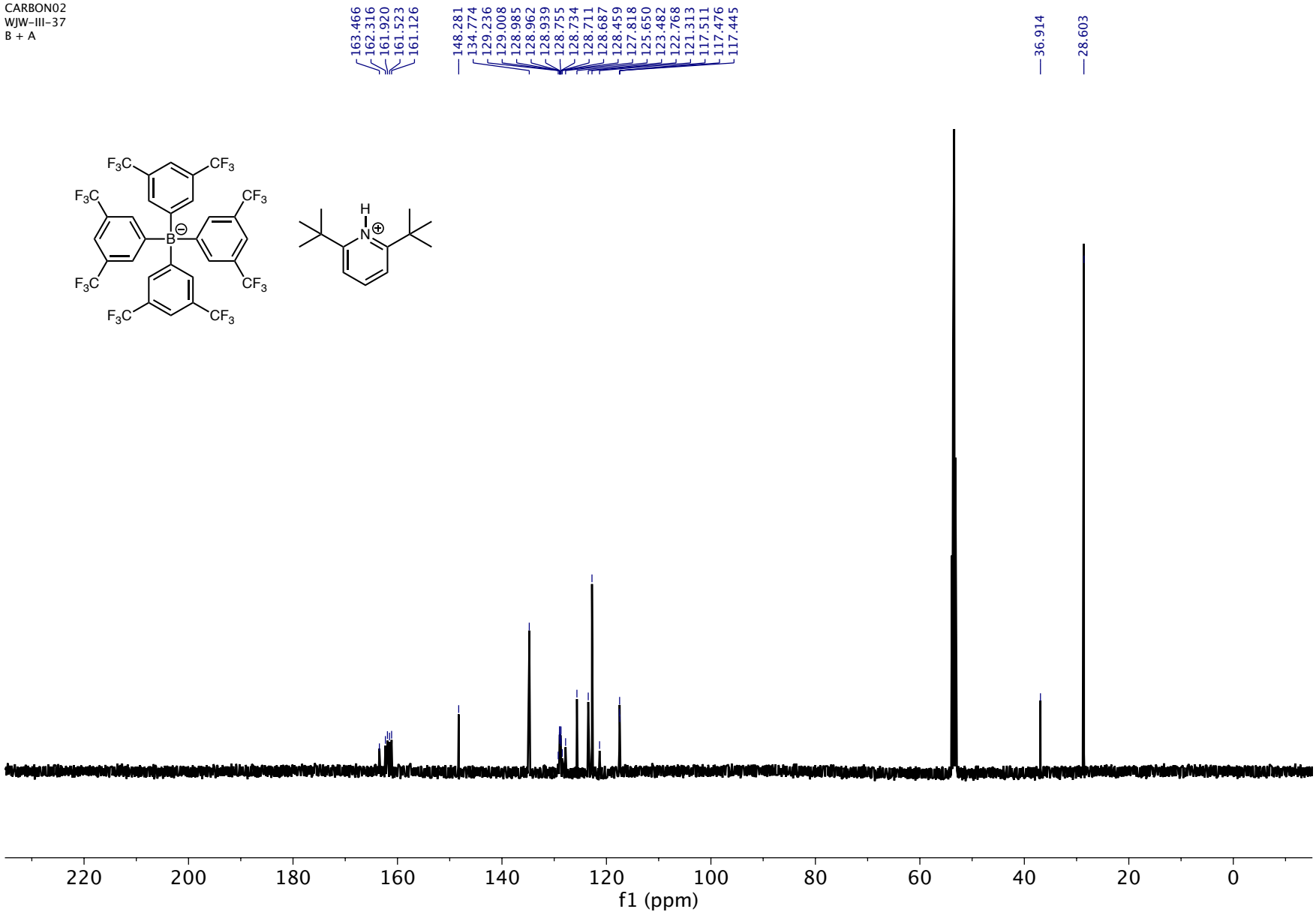
CARBON02
WJW-III-37
B + A
163.466
162.316
161.920
161.523
161.126
148.281
134.774
129.236
129.008
128.985
128.962
128.939
128.755
128.734
128.711
128.687
128.459
127.818
125.650
123.482
122.768
121.313
117.511
117.476
117.445
36.914
28.603
F3C
CF3
B
H
N
220
200
180
160
140
120
100
80
60
40
20
0
f1 (ppm)

^{19}F NMR:

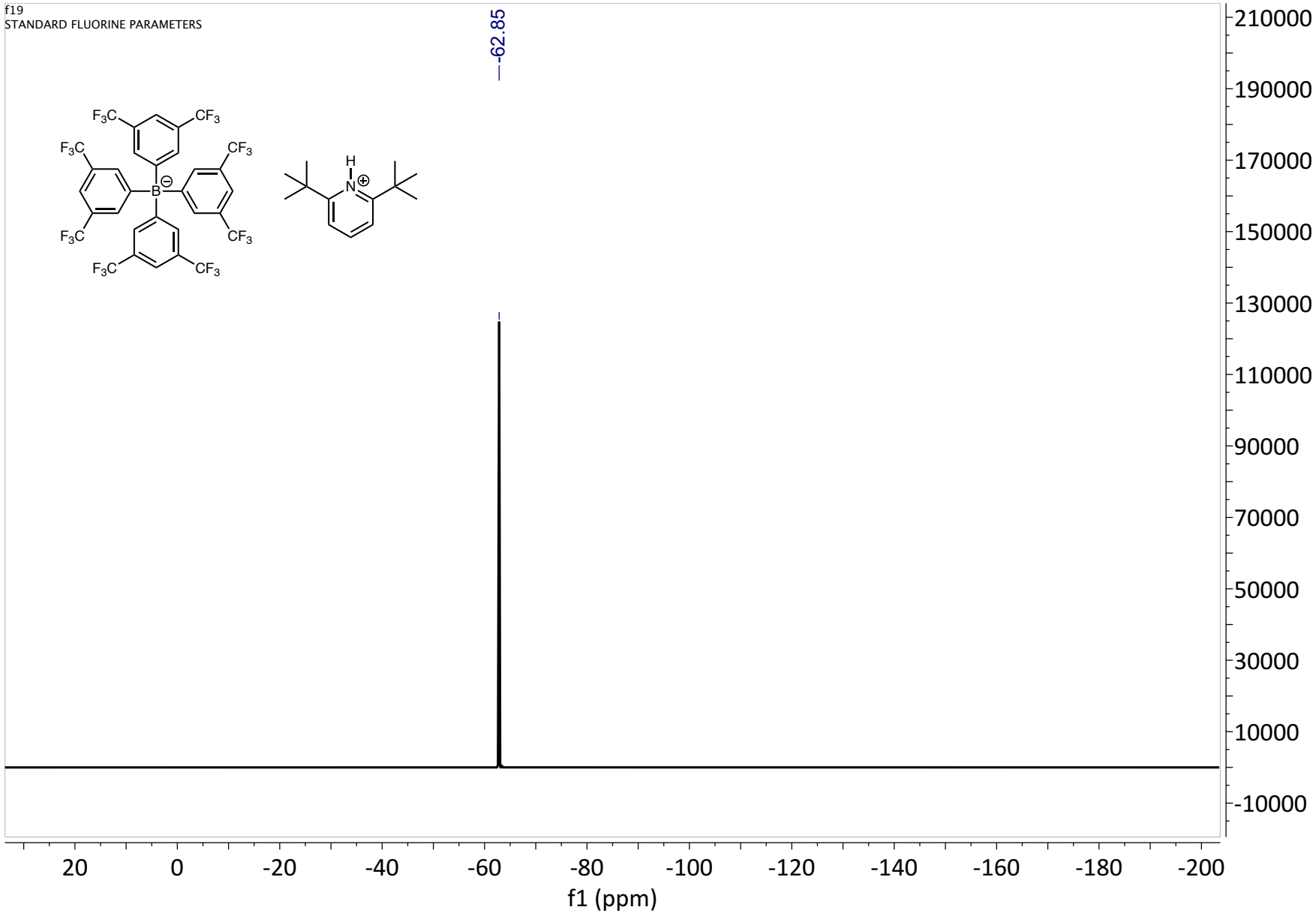
f19
STANDARD FLUORINE PARAMETERS
-62.85
F3C
CF3
B
H
N
210000
190000
170000
150000
130000
110000
90000
70000
50000
30000
10000
-10000
20
0
-20
-40
-60
-80
-100
-120
-140
-160
-180
-200
f1 (ppm)

X-Ray Structure Determination

Low-temperature diffraction data (ϕ-and ω-scans) were collected on a Bruker AXS D8 VENTURE KAPPA diffractometer coupled to a PHOTON 100 CPAD detector with Cu K_α radiation (λ = 1.54178 Å) from an IμS micro-source for the structure of compound P17600. The structure was solved by direct methods using SHELXS[14] and refined against F^2 on all data by full-matrix least squares with SHELXL-2017[15] using established refinement techniques.[16] All non-hydrogen atoms were refined anisotropically. All hydrogen atoms were included into the model at geometrically calculated positions and refined using a riding model. The isotropic displacement parameters of all hydrogen atoms were fixed to 1.2 times the *U* value of the atoms they are linked to (1.5 times for methyl groups). Compound P17600 crystallizes in the triclinic space group *P*-1 with one molecule in the asymmetric unit.

Table S7. Crystal data and structure refinement for P17600.

Identification code	P17600	
Empirical formula	C_{39} H_{49} Cl_2 N_3 Ru	
Formula weight	731.78	
Temperature	100(2) K	
Wavelength	1.54178 Å	
Crystal system	Triclinic	
Space group	P-1	
Unit cell dimensions	a = 10.3622(11) Å	a= 93.849(5)°.
	b = 12.0606(10) Å	b= 91.457(8)°.
	c = 15.3918(14) Å	g = 110.577(10)°.
Volume	1794.3(3) Å^3	
Z	2	
Density (calculated)	1.354 Mg/m^3	
Absorption coefficient	5.131 mm^{-1}	
F(000)	764	
Crystal size	0.400 x 0.150 x 0.050 mm^3	
Theta range for data collection	2.881 to 74.598°.	
Index ranges	-12<=h<=11, -15<=k<=15, -19<=l<=19	
Reflections collected	26663	
Independent reflections	7273 [R(int) = 0.0598]	
Completeness to theta = 67.679°	99.8 %	
Absorption correction	Semi-empirical from equivalents	
Refinement method	Full-matrix least-squares on F^2	
Data / restraints / parameters	7273 / 0 / 414	
Goodness-of-fit on F^2	1.034	
Final R indices [I>2sigma(I)]	R1 = 0.0386, wR2 = 0.0893	

R indices (all data)	R1 = 0.0469, wR2 = 0.0925
Extinction coefficient	n/a
Largest diff. peak and hole	1.980 and -0.818 e.Å^{-3}

Table S8. Atomic coordinates (x 10^4) and equivalent isotropic displacement parameters (Å^{2}x 10^3) for P17600. U(eq) is defined as one third of the trace of the orthogonalized U^{ij} tensor.

	x	y	z	U(eq)
Cl(1)	3834(1)	6135(1)	4063(1)	21(1)
Cl(2)	616(1)	6819(1)	2216(1)	19(1)
Ru(1)	2467(1)	6817(1)	3138(1)	15(1)
C(1)	3435(2)	6708(2)	2007(2)	15(1)
N(1)	4076(2)	7557(2)	1469(2)	17(1)
C(11)	4736(3)	8804(2)	1706(2)	18(1)
C(12)	4068(3)	9587(3)	1496(2)	19(1)
C(17)	2730(3)	9169(2)	948(2)	19(1)
C(18)	3018(3)	9523(3)	14(2)	26(1)
C(19)	1669(3)	9673(3)	1304(2)	27(1)
C(13)	4719(3)	10787(3)	1777(2)	25(1)
C(14)	5999(3)	11191(3)	2224(2)	28(1)
C(15)	6677(3)	10413(3)	2373(2)	27(1)
C(16)	6074(3)	9197(3)	2116(2)	22(1)
C(20)	6855(3)	8373(3)	2275(2)	26(1)
C(21)	7188(4)	8332(4)	3243(3)	38(1)
C(22)	8176(3)	8714(4)	1774(3)	36(1)
C(2)	4402(3)	7057(3)	634(2)	20(1)
C(3)	3500(3)	5760(3)	634(2)	21(1)
N(2)	3226(2)	5645(2)	1563(2)	16(1)
C(31)	2720(3)	4498(2)	1909(2)	19(1)
C(32)	1352(3)	3739(3)	1697(2)	23(1)
C(37)	386(3)	4062(3)	1098(2)	23(1)
C(38)	-1058(3)	3761(3)	1446(3)	34(1)
C(39)	293(3)	3429(3)	187(2)	29(1)
C(33)	916(4)	2612(3)	2014(2)	30(1)
C(34)	1790(4)	2258(3)	2519(2)	37(1)
C(35)	3145(4)	3002(3)	2699(2)	34(1)

C(36)	3651(3)	4126(3)	2388(2)	25(1)
C(40)	5171(3)	4899(3)	2532(2)	32(1)
C(41)	5887(4)	4595(4)	3319(3)	45(1)
C(42)	5967(4)	4806(4)	1718(3)	44(1)
N(3)	1186(2)	6694(2)	4254(2)	17(1)
C(51)	-189(3)	6091(3)	4178(2)	20(1)
C(52)	-1020(3)	5944(3)	4885(2)	24(1)
C(53)	-430(3)	6439(3)	5700(2)	26(1)
C(54)	977(3)	7065(3)	5783(2)	26(1)
C(55)	1746(3)	7165(3)	5050(2)	22(1)
C(61)	3402(3)	8417(3)	3419(2)	21(1)
C(62)	2923(3)	9335(3)	3785(2)	22(1)
C(63)	1539(3)	9238(3)	3789(2)	24(1)
C(64)	1186(4)	10165(3)	4167(2)	28(1)
C(65)	2202(4)	11191(3)	4541(2)	34(1)
C(66)	3576(4)	11301(3)	4536(2)	32(1)
C(67)	3940(3)	10389(3)	4153(2)	27(1)

Table S9. Bond lengths [Å] and angles [°] for P17600.

Cl(1)-Ru(1)	2.3623(7)	C(22)-H(22A)	0.9800
Cl(2)-Ru(1)	2.3576(7)	C(22)-H(22B)	0.9800
Ru(1)-C(61)	1.844(3)	C(22)-H(22C)	0.9800
Ru(1)-C(1)	2.051(3)	C(2)-C(3)	1.514(4)
Ru(1)-N(3)	2.178(2)	C(2)-H(2A)	0.9900
C(1)-N(2)	1.355(4)	C(2)-H(2B)	0.9900
C(1)-N(1)	1.356(4)	C(3)-N(2)	1.470(4)
N(1)-C(11)	1.433(4)	C(3)-H(3A)	0.9900
N(1)-C(2)	1.479(4)	C(3)-H(3B)	0.9900
C(11)-C(12)	1.402(4)	N(2)-C(31)	1.441(4)
C(11)-C(16)	1.413(4)	C(31)-C(32)	1.406(4)
C(12)-C(13)	1.396(4)	C(31)-C(36)	1.411(4)
C(12)-C(17)	1.510(4)	C(32)-C(33)	1.399(4)
C(17)-C(19)	1.527(4)	C(32)-C(37)	1.510(5)
C(17)-C(18)	1.534(4)	C(37)-C(38)	1.531(4)
C(17)-H(17)	1.0000	C(37)-C(39)	1.535(4)
C(18)-H(18A)	0.9800	C(37)-H(37)	1.0000
C(18)-H(18B)	0.9800	C(38)-H(38A)	0.9800
C(18)-H(18C)	0.9800	C(38)-H(38B)	0.9800
C(19)-H(19A)	0.9800	C(38)-H(38C)	0.9800
C(19)-H(19B)	0.9800	C(39)-H(39A)	0.9800
C(19)-H(19C)	0.9800	C(39)-H(39B)	0.9800
C(13)-C(14)	1.388(5)	C(39)-H(39C)	0.9800
C(13)-H(13)	0.9500	C(33)-C(34)	1.374(5)
C(14)-C(15)	1.382(5)	C(33)-H(33)	0.9500
C(14)-H(14)	0.9500	C(34)-C(35)	1.384(6)
C(15)-C(16)	1.401(4)	C(34)-H(34)	0.9500
C(15)-H(15)	0.9500	C(35)-C(36)	1.393(5)
C(16)-C(20)	1.514(5)	C(35)-H(35)	0.9500
C(20)-C(21)	1.528(5)	C(36)-C(40)	1.524(5)
C(20)-C(22)	1.529(4)	C(40)-C(41)	1.536(5)
C(20)-H(20)	1.0000	C(40)-C(42)	1.537(5)
C(21)-H(21A)	0.9800	C(40)-H(40)	1.0000
C(21)-H(21B)	0.9800	C(41)-H(41A)	0.9800
C(21)-H(21C)	0.9800	C(41)-H(41B)	0.9800

C(41)-H(41C)	0.9800
C(42)-H(42A)	0.9800
C(42)-H(42B)	0.9800
C(42)-H(42C)	0.9800
N(3)-C(55)	1.342(4)
N(3)-C(51)	1.350(4)
C(51)-C(52)	1.387(4)
C(51)-H(51)	0.9500
C(52)-C(53)	1.381(5)
C(52)-H(52)	0.9500
C(53)-C(54)	1.384(5)
C(53)-H(53)	0.9500
C(54)-C(55)	1.385(4)
C(54)-H(54)	0.9500
C(55)-H(55)	0.9500
C(61)-C(62)	1.451(4)
C(61)-H(61)	0.9500
C(62)-C(63)	1.398(4)
C(62)-C(67)	1.407(4)
C(63)-C(64)	1.390(4)
C(63)-H(63)	0.9500
C(64)-C(65)	1.388(5)
C(64)-H(64)	0.9500
C(65)-C(66)	1.383(5)
C(65)-H(65)	0.9500
C(66)-C(67)	1.384(5)
C(66)-H(66)	0.9500
C(67)-H(67)	0.9500
C(61)-Ru(1)-C(1)	96.19(12)
C(61)-Ru(1)-N(3)	91.79(11)
C(1)-Ru(1)-N(3)	171.31(9)
C(61)-Ru(1)-Cl(2)	102.29(10)
C(1)-Ru(1)-Cl(2)	85.31(7)
N(3)-Ru(1)-Cl(2)	89.66(7)
C(61)-Ru(1)-Cl(1)	96.47(10)
C(1)-Ru(1)-Cl(1)	97.70(8)
N(3)-Ru(1)-Cl(1)	84.76(7)
Cl(2)-Ru(1)-Cl(1)	160.58(2)
N(2)-C(1)-N(1)	106.7(2)
N(2)-C(1)-Ru(1)	121.10(19)
N(1)-C(1)-Ru(1)	130.5(2)
C(1)-N(1)-C(11)	126.7(2)
C(1)-N(1)-C(2)	112.7(2)
C(11)-N(1)-C(2)	118.6(2)
C(12)-C(11)-C(16)	122.6(3)
C(12)-C(11)-N(1)	119.5(2)
C(16)-C(11)-N(1)	117.8(3)
C(13)-C(12)-C(11)	117.6(3)
C(13)-C(12)-C(17)	120.7(3)
C(11)-C(12)-C(17)	121.6(3)
C(12)-C(17)-C(19)	113.1(3)
C(12)-C(17)-C(18)	109.6(2)
C(19)-C(17)-C(18)	108.9(3)
C(12)-C(17)-H(17)	108.4
C(19)-C(17)-H(17)	108.4
C(18)-C(17)-H(17)	108.4
C(17)-C(18)-H(18A)	109.5
C(17)-C(18)-H(18B)	109.5
H(18A)-C(18)-H(18B)	109.5
C(17)-C(18)-H(18C)	109.5
H(18A)-C(18)-H(18C)	109.5
H(18B)-C(18)-H(18C)	109.5
C(17)-C(19)-H(19A)	109.5
C(17)-C(19)-H(19B)	109.5
H(19A)-C(19)-H(19B)	109.5
C(17)-C(19)-H(19C)	109.5
H(19A)-C(19)-H(19C)	109.5
H(19B)-C(19)-H(19C)	109.5
C(14)-C(13)-C(12)	121.0(3)
C(14)-C(13)-H(13)	119.5
C(12)-C(13)-H(13)	119.5
C(15)-C(14)-C(13)	120.2(3)
C(15)-C(14)-H(14)	119.9

C(13)-C(14)-H(14)	119.9	C(1)-N(2)-C(31)	126.3(2)
C(14)-C(15)-C(16)	121.5(3)	C(1)-N(2)-C(3)	112.3(2)
C(14)-C(15)-H(15)	119.3	C(31)-N(2)-C(3)	121.2(2)
C(16)-C(15)-H(15)	119.3	C(32)-C(31)-C(36)	121.6(3)
C(15)-C(16)-C(11)	116.8(3)	C(32)-C(31)-N(2)	119.4(3)
C(15)-C(16)-C(20)	120.1(3)	C(36)-C(31)-N(2)	118.7(3)
C(11)-C(16)-C(20)	123.1(3)	C(33)-C(32)-C(31)	117.8(3)
C(16)-C(20)-C(21)	112.8(3)	C(33)-C(32)-C(37)	119.5(3)
C(16)-C(20)-C(22)	110.8(3)	C(31)-C(32)-C(37)	122.6(3)
C(21)-C(20)-C(22)	110.3(3)	C(32)-C(37)-C(38)	112.4(3)
C(16)-C(20)-H(20)	107.6	C(32)-C(37)-C(39)	109.9(3)
C(21)-C(20)-H(20)	107.6	C(38)-C(37)-C(39)	109.9(3)
C(22)-C(20)-H(20)	107.6	C(32)-C(37)-H(37)	108.1
C(20)-C(21)-H(21A)	109.5	C(38)-C(37)-H(37)	108.1
C(20)-C(21)-H(21B)	109.5	C(39)-C(37)-H(37)	108.1
H(21A)-C(21)-H(21B)	109.5	C(37)-C(38)-H(38A)	109.5
C(20)-C(21)-H(21C)	109.5	C(37)-C(38)-H(38B)	109.5
H(21A)-C(21)-H(21C)	109.5	H(38A)-C(38)-H(38B)	109.5
H(21B)-C(21)-H(21C)	109.5	C(37)-C(38)-H(38C)	109.5
C(20)-C(22)-H(22A)	109.5	H(38A)-C(38)-H(38C)	109.5
C(20)-C(22)-H(22B)	109.5	H(38B)-C(38)-H(38C)	109.5
H(22A)-C(22)-H(22B)	109.5	C(37)-C(39)-H(39A)	109.5
C(20)-C(22)-H(22C)	109.5	C(37)-C(39)-H(39B)	109.5
H(22A)-C(22)-H(22C)	109.5	H(39A)-C(39)-H(39B)	109.5
H(22B)-C(22)-H(22C)	109.5	C(37)-C(39)-H(39C)	109.5
N(1)-C(2)-C(3)	101.6(2)	H(39A)-C(39)-H(39C)	109.5
N(1)-C(2)-H(2A)	111.5	H(39B)-C(39)-H(39C)	109.5
C(3)-C(2)-H(2A)	111.5	C(34)-C(33)-C(32)	121.3(3)
N(1)-C(2)-H(2B)	111.5	C(34)-C(33)-H(33)	119.3
C(3)-C(2)-H(2B)	111.5	C(32)-C(33)-H(33)	119.3
H(2A)-C(2)-H(2B)	109.3	C(33)-C(34)-C(35)	120.2(3)
N(2)-C(3)-C(2)	102.0(2)	C(33)-C(34)-H(34)	119.9
N(2)-C(3)-H(3A)	111.4	C(35)-C(34)-H(34)	119.9
C(2)-C(3)-H(3A)	111.4	C(34)-C(35)-C(36)	121.3(3)
N(2)-C(3)-H(3B)	111.4	C(34)-C(35)-H(35)	119.3
C(2)-C(3)-H(3B)	111.4	C(36)-C(35)-H(35)	119.3
H(3A)-C(3)-H(3B)	109.2	C(35)-C(36)-C(31)	117.7(3)

C(35)-C(36)-C(40)	120.9(3)	C(52)-C(53)-H(53)	120.6
C(31)-C(36)-C(40)	121.4(3)	C(54)-C(53)-H(53)	120.6
C(36)-C(40)-C(41)	113.4(3)	C(53)-C(54)-C(55)	119.0(3)
C(36)-C(40)-C(42)	110.9(3)	C(53)-C(54)-H(54)	120.5
C(41)-C(40)-C(42)	108.6(3)	C(55)-C(54)-H(54)	120.5
C(36)-C(40)-H(40)	107.9	N(3)-C(55)-C(54)	122.9(3)
C(41)-C(40)-H(40)	107.9	N(3)-C(55)-H(55)	118.5
C(42)-C(40)-H(40)	107.9	C(54)-C(55)-H(55)	118.5
C(40)-C(41)-H(41A)	109.5	C(62)-C(61)-Ru(1)	130.7(2)
C(40)-C(41)-H(41B)	109.5	C(62)-C(61)-H(61)	114.7
H(41A)-C(41)-H(41B)	109.5	Ru(1)-C(61)-H(61)	114.7
C(40)-C(41)-H(41C)	109.5	C(63)-C(62)-C(67)	118.8(3)
H(41A)-C(41)-H(41C)	109.5	C(63)-C(62)-C(61)	124.5(3)
H(41B)-C(41)-H(41C)	109.5	C(67)-C(62)-C(61)	116.7(3)
C(40)-C(42)-H(42A)	109.5	C(64)-C(63)-C(62)	120.0(3)
C(40)-C(42)-H(42B)	109.5	C(64)-C(63)-H(63)	120.0
H(42A)-C(42)-H(42B)	109.5	C(62)-C(63)-H(63)	120.0
C(40)-C(42)-H(42C)	109.5	C(65)-C(64)-C(63)	120.4(3)
H(42A)-C(42)-H(42C)	109.5	C(65)-C(64)-H(64)	119.8
H(42B)-C(42)-H(42C)	109.5	C(63)-C(64)-H(64)	119.8
C(55)-N(3)-C(51)	117.6(2)	C(66)-C(65)-C(64)	120.2(3)
C(55)-N(3)-Ru(1)	121.06(18)	C(66)-C(65)-H(65)	119.9
C(51)-N(3)-Ru(1)	121.3(2)	C(64)-C(65)-H(65)	119.9
N(3)-C(51)-C(52)	122.6(3)	C(65)-C(66)-C(67)	119.9(3)
N(3)-C(51)-H(51)	118.7	C(65)-C(66)-H(66)	120.0
C(52)-C(51)-H(51)	118.7	C(67)-C(66)-H(66)	120.0
C(53)-C(52)-C(51)	119.2(3)	C(66)-C(67)-C(62)	120.7(3)
C(53)-C(52)-H(52)	120.4	C(66)-C(67)-H(67)	119.7
C(51)-C(52)-H(52)	120.4	C(62)-C(67)-H(67)	119.7
C(52)-C(53)-C(54)	118.7(3)		

Symmetry transformations used to generate equivalent atoms:

Table S10. Anisotropic displacement parameters ($Å^2 x\ 10^3$) for P17600. The anisotropic displacement factor exponent takes the form: $-2p^2[\ h^2\ a^{*2}U^{11} + ...\ + 2\ h\ k\ a^*\ b^*\ U^{12}\ ]$

	U^{11}	U^{22}	U^{33}	U^{23}	U^{13}	U^{12}
Cl(1)	16(1)	26(1)	21(1)	3(1)	1(1)	7(1)
Cl(2)	15(1)	23(1)	19(1)	1(1)	0(1)	6(1)
Ru(1)	11(1)	16(1)	16(1)	0(1)	1(1)	2(1)
C(1)	9(1)	19(1)	18(1)	1(1)	-2(1)	5(1)
N(1)	13(1)	16(1)	18(1)	0(1)	3(1)	1(1)
C(11)	13(1)	17(1)	18(1)	0(1)	4(1)	0(1)
C(12)	14(1)	20(1)	20(1)	1(1)	5(1)	3(1)
C(17)	15(1)	17(1)	25(2)	4(1)	2(1)	4(1)
C(18)	17(1)	32(2)	27(2)	4(1)	2(1)	5(1)
C(19)	20(1)	27(2)	34(2)	3(1)	5(1)	10(1)
C(13)	23(1)	18(1)	30(2)	0(1)	8(1)	3(1)
C(14)	22(1)	20(1)	30(2)	-6(1)	5(1)	-6(1)
C(15)	17(1)	27(2)	25(2)	-5(1)	2(1)	-4(1)
C(16)	14(1)	27(2)	19(1)	-1(1)	2(1)	0(1)
C(20)	14(1)	32(2)	28(2)	5(1)	0(1)	3(1)
C(21)	27(2)	47(2)	34(2)	11(2)	-4(1)	5(2)
C(22)	23(2)	47(2)	42(2)	16(2)	11(1)	15(1)
C(2)	18(1)	22(1)	19(1)	1(1)	5(1)	5(1)
C(3)	23(1)	22(1)	17(1)	2(1)	3(1)	7(1)
N(2)	16(1)	17(1)	15(1)	1(1)	1(1)	5(1)
C(31)	24(1)	17(1)	17(1)	2(1)	3(1)	9(1)
C(32)	32(2)	16(1)	19(1)	0(1)	6(1)	6(1)
C(37)	17(1)	21(1)	24(2)	0(1)	0(1)	-1(1)
C(38)	20(2)	31(2)	44(2)	0(2)	5(1)	0(1)
C(39)	28(2)	24(2)	27(2)	-2(1)	-4(1)	0(1)
C(33)	44(2)	18(1)	22(2)	1(1)	5(1)	4(1)
C(34)	68(2)	20(2)	23(2)	6(1)	9(2)	17(2)
C(35)	60(2)	32(2)	23(2)	4(1)	3(2)	30(2)
C(36)	35(2)	29(2)	19(2)	1(1)	2(1)	21(1)
C(40)	29(2)	48(2)	28(2)	2(2)	0(1)	24(2)
C(41)	44(2)	68(3)	37(2)	1(2)	-9(2)	37(2)
C(42)	38(2)	75(3)	31(2)	0(2)	4(2)	36(2)

N(3)	16(1)	19(1)	16(1)	2(1)	6(1)	4(1)
C(51)	15(1)	20(1)	24(2)	1(1)	1(1)	4(1)
C(52)	18(1)	26(2)	27(2)	5(1)	6(1)	7(1)
C(53)	28(2)	28(2)	24(2)	5(1)	12(1)	14(1)
C(54)	32(2)	25(2)	20(2)	-3(1)	4(1)	8(1)
C(55)	22(1)	19(1)	19(1)	0(1)	3(1)	1(1)
C(61)	18(1)	24(1)	17(1)	-2(1)	3(1)	2(1)
C(62)	30(2)	16(1)	17(1)	2(1)	5(1)	4(1)
C(63)	29(2)	20(1)	21(2)	2(1)	3(1)	6(1)
C(64)	40(2)	31(2)	21(2)	5(1)	5(1)	21(1)
C(65)	59(2)	26(2)	24(2)	1(1)	1(2)	24(2)
C(66)	48(2)	20(2)	24(2)	-1(1)	1(1)	8(1)
C(67)	34(2)	23(2)	19(2)	3(1)	2(1)	5(1)

Table S11. Hydrogen coordinates (x 10^4) and isotropic displacement parameters (Å^{2}x 10^3) for P17600.

	x	y	z	U(eq)
H(17)	2326	8283	930	23
H(18A)	3427	10390	20	39
H(18B)	2151	9237	-344	39
H(18C)	3660	9167	-232	39
H(19A)	1505	9477	1909	40
H(19B)	803	9326	949	40
H(19C)	2020	10538	1282	40
H(13)	4278	11335	1659	30
H(14)	6411	12005	2430	34
H(15)	7572	10709	2655	32
H(20)	6254	7554	2045	31
H(21A)	7710	9137	3500	57
H(21B)	7740	7826	3308	57
H(21C)	6327	8006	3542	57
H(22A)	7943	8695	1151	53
H(22B)	8644	8149	1864	53
H(22C)	8788	9517	1986	53
H(2A)	5392	7159	626	24
H(2B)	4151	7425	132	24
H(3A)	2634	5577	274	25
H(3B)	3991	5233	420	25
H(37)	779	4938	1045	27
H(38A)	-1490	2898	1460	52
H(38B)	-1622	4049	1063	52
H(38C)	-987	4144	2036	52
H(39A)	1216	3650	-41	44
H(39B)	-309	3665	-204	44
H(39C)	-89	2567	224	44
H(33)	-1	2081	1876	35
H(34)	1462	1500	2746	44
H(35)	3742	2742	3042	41

H(40)	5231	5744	2637	39
H(41A)	5349	4590	3834	68
H(41B)	6815	5192	3428	68
H(41C)	5953	3810	3198	68
H(42A)	5883	3977	1584	66
H(42B)	6943	5300	1829	66
H(42C)	5584	5082	1223	66
H(51)	-603	5754	3618	24
H(52)	-1983	5509	4810	28
H(53)	-979	6352	6193	31
H(54)	1409	7419	6335	32
H(55)	2713	7588	5114	26
H(61)	4355	8685	3305	26
H(63)	839	8539	3534	29
H(64)	245	10097	4169	34
H(65)	1952	11818	4801	40
H(66)	4269	12002	4795	38
H(67)	4887	10476	4139	32

Table S12. Torsion angles [°] for P17600.

N(2)-C(1)-N(1)-C(11)	-167.2(2)
Ru(1)-C(1)-N(1)-C(11)	27.8(4)
N(2)-C(1)-N(1)-C(2)	-3.8(3)
Ru(1)-C(1)-N(1)-C(2)	-168.84(19)
C(1)-N(1)-C(11)-C(12)	-103.6(3)
C(2)-N(1)-C(11)-C(12)	93.9(3)
C(1)-N(1)-C(11)-C(16)	79.0(3)
C(2)-N(1)-C(11)-C(16)	-83.5(3)
C(16)-C(11)-C(12)-C(13)	-5.7(4)
N(1)-C(11)-C(12)-C(13)	177.0(3)
C(16)-C(11)-C(12)-C(17)	171.3(3)
N(1)-C(11)-C(12)-C(17)	-6.0(4)
C(13)-C(12)-C(17)-C(19)	-47.0(4)
C(11)-C(12)-C(17)-C(19)	136.1(3)
C(13)-C(12)-C(17)-C(18)	74.6(3)
C(11)-C(12)-C(17)-C(18)	-102.2(3)
C(11)-C(12)-C(13)-C(14)	1.9(4)
C(17)-C(12)-C(13)-C(14)	-175.1(3)
C(12)-C(13)-C(14)-C(15)	2.4(5)
C(13)-C(14)-C(15)-C(16)	-3.0(5)
C(14)-C(15)-C(16)-C(11)	-0.6(5)
C(14)-C(15)-C(16)-C(20)	179.0(3)
C(12)-C(11)-C(16)-C(15)	5.0(4)
N(1)-C(11)-C(16)-C(15)	-177.6(3)
C(12)-C(11)-C(16)-C(20)	-174.5(3)
N(1)-C(11)-C(16)-C(20)	2.9(4)
C(15)-C(16)-C(20)-C(21)	61.8(4)
C(11)-C(16)-C(20)-C(21)	-118.7(3)
C(15)-C(16)-C(20)-C(22)	-62.4(4)
C(11)-C(16)-C(20)-C(22)	117.1(3)
C(1)-N(1)-C(2)-C(3)	15.8(3)
C(11)-N(1)-C(2)-C(3)	-179.4(2)
N(1)-C(2)-C(3)-N(2)	-20.0(3)
N(1)-C(1)-N(2)-C(31)	172.5(2)
Ru(1)-C(1)-N(2)-C(31)	-20.7(4)

N(1)-C(1)-N(2)-C(3)	-11.0(3)
Ru(1)-C(1)-N(2)-C(3)	155.83(19)
C(2)-C(3)-N(2)-C(1)	20.3(3)
C(2)-C(3)-N(2)-C(31)	-163.0(2)
C(1)-N(2)-C(31)-C(32)	104.9(3)
C(3)-N(2)-C(31)-C(32)	-71.4(3)
C(1)-N(2)-C(31)-C(36)	-80.7(4)
C(3)-N(2)-C(31)-C(36)	103.0(3)
C(36)-C(31)-C(32)-C(33)	3.0(4)
N(2)-C(31)-C(32)-C(33)	177.2(3)
C(36)-C(31)-C(32)-C(37)	-172.6(3)
N(2)-C(31)-C(32)-C(37)	1.6(4)
C(33)-C(32)-C(37)-C(38)	48.5(4)
C(31)-C(32)-C(37)-C(38)	-136.0(3)
C(33)-C(32)-C(37)-C(39)	-74.4(3)
C(31)-C(32)-C(37)-C(39)	101.2(3)
C(31)-C(32)-C(33)-C(34)	0.5(5)
C(37)-C(32)-C(33)-C(34)	176.2(3)
C(32)-C(33)-C(34)-C(35)	-2.4(5)
C(33)-C(34)-C(35)-C(36)	1.0(5)
C(34)-C(35)-C(36)-C(31)	2.3(5)
C(34)-C(35)-C(36)-C(40)	-175.3(3)
C(32)-C(31)-C(36)-C(35)	-4.3(4)
N(2)-C(31)-C(36)-C(35)	-178.6(3)
C(32)-C(31)-C(36)-C(40)	173.3(3)
N(2)-C(31)-C(36)-C(40)	-1.0(4)
C(35)-C(36)-C(40)-C(41)	-24.0(4)
C(31)-C(36)-C(40)-C(41)	158.5(3)
C(35)-C(36)-C(40)-C(42)	98.5(4)
C(31)-C(36)-C(40)-C(42)	-79.0(4)
C(55)-N(3)-C(51)-C(52)	-0.3(4)
Ru(1)-N(3)-C(51)-C(52)	176.5(2)
N(3)-C(51)-C(52)-C(53)	0.5(5)
C(51)-C(52)-C(53)-C(54)	-0.2(5)
C(52)-C(53)-C(54)-C(55)	-0.5(5)
C(51)-N(3)-C(55)-C(54)	-0.4(4)
Ru(1)-N(3)-C(55)-C(54)	-177.2(2)

C(53)-C(54)-C(55)-N(3)	0.8(5)
C(1)-Ru(1)-C(61)-C(62)	140.5(3)
N(3)-Ru(1)-C(61)-C(62)	-36.1(3)
Cl(2)-Ru(1)-C(61)-C(62)	54.0(3)
Cl(1)-Ru(1)-C(61)-C(62)	-121.0(3)
Ru(1)-C(61)-C(62)-C(63)	-18.0(5)
Ru(1)-C(61)-C(62)-C(67)	162.4(2)
C(67)-C(62)-C(63)-C(64)	-1.2(5)
C(61)-C(62)-C(63)-C(64)	179.2(3)
C(62)-C(63)-C(64)-C(65)	0.1(5)
C(63)-C(64)-C(65)-C(66)	0.4(5)
C(64)-C(65)-C(66)-C(67)	0.3(5)
C(65)-C(66)-C(67)-C(62)	-1.5(5)
C(63)-C(62)-C(67)-C(66)	2.0(5)
C(61)-C(62)-C(67)-C(66)	-178.4(3)

Symmetry transformations used to generate equivalent atoms:

References

(1) Alder, K.; Roth, W. Die Synthese der stereoisomeren Iso-santene. Darstellung des 2.3-Dimethylen-1.4-endomethylen-cyclohexans und seine Überführung in Santen (mitbearbeitet von Adolf Grell). *Chem. Ber.* **1955**, *88* (3), 407–419. https://doi.org/10.1002/cber.19550880317.

(2) Gajewski, J. J.; Salazar, J. D. C. Degenerate Thermal Rearrangement of 1,3-Dimethylenecyclopentane. Evidence for Partially Stereospecific Biradical Formation and Closure in a 1,3 Shift. *J. Am. Chem. Soc.* **1981**, *103* (14), 4145–4154. https://doi.org/10.1021/ja00404a028.

(3) Chang, A. B.; Lin, T.-P.; Thompson, N. B.; Luo, S.-X.; Liberman-Martin, A. L.; Chen, H.-Y.; Lee, B.; Grubbs, R. H. Design, Synthesis, and Self-Assembly of Polymers with Tailored Graft Distributions. *J. Am. Chem. Soc.* **2017**, *139* (48), 17683–17693. https://doi.org/10.1021/jacs.7b10525.

(4) Bates, C. M.; Chang, A. B.; Momčilović, N.; Jones, S. C.; Grubbs, R. H. ABA Triblock Brush Polymers: Synthesis, Self-Assembly, Conductivity, and Rheological Properties. *Macromolecules* **2015**, *48* (14), 4967–4973. https://doi.org/10.1021/acs.macromol.5b00880.

(5) Lin, T.-P.; Chang, A. B.; Chen, H.-Y.; Liberman-Martin, A. L.; Bates, C. M.; Voegtle, M. J.; Bauer, C. A.; Grubbs, R. H. Control of Grafting Density and Distribution in Graft Polymers by Living Ring-Opening Metathesis Copolymerization. *J. Am. Chem. Soc.* **2017**, *139* (10), 3896–3903. https://doi.org/10.1021/jacs.7b00791.

(6) Sanford, M. S.; Love, J. A.; Grubbs, R. H. A Versatile Precursor for the Synthesis of New Ruthenium Olefin Metathesis Catalysts. *Organometallics* **2001**, *20* (25), 5314–5318. https://doi.org/10.1021/om010599r.

(7) Leitao, E. M.; Piers, W. E.; Parvez, M. A Thermally Robust Ruthenium Phosphonium Alkylidene Catalyst — the Effect of More Bulky N-Heterocyclic Carbene Ligands on Catalyst Performance in Olefin Metathesis Reactions. *Can. J. Chem.* **2013**, *91* (10), 935–942. https://doi.org/10.1139/cjc-2013-0156.
(8) Walsh, D. J.; Lau, S. H.; Hyatt, M. G.; Guironnet, D. Kinetic Study of Living Ring-Opening Metathesis Polymerization with Third-Generation Grubbs Catalysts. *J. Am. Chem. Soc.* **2017**, *139* (39), 13644–13647. https://doi.org/10.1021/jacs.7b08010.
(9) Falivene, L.; Credendino, R.; Poater, A.; Petta, A.; Serra, L.; Oliva, R.; Scarano, V.; Cavallo, L. SambVca 2. A Web Tool for Analyzing Catalytic Pockets with Topographic Steric Maps. *Organometallics* **2016**, *35* (13), 2286–2293. https://doi.org/10.1021/acs.organomet.6b00371.
(10) Green, M. L. H.; Conway, S. L. J.; Doerrer, L. H. Hydrogen/Deuterium Exchange in Alkyl-Hydride Derivatives of Ansa-Tungstenocene Compounds. *Polyhedron* **2005**, *24* (11), 1388–1403. https://doi.org/10.1016/j.poly.2005.05.004.
(11) Benoit, R. L.; Fréchette, M.; Lefebvre, D. 2,6-Di- *Tert* -Butylpyridine: An Unusually Weak Base in Dimethylsulfoxide. *Can. J. Chem.* **1988**, *66* (5), 1159–1162. https://doi.org/10.1139/v88-190.
(12) Mugridge Jeffrey S.; Bergman Robert G.; Raymond Kenneth N. Does Size Really Matter? The Steric Isotope Effect in a Supramolecular Host–Guest Exchange Reaction. *Angew. Chem. Int. Ed.* **2010**, *49* (21), 3635–3637. https://doi.org/10.1002/anie.200906569.
(13) Bielawski, C. W.; Grubbs, R. H. Increasing the Initiation Efficiency of Ruthenium-Based Ring-Opening Metathesis Initiators: Effect of Excess Phosphine. *Macromolecules* **2001**, *34* (26), 8838–8840. https://doi.org/10.1021/ma011214j.
(14) Sheldrick, G. M. Phase Annealing in SHELX-90: Direct Methods for Larger Structures. *Acta Crystallogr. A* **1990**, *46* (6), 467–473. https://doi.org/10.1107/S0108767390000277.
(15) Sheldrick, G. M. Crystal Structure Refinement with SHELXL. *Acta Crystallogr. Sect. C Struct. Chem.* **2015**, *71* (1), 3–8. https://doi.org/10.1107/S2053229614024218.
(16) Müller, P. Practical Suggestions for Better Crystal Structures. *Crystallogr. Rev.* **2009**, *15* (1), 57–83. https://doi.org/10.1080/08893110802547240.